CONDENSER PERFORMANCE, CONTROL, AND HEAT TRANSFER ENHANCEMENT ISSUES RESULTING FROM ELLIPTIC-SENSITIVITY OF SHEAR DRIVEN INTERNAL CONDENSING FLOWS

Shantanu Kulkarni, Amitabh Narain (Email: narain@mtu.edu), Michael Kivisalu, Soumya Mitra, and Mohammad M. Hasan*

Department of Mechanical Engineering-Engineering Mechanics
Michigan Technological University
Houghton, MI 49931
*NASA Glenn Research Center, MS 77-5
Cleveland, OH 44135

ABSTRACT

This paper presents unsteady computational simulation results and supporting experimental evidence that show a certain fundamental feature of a purely shear driven annular/stratified internal condensing flow with respect to its sensitivity to boundary conditions. This feature is termed "elliptic sensitivity." Shear driven condensing flows occur in 0g, horizontal channels, and micro-meter scale ducts of any orientation and they often have, or are designed to have, a significant annular/stratified regime. This fundamental feature of the flow allows imposition of several possible values of the mean pressure-difference (unlike the usual situation of having only *one* pressure difference value) for a given set of quasi-steady values of mass-flow rate, inlet or outlet pressure, and a steady cooling approach for the condensing-surface. By a quasi-steady time-varying flow variable, it is meant that the variable exhibits a steady-in-the-mean value with suitable time periodic fluctuation (s) superposed on it. For most common cooling approaches, when a quasi-steady value of the pressure-difference is changed (even by an amount in the range of 5 – 200 Pa) *in time* to another quasi-steady value, it often triggers significant changes in the mean condensate thickness, heat transfer rates which induces significant thermal transients, and system characteristics outside the condenser. However if the

system always allows the flow to self-seek a "natural" pressure-difference across the condenser, then purely shear driven flows behave like gravity driven and dominated flows in the sense that they are able to achieve a unique and *stable* realization of a quasi-*steady* flow with a *unique* (termed "natural") value of the pressure-difference. The reported "elliptic" sensitivity feature is absent for gravity dominated flows for which gravity is so strong that it determines the condensate motion as well as its mean interface location.

1. INTRODUCTION

Reliable design and effective integration of condensers in traditional macro-scale as well as modern micro-scale thermal systems require good flow prediction capabilities (simulations, experimentally validated correlations, etc.) and proper flow control strategies. For this, one needs to investigate issues pertaining to attainability and control of quasi-steady condensing flows in different flow categories (gravity driven, shear driven, etc.) and flow regimes (annular, plug/slug, etc.). Most micro-scale condensers and many macro-scale condensers (particularly space-based or horizontal condensers) are shear/pressure driven. There is a special need for flow prediction and control capabilities for these shear/pressure driven condensers.

Typical flow morphologies that are encountered in internal condensing flows (see Carey [1]) are annular/stratified, plug/slug, bubbly, etc. Of these regimes, particular interest is in attainability and controllability of annular/stratified flow regimes under gravity or shear driven conditions. This paper's emphasis on annular/stratified flows is partly because of their high heat exchange rates at relatively lower pumping powers. Another reason for the focus on this regime is because our simulation capabilities are currently limited to annular/stratified flows, and these simulations are required for a good understanding of the boundary condition sensitivities.

Available background and knowledge for condensing flows that are relevant to this paper can be put in the following categories: (i) excellent available knowledge with regard to exact and approximate model equations for mm-μm scale flows and conditions at the interface (Delhaye [2], Carey [1], Faghri et al. [3] - [5], etc.); (ii) classical solutions for *external* film condensation flows over vertical, horizontal, and inclined walls (Nusselt [6], Sparrow and Gregg [7], Koh [8], etc.) and their subsequent modifications and extensions (Rohsenow [9], Chen [10], Dhir and Lienhard [11], Fujii and Uehara [12], Phan and Narain [13], Kulkarni et al. [14], etc.); (iii) experimental data and correlation for heat transfer rates for the various *external* condensing flow regimes (Labuntsov [15], Kutateladze [16], Gregorig et al. [17], etc.) as well as *internal* condensing flows (Carpenter and Colburn [18], Cavallini and Zecchin [19], Shah [20], Dobson and Chato [21], Shao and Grannid [22], Garimella et al. [23]-[24], Kurita et al. [25], etc.); and (iv) flow regime maps for internal condensing flows (Carey [1], Hewitt et al. [26], Cheng et al. [27] – [28], Shao and Grannid [22], Garimella et al. [23]-[24], etc.).

Despite the helpful availability of the above knowledge for condensing flows, some of the outstanding issues are: (i) poor agreement between experiments and correlations when general purpose correlations are sought or used (see Palen et al. [29]), (ii) incomplete understanding of parameters and conditions that may make development of flow regime maps, particularly for experiments dealing with shear driven flows (see Cheng et al. [26]-[27], Garimella et al. [23]-[24], etc.) more reliable and repeatable, and (iii) insufficient understanding of the sensitivities of these flows to condensing surface vibrations, inlet/outlet flow fluctuations, and pressure-difference impositions across a condenser that is exposed to popular cooling approaches in commonly occurring closed-loop systems for various applications.

The computational/experimental research results reported in this paper contribute towards addressing some of the outstanding issues alluded to above. This is because of the reported identification of a fundamental feature (termed "elliptic sensitivity") of purely shear/pressure driven annular/stratified internal condensing flows. This fundamental feature of the flow allows imposition of several possible values for the mean pressure-difference (unlike the usual situation of having only *one* pressure difference value) even as the flow operates at a specified set of quasi-steady values for: mass-flow rate, inlet or outlet pressure, and a cooling approach for the condensing-surface. Since quasi-steady flows mean presence of time-periodic fluctuations superposed on a steady mean value of a flow variable, and such fluctuations are ubiquitous because of presence of compressors and pumps in real systems, the impact of the identified fundamental feature of "elliptic sensitivity" is quite significant in making sense of experimental data in the literature, in practice, and those reported here. Because of this, the reported results on this fundamental feature of internal flow condensation (which is possibly also applicable to internal flow boiling) is expected to assist in mapping a course for future research for: (a) better control of these flows, (b) enhanced heat transfer rates, and (c) ensuring repeatable behavior of the condenser (or boiler) by properly designing closed loop systems that employ flow condensers and/or flow boilers.

The computational results in this paper corrects some of our earlier results ([30]-[34]) on "elliptic sensitivity" of internal condensing flows. Both the earlier results ([30]-[34]) and this paper agree on the existence of a "natural" steady solution of the strictly steady governing equations when the flow is allowed to self-seek its "natural" pressure-difference under "parabolic" boundary conditions (e.g. a given steady inlet vapor mass flow rate, steady inlet or exit pressure, and a known steady cooling approach for the condensing-surface that defines its

thermal boundary condition). The error in the earlier results ([30]-[34]) was that it said multiple steady pressure-difference impositions were possible (termed "elliptic" behavior) and that this led to multiple steady solutions of the inherently "elliptic" steady governing equations. The corrected result in this paper says that there is only one *unique* "natural" steady solution of the strictly *steady* governing equations - which are, therefore, "parabolic" in nature. However, in most practical situations, there are multiple quasi-steady solutions because it is the *unsteady* equations (not the steady equations) that are inherently "elliptic" and hence allow multiple quasi-steady pressure-difference impositions. The multiplicity of the steady solutions was erroneously concluded in the earlier results because the reported quasi-steady solutions are often very close to the strictly steady solution, and computational errors in [30]-[34] went unnoticed and uncorrected at the time of their reporting. Furthermore, at this time, we also have an independent one-dimensional solver ([35]) which confirms the inherently "unique" solution of the strictly steady governing equations under "parabolic" boundary conditions (see definition in section-2).

Besides the computational results reported in this paper, the experimental results reported in this paper also confirm the fact that shear driven internal condensing flows allow multiple quasi-steady flow realizations due to multiple quasi-steady pressure difference impositions (i.e. the flows exhibit "elliptic sensitivity"). This result appears to be quite general because the thermal-conditions for the condensing-surface that is used for the computational simulations is one of steady uniform temperature whereas the one imposed in the experiments is one of the more common steady convection-type thermal boundary condition (see sections 2 and 6).

2. TERMINOLOGY AND ESSENTIAL RESULTS AS A MOTIVATION FOR THIS PAPER

2.1 Terminology

The liquid and vapor phases in the flow (see Fig. 1) are denoted by $\mathcal{L}$ (subscript I: I = 1) for liquid and $\mathcal{V}$ (I = 2) for vapor. The fluid properties (density ρ, viscosity μ, specific heat C_p, and thermal conductivity k) with subscript I are assumed to take their representative constant values for each phase (I = 1 or 2). Let T_I be the temperature fields, p_I be the pressure fields, $T_s(p)$ be the saturation temperature of the vapor as a function of local pressure at the interface p, Δ be the film thickness, $\dot{m}$ be the local interfacial mass flux, $T_w(x)$ ($< T_s(p)$) be a known temperature variation of the condensing surface (with its length average mean value being $\overline{T}_W$), and $\mathbf{v}_I = u_I\hat{\mathbf{i}}+v_I\hat{\mathbf{j}}$ be the velocity fields. The flow fields are defined at every point **x** (a 3-D Euclidean position vector) and time *t*. Furthermore, the characteristic length L_c for the channel geometry is its channel gap 'h' shown in Fig. 1 and, for the tube geometry (see [35]), L_c is the diameter D. Let g_x and g_y be the components of gravity along x and y axes, p_0 be the inlet pressure, $\Delta T \equiv T_s(p_0) - \overline{T}_W$ be a representative controlling temperature difference between the vapor and the bottom plate, h_{fg} be the heat of vaporization at temperature $T_s(p)$, and U be the average inlet vapor speed determined by the inlet mass flow rate $\dot{M}_{in}$ ($\equiv \rho_2 \cdot U \cdot h$ for the channel flow). Let t represent the actual time and (x, y) represent the physical distances of a point with respect to the axes shown in Fig. 1 for the channel flow (for tube flows in [35], $x = 0$ is at the inlet, $y = 0$ is at the tube wall). For the channel of height 'h,' y = h is an isothermal plate and is a slightly superheated non-condensing surface. For the tube in [35], y = D/2 (i.e. r = 0) is the center-line where symmetry condition holds for all flow variables of interest. Note that, $y \equiv L_c.y$ represents the distance from the

condenser surface, for both channel (Fig. 1) and in-tube (see [35]) flows. We introduce a new list of fundamental non-dimensional variables – viz. $(x, y, t, \delta, u_I, v_I, \pi_I, \theta_I, \dot{m})$ through the following definitions:

$$\{\chi, y, \Delta, u_1, \dot{m}\} \equiv \{L_C \cdot x, L_C \cdot y, L_C \cdot \delta, U \cdot u_1, \rho_l \cdot U \cdot \dot{m}\}$$
$$\{v_1, T_I, p_I, t\} \equiv \{U \cdot v_1, (\Delta T) \cdot \theta_1, p_0 + \rho_l U^2 \cdot \pi_I, (L_C / U) \cdot t\}. \quad (1)$$

2.2 Steady and Unsteady Flow Behavior of Condensing Flows

For the convenience of communication of the rather unique nature of the shear driven condensing flows we propose a distinction among: (i) parabolic/elliptic boundary conditions, (ii) parabolic/elliptic governing equations, and (iii) parabolic/elliptic flow behavior. These terms are defined as:

Parabolic Boundary Conditions

In one computational approach, parabolic boundary conditions for the two dimensional flow in Fig. 1 requires prescription of the values of inlet mass flow rate $\dot{M}_{in}$ (more precisely, for 2-D computations, x-velocity profile $u_2(0, y, t)$ and a suitable $v_2(0, y, t)$), inlet temperature $T_2(0, y, t)$, the thermal and hydrodynamic wall conditions on the channel walls (at $y = 0$ and $y = h$), and either the inlet pressure p_{in} (= $p_2(0, y, t)$) or the exit pressure p_{exit} (= $p_2(x_e, y, t)$) at any "one point" on the inlet or the outlet cross-section. The procedure for specifying pressure at a point is quite similar to specifying reference pressure at one point ([36]) in an incompressible single-phase flow. In a second computational approach, parabolic boundary conditions for a two dimensional problem consists of: prescription of the inlet pressure p_{in} (= $p_2(0, y, t)$) and the exit pressure p_{exit} (= $p_2(x_e, y, t)$ that are concurrently specified across an arbitrary line $y = y^*$ and $0 \le x \le x_e$ (i.e. the

pressure-difference $\Delta p \equiv p_{in} - p_{exit}$ is specified), inlet temperature $T_2(0, y, t)$, the thermal and hydrodynamic wall conditions on the channel walls (at $y = 0$ and $y = h$), and, in addition, the specification of the complete pressure variation across either the inlet *or* the exit cross-section as the normal stress for the stress boundary condition (which requires normal and tangential stresses) on that boundary.

Elliptic Boundary Conditions

In addition to the parabolic boundary conditions in the first computational approach described above, if one can specify the pressure variation across the boundary (say the inlet or the outlet) where the "pressure at a point" was *not* specified as part of the parabolic boundary condition, then such a specification is called an elliptic boundary condition. In the second computational approach for the parabolic boundary conditions, if besides the point pressure p_{in}, point pressure p_{exit}, and a cross-sectional pressure variation (over an inlet or outlet boundary); one specifies the inlet mass flow rate then this specification will be called an elliptic boundary condition.

Parabolic Governing Equations

If the duct flow governing equations (steady or unsteady) are such that the parabolic boundary conditions in the first approach are sufficient to fully determine the pressure, velocity, and temperature fields elsewhere, then the governing equations are said to be parabolic. The parabolic governing equations discretization and solution technique in this computational approach (for which the "pressure at a point" at the inlet is prescribed) are such that to determine the value of a flow variable at a point one does not need information from any downstream location. If the governing equations (steady or unsteady) are such that the parabolic boundary

conditions for the second computational approach are sufficient to fully determine the mass flow rate $\dot{M}_{in}$ (more precisely, the x-velocity profile $u_2(0, y, t)$ and a suitable y-velocity profile $v_2(0, y, t)$), then again the governing equations are said to be parabolic. Different approaches (e.g. the second approach discussed above) to specify parabolic boundary conditions are all equivalent to the first approach (for which the "pressure at a point" on the inlet was specified) because they all indirectly exploit the parabolic governing equations' feature that the flow at a point is only affected by the upstream conditions.

Elliptic Governing Equations

If the duct flow governing equations (steady or unsteady) are such that the elliptic boundary conditions need to be added to parabolic boundary conditions for either the first or the second approach to fully determine (within the domain and relevant parts of its boundary) the pressure, velocity, and temperature fields, then the governing equations are said to be elliptic.

Strictly Parabolic Flow Behavior

Steady or unsteady incompressible single phase flows (and some immiscible two-fluid flows) are examples of strictly parabolic flows. A strict parabolic problem has the following two features: (i) for repeatable realization of the flow, the available knowledge of the parabolic boundary conditions is sufficient without any knowledge or specification of the remaining "elliptic" boundary condition, and (ii) any impositions (with or without fluctuations) of the remaining "elliptic" boundary condition is impossible as it can only affect the flow outside the flow domain of interest.

Strictly Elliptic Flow Behavior

A *strictly* "elliptic" flow (steady or unsteady) will have the following feature: for repeatable realization of the flow, one needs specifications or knowledge of all the boundary conditions – the parabolic *and* elliptic boundary conditions defined above.

Incompressible single-phase flows of common experience are always parabolic in behavior and never elliptic. This is because information to an interior point does not travel from both upstream and downstream locations. Some compressible duct flows are, however, elliptic in the above sense.

Unique and Mixed (Parabolic and Elliptic) Nature of Internal Condensing Flow Behavior

These flows' behavior are characterized by the fact that: (i) steady condensing flow governing equations are parabolic, (ii) unsteady condensing flow governing equations can be parabolic for unspecified exit conditions (i. e. parabolic boundary conditions), and (iii) unsteady condensing flow governing equations can also be typically (i.e. for most thermal boundary conditions for the condensing surface) elliptic for elliptic boundary condition specification.

The *steady* internal condensing flows governing equations under steady parabolic boundary conditions for the first computational approach yield unique solutions that predict the entire velocity, temperature (including condensing-surface temperature if it was not directly specified as a thermal boundary condition), and pressure variations. This means that the steady governing equations are parabolic and they define a unique self sought value of the steady pressure difference $\Delta p_{lNa} \equiv p_{in} - p_{exit}$. However shear driven internal condensing flows behavior itself does not exhibit *strictly* parabolic behavior because the *unsteady* governing equations allow

unsteady prescription of elliptic boundary conditions leading to unsteady flows for most thermal boundary conditions. The thermal boundary condition for which the wall heat flux profile for the condensing surface is fixed is an exception because flows with this boundary condition exhibit parabolic behavior. A thermal boundary condition that does not fix a steady wall heat flux for the condensing-surface is the one which is usually encountered in practice and is investigated here. The ability to impose unsteady elliptic boundary condition for shear driven internal condensing flows was found to become gradually impossible as gravity component in the direction of the flow becomes large enough to make the flow gravity dominant (see [35]). For example, for a representative horizontal channel flow, the flow becomes gravity dominated (see [35]) as the condensing plate is given an approximate 1° downward tilt.

For partially condensing annular/stratified flows in Fig. 1, if the inlet pressure p_{in} at a point is specified as part of the parabolic boundary conditions in the first computational approach, the elliptic boundary condition specification of the exit pressure across the exit boundary is found to be equivalent to specification of the exit liquid (or vapor) mass flow rate $\dot{M}_{L-e}(t) \equiv \int_0^{\Delta} \rho_1 u_1(x_e, y, t)dy \equiv \rho_1 U h \int_0^{\delta} u_1 dy \equiv \rho_1 U h \hat{\dot{M}}_{L-e}(t)$. With regard to the ability to impose unsteady exit liquid mass flow rate as an elliptic boundary condition for partially condensing flows when the parabolic boundary conditions described above (for the first computational approach) are steady in time, it is found that both the elliptic exit condition and the resulting flow must be unsteady in order to impose elliptic boundary condition. For the condensing surface thermal boundary condition of fixed and steady temperatures (i.e. $T_w(x,t) = T_w(x) =$ constant), there are two types of unsteady elliptic boundary condition specifications that are computationally considered here. These are:

i. A truly unsteady exit condition specification (e.g. an unsteady specification of $\hat{\dot{M}}_{L-e}(t)$ in Fig. 2a) leads to a truly unsteady solution – this is demonstrated by the resulting unique solution's unsteady film thickness δ(x,t) values in Fig. 2b.

ii. A quasi-steady specification of the exit condition (e.g. through a steady-in-the-mean specification of $\hat{\dot{M}}_{L-e}(t)$, the blue curve in Fig. 3) leads to a quasi-steady solution (as shown by a steady-in-the-mean δ(x,t) values with $\overline{\delta(x,t)} \neq \delta_{Na}(x)$) associated with the blue curves in Fig. 4. Note that the mean quasi-steady specification does not allow just any time-periodic fluctuations on it for the resulting flow to be quasi-steady. The superposed fluctuations must be in a class that is compatible with it. The fact that these steady-in-the-mean (quasi-steady) elliptic boundary condition impositions are attainable in the presence of suitable superposed time-periodic fluctuations of one or more hydrodynamic (pressure and/or flow rate/velocity field) boundary conditions illustrates the unique "mixed" behavior of the shear dominated condensing flows.

The ellipticity of the unsteady equations or quasi-steady "elliptic–sensitivity" of the steady parabolic boundary conditions computationally demonstrated above (in Figs. 2-3) is not limited to the thermal boundary condition that have been considered here (in which condensing surface temperature was held steady (at $T_w(x,t) = T_w(x)$ = constant). This elliptic–sensitivity is found to manifest - with some variations in the dynamic response - for many other commonly occurring steady cooling approaches for the condensing surface. For example, the condensing surface thermal boundary condition for the cooling approach in which the condensing-surface rejects heat through a negligible thermal resistance slab into a steady coolant flow of constant temperature T_{res}, is modeled by: $q''_W(x,0,t) \equiv h_{ext}[T(x,0,t) - T_{res}] \equiv -k_1 \frac{\partial T_1}{\partial y}|_{y=0}$ - where

the cooling approach itself is steady because the value of the external thermal resistance ($1/ h_{ext}$) on a per unit area basis as well as the coolant temperature T_{res} are steady. In this paper, the elliptic-sensitivity of the quasi-steady condensing flows is experimentally demonstrated for the above types of cooling approaches.

For the shear driven fully condensing flow experiment employing a rectangular cross-section (2 mm x 15 mm) horizontal channel modeled as a 2-D channel of Fig. 5, the thermal boundary conditions is predominantly of convection type (see section 6), i.e. $h_{ext}[T(x,0,t) - T_{res}] \equiv -k_1 \frac{\partial T_1}{\partial y}|_{y=0}$, at all locations except locations marked HFX-1/TEC-1 and TEC-2 in Fig. 5. The reported experiment is able to fix a steady set of parabolic boundary condition, namely: cooling approach, the mean value of exit pressure p_{exit}, and the mean value of inlet mass flow rate $\dot{M}_{in}$. One set of experiments are done when the inlet pressure is free to self select its value for the above described quasi-steady "parabolic" boundary conditions. A repeatable quasi-steady (because of unavoidable fluctuations) flow is achieved for $t \leq t_0$ shown in Figs.6a–6b. The Figs. 6a–6b show the experimentally achieved quasi-steady values of p_{exit}, $\dot{M}_{in}$, $p_{in|Na}$, Δp, and average heat flux $q''_{W|HFX-1}$ over HFX-1. Experimental data reported in Figs. 5-6 are good only for the time-averaged mean values and currently they do not precisely measure the fluctuations over the reported mean values. Fig. 6c shows that in response to a transient (or unsteady) imposition of inlet pressure $p_{in}(t) \neq p_{in|Na}$ (over $t_0 \leq t \leq t_0 + 10$ - not shown), the elliptic–sensitivity of the flow induces a longer transient (about 65 minutes long) in the wall temperatures (see Fig. 6c) and a shorter 8 min transient in heat-flux values $q''_{W|HFX-1}$ (note that heat flux values are being reported for a location where the condensing surface temperature was held fixed). The observed time varying thermal transient in the condensing-surface temperature (which would be part of the

unsteady solution if the problem was computationally solved) proves the unsteady elliptic response of the flow due to unsteady elliptic boundary condition imposition (as in Figs. 2-3). Unlike computations where the condensing-surface temperature is fixed, the experimental steady cooling approach allows (see section 6) thermal transients in the form of induced unsteady values for the condensing-surface temperature $T_w(x, t)$. Since the imposed inlet pressure p_{in} (t) is eventually steady for $t > t_0 + 10$, a different quasi-steady flow with a different condensing-surface temperature distribution, (see Fig. 7) is achieved for $t > t_0 + 65$. As a result, very different heat transfer rates were observed (e.g. there is an almost 40% enhancement in $q''_{W|HFX-1}$ in Fig. 6 over the condenser surface area covered by HFX -1) as compared to the original quasi-steady flow at $t < t_0$. The relationship between the two quasi-steady flows for the experimental thermal boundary condition and the relationship between steady and quasi-steady flows in Figs. 2-3 for the theoretical thermal boundary condition of constant temperatures are, however, qualitatively different (see section 6).

The Figs. 6-7 showing unsteady experimental response resulting from unsteady elliptic boundary condition imposition over $t_0 \leq t \leq t_0 + 10$ confirms a generalized version of the computationally established unsteady elliptic behavior in Fig. 2.

The above described unique qualitative feature of the steady equations' parabolicity and the unsteady equations' ellipticity arise from the fact that the macroscopic characterization of the governing equations are only supposed to reflect the unique and different physics of the acoustic waves and interface location fluctuation that underlie the macroscopic governing equations. This physics is hidden in the governing equations because the time scale "δt" and fluid element volume "δv" of interest associated with these equations are significantly larger than the relatively

minuscule time scales "δt_a" and fluid element volume "δv_a" that are required to capture the signatures of the underlying fast moving acoustic waves and their coupling with interfacial locations and mass transfer fluctuations.

As an example, when people are talking and listening, at the larger length and time scales of interest, the quiescent air satisfies the governing equations of motion whose solutions are: zero velocity, hydrostatic pressure variation, isothermal temperatures, and constant density. Yet the governing equations at the smaller length and time scales of interest that capture acoustic waves yield solutions that have: non-zero velocity fluctuations, non-isothermal temperature fluctuations, non-constant density fluctuations, etc.

Therefore different physical situations (condensing flow, single phase flow, etc.) that lead to different parabolic/elliptic sensitivities at the larger length and time scales arise from different physics of acoustic waves and other fluctuations with regard to their transmission, reflection, and absorption characteristics within the control volume and its boundaries. For example, the unsteady elliptic behavior of laminar/laminar internal condensing flows results from the fact that, under unsteady elliptic boundary condition impositions, a fluid element in the interior – particularly at the interface (which has interfacial waves travelling only in the downwind direction (see [33]))– receives and accumulates acoustic waves and the interfacial fluctuations. This happens in a way that information from both the upstream and the downstream locations matter and one still does not need changes in the incompressible governing equations for the larger length and time scales. The net result of this feature is that if one increases in time the exit pressure on the vapor phase (for shear driven flows whose condensing-surface cooling conditions do not restrict changes in heat-flux values) above its "natural" value, the vapor tries to accommodate this by slowing down and accordingly increasing the interfacial mass transfer

rates, decreasing the film thickness, increasing the heat-transfer rates, and suitably changing the interfacial shear (that keeps the exit pressure for the liquid condensate consistent with the imposed pressure on the vapor phase). Analogous but opposite trends occur if the imposed exit pressure decreases in time. However it is very important to note that if the time-periodic elliptic imposition leads to quasi-steady annular flows, the fluctuations in the interior and the boundaries for any two different flow variables must correlate in time in such a way so as to yield non-zero time-averaged correlations. This is consistent with the computational results in section-5 and the discussions in section 6 for the experimental results.

3. BACKGROUND FOR COMPUTATIONAL AND THEORETICAL RESULTS/INVESTIGATIONS

This section summarizes the 2-dimensional (steady or unsteady) governing equations and computational approaches for internal condensing flows in channels (or vertical tubes). These approaches/techniques are used to investigate gravity driven, shear driven, and mixed driven flows.

3.1 Two-Dimensional (2-D) Governing Equations

Interior Equations

The non-dimensional differential forms of mass, momentum (x and y components), and energy equations for the two-dimensional flow in the interior of either of the incompressible phases are the well-known equations:

$$\frac{\partial u_I}{\partial x} + \frac{\partial v_I}{\partial y} = 0$$

$$\frac{\partial u_I}{\partial t} + u_I \frac{\partial u_I}{\partial x} + v_I \frac{\partial u_I}{\partial y} = -\left(\frac{\partial \pi_I}{\partial x}\right) + Fr_x^{-1} + \frac{1}{Re_I}\left(\frac{\partial^2 u_I}{\partial x^2} + \frac{\partial^2 u_I}{\partial y^2}\right)$$

$$\frac{\partial v_I}{\partial t} + u_I \frac{\partial v_I}{\partial x} + v_I \frac{\partial v_I}{\partial y} = -\left(\frac{\partial \pi_I}{\partial y}\right) + Fr_y^{-1} + \frac{1}{Re_I}\left(\frac{\partial^2 v_I}{\partial x^2} + \frac{\partial^2 v_I}{\partial y^2}\right) \tag{2}$$

$$\frac{\partial \theta_I}{\partial t} + u_I \frac{\partial \theta_I}{\partial x} + v_I \frac{\partial \theta_I}{\partial y} \approx \frac{1}{Re_I Pr_I}\left(\frac{\partial^2 \theta_I}{\partial x^2} + \frac{\partial^2 \theta_I}{\partial y^2}\right),$$

where $Re_I \equiv \rho_I U h / \mu_I, Pr_I \equiv \mu_I C_{pI} / k_I, Fr_x^{-1} \equiv g_x h / U^2$ and $Fr_y^{-1} \equiv g_y h / U^2$.

Interface Conditions

The nearly exact interface conditions (see Delhaye [2], Narain et. al. [33] etc.) for condensing flows are given in the Appendix A-1 (see Eqs. (A.1) - (A.8)). Utilizing a superscript "i" for values of flow variables at the interface located as $\phi \equiv y - \Delta(x,t) = 0$, non-dimensional forms of the interface conditions are given below.

• The non-dimensional form of the requirement of continuity of tangential component of velocities (see Eq. (A. 2)) becomes:

$$u_2^i = u_1^i - \delta_x (v_2^i - v_1^i), \tag{3}$$

where $\delta_x \equiv \partial\delta/\partial x$.

• The non-dimensional form of the normal component of momentum balance at the interface (see Eq. (A. 3)) becomes:

$$\pi_1^i = \frac{\rho_2}{\rho_1}\pi_2^i - \frac{1}{We}\left(\frac{\delta_{xx}}{[1+\delta_x^2]^{3/2}}\right) + \dot{m}^2\left(\frac{\rho_1}{\rho_2} - 1\right), \tag{4}$$

where $We \equiv \rho_1 U^2 h/\sigma$, and surface tension $\sigma = \sigma(T)$ where T is the interfacial temperature.

• The tangential component of momentum balance at the interface (see Eq. (A. 4) in Narain et al. [33]) becomes:

$$\left.\frac{\partial u_1}{\partial y}\right|^i = \frac{\mu_2}{\mu_1}\left.\frac{\partial u_2}{\partial y}\right|^i + [t], \tag{5}$$

where the term [t] in Eq. (5) is defined in Eq. (A.9).

• The non-dimensional form of non-zero physical values of interfacial mass fluxes $\dot{m}_{LK}$ and $\dot{m}_{VK}$ (defined in Eq. (A.5)) are required to satisfy kinematic constraints associated with the liquid and vapor velocity values of the interface. In the non-dimensional form these are given by:

$$\begin{aligned} \dot{m}_{LK} &\equiv \left[u_1^i(\partial\delta/\partial x) - (v_1^i - \partial\delta/\partial t)\right]/\sqrt{1+(\partial\delta/\partial x)^2}, \text{ and} \\ \dot{m}_{VK} &\equiv (\rho_2/\rho_1)\left[u_2^i(\partial\delta/\partial x) - (v_2^i - \partial\delta/\partial t)\right]/\sqrt{1+(\partial\delta/\partial x)^2}. \end{aligned} \tag{6}$$

• The non-dimensional form of non-zero physical values of interfacial mass flux $\dot{m}_{Energy}$ (as given by Eq. (A.6)) represents the constraint imposed by the net energy transfer across the interface and is given by:

$$\dot{m}_{Energy} \equiv Ja/(Re_1\, Pr_1)\{\partial\theta_1/\partial n\big|^i - (k_2/k_1)\partial\theta_2/\partial n\big|^i\}, \tag{7}$$

where $Ja \equiv C_{p1}\Delta T / h^0_{fg}$, and $h^0_{fg} \equiv h_{fg}(T_s(p_o)) \cong h_{fg}(T_s(p_2^i))$.

• The interfacial mass balance requires that the net mass flux (in kg/m^2/s) at a point on the interface, as given by Eq. (A.7), be single-valued regardless of which physical process is used to obtain it. The non-dimensional form of this requirement becomes:

$$\dot{m}_{LK} = \dot{m}_{VK} = \dot{m}_{Energy} \equiv \dot{m}. \tag{8}$$

It should be noted that negligible interfacial thermal resistance and equilibrium thermodynamics on either side of the interface is assumed to hold for x – values downstream of the origin (i. e., second or third computational cell onwards). Hence, as per discussions leading to Eq. (A.8) in Appendix A-1, no model for the interfacial mass-flux $\dot{m}$ is needed to obtain a solution.

• The non-dimensional thermodynamic restriction on interfacial temperatures (as given by Eq. (A.8)) becomes:

$$\theta_1^i \cong \theta_2^i = T_s\left(p_2^i\right)\Big/\Delta T \equiv \theta_s\left(\pi_2^i\right) \ . \tag{9}$$

within the vapor phase, for the refrigerants considered here, changes in absolute pressure relative to the inlet pressure are big enough to affect vapor motion but, at the same time, they are usually too small to significantly affect saturation temperatures (except in micro-scale ducts). Therefore, we have $\theta_s(\pi_2^i) \cong \theta_s(0)$.

Boundary Conditions

The problem posed by Eqs. (2) – (9) is computationally solved subject to the well-known (see [33]) boundary conditions on the top and bottom walls.

Top wall: The upper wall temperature $T_2(x, h, t) = T_2|_0 > T_{sat}(p_0)$ is at a superheated value (to prevent condensation on this surface) close to saturation temperature to allow the assumption of a nearly constant saturation temperature for the vapor at all location. This is reasonable because effects of superheat (in the typical 5 – 10^{o}C range) on the condensation process are quite negligible.

Bottom wall: Besides the no-slip condition ($u_1(x, 0, t) = v_1(x, 0, t) = 0$) at the condensing surface, one could have several types of thermal boundary conditions. Typically, on different portions of the condensing surface, one could have any of the following three types of boundary conditions. If the condensing-surface temperature ($T_1(x, 0, t) = T_w(x)$) is prescribed or known, the non-dimensional form of this condition is written as

$$\theta_1(x, 0, t) = \theta_W(x) \equiv T_W(x) \,/\, \Delta T \tag{10}$$

Here Eq. (10) is known as steady temperature boundary condition for a known condensing surface temperature distribution $T_W(x)$. The computational results presented in this paper limit itself to uniform values of this type of boundary condition.

Alternatively, one could have the physical heat flux (i.e. $q''_w(x) = - k_1(\partial T_1/\partial y) |_{y=0} = q''_{w0} * \tilde{q}''(x)$) specified directly or indirectly (through convection type boundary condition). For direct specification of heat flux, the non-dimensional function $q''_w(x, t)$ is a known function of x and t hence the thermal boundary condition becomes:

$$(\partial\theta_1/\partial y)\,(x, 0, t) = (q''_{w0} \cdot h \cdot \tilde{q}''(x, t)) / (k_1 \cdot \Delta T) \qquad (11)$$

Equation (11) is known as *steady* heat flux boundary condition if the non dimensional form of $q''_w(x, t)$ is $q''_w(x)$. This type of boundary condition does not allow flows to exhibit 'elliptical sensitivity' as described in section 2 and is not considered here. Often the heat-flux $q''_w(x, t)$ is only implicitly known through the convection condition of the type:

$$(\partial\theta_1/\partial y)\,(x, 0, t) = (h_{ext}h/k_1)\,\{\theta_1(x,0,t) - \theta_{res}\} \qquad (12)$$

where, $(1/h_{ext})$ is known as external thermal resistance and $\theta_{res} = T_{res} / \Delta T$ is the non dimensional value of the reference temperature.

Inlet Conditions: At the inlet x = 0, we have $u_2 = U$ and we prescribe:

$$u_2(0, y, t) = 1\,,\ \partial v_2/\partial x\big|_{x=0} = 0\,. \qquad (13)$$

Pressure is not prescribed across the entire inlet boundary but its value p_0 is prescribed at a point on the inlet boundary – and its value also appears indirectly through important thermodynamic properties such as $h_{fg}(p_2^i) \approx h_{fg}(p_0)$ and $T_{sat}(p_2^i) \approx T_{sat}(p_0)$. The interfacial pressure variations are obtained from the computed values of non dimensional pressures $\pi_2^i(x, y, t)$ and the relation $p_2 = p_0 + \rho_2.U^2\,\pi_2\,(x, \delta(x, t), t)$.

Exit Conditions:

In the computational study reported here, "parabolic" boundary conditions for the steady problem – as described in section 2 – are the steady inlet pressure p_0 (which is prescribed only at a point on the inlet boundary), inlet vapor mass flow rate, and the steady wall temperature. Therefore, for the *steady* parabolic problem, no exit boundary condition is specified. For the unsteady problem, as described in section 2, "elliptic" boundary condition specifications are needed.

Unspecified Exit Condition or "Parabolic" Formulation [A]: For partial condensation, the "natural" specification of liquid or vapor exit flow rate (or exit pressure) is one that does not constrain the flow and allows the flow to "self-seek" its exit condition. This is achieved by the imposition of the following "outflow" type condition at the exit:

$$\frac{\partial v_I}{\partial x}\Big|_{x = x_e} \cong 0 \tag{14}$$

for I = 1 and 2, while concurrently ensuring that the x-component of the exit velocities $u_I|_{x=xe}$ are positive (for I = 1 and 2) and satisfy the overall mass balance for the entire partially condensing control volume in Fig. 1.

Formulation [B] for Elliptic Boundary Condition Imposition: For *unsteady* annular/stratified internal condensing flow problems (purely shear driven flows – 0g or horizontal channel in Fig. 1), it is tentatively assumed that exit condition can be specified in terms of exit flow rate (either non dimensional exit vapor flow rate $\hat{\dot{M}}_{V-e}(t)$ at the exit or non dimensional liquid flow rate $\hat{\dot{M}}_{L-e}(t)$ at the exit) or suitable exit pressure specifications (not implemented in this paper). Equation (15)

below shows one way that exit condition can be specified in terms of the time varying non-dimensional liquid exit mass flow rate:

$$\hat{\dot{\mathbf{M}}}_{\mathbf{L-e}}(\mathbf{t}) = \int_{\mathbf{y=0}}^{\boldsymbol{\delta}(\mathbf{x_e},\mathbf{t})} \mathbf{u_1}(\mathbf{x_e},\mathbf{y},\mathbf{t}) \cdot \mathbf{dy} \equiv \frac{1}{\boldsymbol{\rho}_1 \mathbf{U_0 h}} \left[\int_{y=0}^{\delta(x_e,t)} \boldsymbol{\rho}_1 u_1(x_e, y, t) \cdot \mathbf{d}y \right]$$

$$\equiv \text{A known function of time t for each } t \geq 0 \qquad (15)$$

Even though one can test different constants or time varying values on the right hand side of Eq. (15), we already know from our steady solution that there must exist only one unique time independent *constant* value for the right side of Eq. (15) for which a long term ($t \rightarrow \infty$) steady solution can be obtained for the time independent exit condition imposition in Eq. (15). This unique constant must be the same as the one obtained from the solution of the steady equations under formulation [A]. Physically these solutions are only realized when one does not constrain the flow from self seeking its "natural" exit condition. The question here is whether other unsteady or steady-in-the-mean time-periodic specifications of $\hat{\dot{M}}_{L-e}(t)$ in Eq. (15) – corresponding to a range of system imposed mean exit conditions superposed with suitable time-periodic fluctuations can or cannot be imposed to obtain a corresponding range of unsteady or quasi-steady solutions.

Initial Conditions

If t = 0 is chosen to be the time when saturated vapor first comes in contact and condenses on a dry sub-cooled ($T_w(x) < T_s(p_0)$) bottom plate, the above described *continuum* equations do not apply at very early times (t ~ 0). This is because these equations do not model and incorporate various inter-molecular forces that are important in determining the time evolution of very thin (10 - 100 nm) condensate film thickness δ (x,t). Because of the above

modeling limitations, the strategy here is to start at a time (t = 0) for which one has a sufficiently thick arbitrary *guess* or one starts at the *steady* solution of the *continuum* equations (where all the governing equations clearly apply) and then, from there, one can obtain the natural large time ($t \rightarrow \infty$) steady/quasi-steady solutions with the help of the unsteady equations. That is, if $\phi(x,y,t)$ is any variable (such as u_I, v_I, π_I, θ_I, etc.), the initial values of ϕ and film thickness $\delta(x,t)$ are such that:

$$\phi(x, y,0) = \phi_{steady}(x, y) \text{ or } \phi_{guess}(x,y)$$

$$\text{and } \delta(x,0) = \delta_{steady}(x) \text{ or } \delta_{guess}(x) \qquad (16)$$

where ϕ_{guess} and δ_{guess} are respectively reasonable but arbitrary initial guesses whereas ϕ_{steady} and δ_{steady} are solutions of the governing equations obtained by dropping all time dependencies in equations (2) – (13) and solving the resulting steady equations for parabolic boundary conditions (i.e. by not imposing the exit conditions).

3.2 Quasi One-Dimensional (1-D) Governing Equations and Computational Approach

The steady solutions for shear and gravity driven flows that have been obtained by the 2-D approach described above, can also be obtained by a computationally more efficient and powerful (though more approximate) 1-D solution technique [35] that has been recently developed to support and reinforce the 2-D results. This 1-D technique [35] is based on solutions of a coupled set of ordinary differential equations and is not described here for brevity. This technique, a brief summary of results obtained from it, and a comparison of some of its basic results from those obtained from the 2-D results are reported in this paper.

The quasi 1-D solution technique in [35] is prefixed "quasi" because it uses the exact 2-D analytical solutions of the underlying equations obtained from thin film approximations that model the condensate motion and its temperature profiles. Only the vapor phase momentum and mass balance equations used in this approximation are integral or one-dimensional in nature. Therefore accuracy of results obtained from these integral balance law statements depend solely on the reasonableness of the choice for vapor velocity profile $u_2(x, y)$.

4. ALGORITHM AND REGULARITIES AND ACCURACY OF THE 2-D COMPUTATIONAL METHODS

2-D Approach

For a computational solution to be accurate, it needs to meet the following criteria: (i) satisfaction of the convergence criteria in the interior of each fluid (since finite volume SIMPLER technique is used, it means smallness of "b" defined on p.125 of Patankar [36]), (ii) satisfaction of all the interface conditions, (iii) grid independence of solutions for grids that are sufficiently refined, and (iv) unsteady simulations' time varying predictions of the interface location should be free of computational noise in the absence of physical noise. The steady and unsteady simulation results presented here satisfy all the above criteria.

The satisfaction of the governing equations in the interior and all the conditions at the interface is demonstrated in Liang et al [32]. Let the number of spatial grid lines $\left(n_i \times n_{j|L} \times n_{j|V}\right)_{I \text{ or } II}$ in grid-I or grid-II respectively indicate the number of grid lines over $0 < x < x_e$, $0 < y < \delta_{steady}(x)$, and $\delta_{steady}(x) < y < 1$ for the interface location at $t = 0$. These numbers undergo minor changes as one marches forward in time in integer multiples of a time step Δt. We

consider two different sufficiently refined choices of grid, viz. grid-I and grid-II, for computing the unsteady results in Fig. 9. For these grids I and II, we have: $(n_i \times n_{j|L} \times n_{j|V})_I \times \Delta t = (30 \times 30 \times 20) \times 2.5$ and $(n_i \times n_{j|L} \times n_{j|V})_{II} \times \Delta t = (50 \times 50 \times 30) \times 5$. For these two refined grids, the combined sum of truncation and round off errors are minimized to a plateau level and the solutions in Fig. 9 are seen to be grid independent to within 1–2%. For a technical estimate of total discretization error – section 3.10 in Ferziger and Peric [37] is used for estimating the error on a representative flow variable, say film thickness in Fig. 9. This estimate leads to an approximate total error to be within 3%. The error in other converged flow variables for this representative flow situation was found to be of the same order of magnitude (within 2-5 %).

Computational Algorithm Outline

In the computational approach, at any instance of time t, the liquid domain and the vapor domain in Figs. 8a-8b are solved separately after a tentative guess of interfacial location δ. The liquid domain is solved subject to stress boundary conditions (namely shear stress τ^i and pressure p^i in Fig. 8a) and the vapor domain is solved subject to the velocity boundary condition (u_2^i and v_2^i in Fig. 8b). The grid details are given in Liang [38]. The temperature boundary condition at the interface viz. values of θ_1^i and θ_2^i are determined by the saturation condition in Eq. (9) – which, for all current purposes, equal known temperatures $\theta_s(0)$. In this approach, the five guesses of $\{u_2^i, v_2^i, \tau_1^i, p_1^i, \delta\}$ are equivalent to the five guesses of $\{u_2^i, v_2^i, u_{1s}^i, v_{1s}^i, \delta\}$ where, $\{\tau_1^i, p_1^i\}$ are replaced, in Fig. 8a, by $\{u_{1s}^i, v_{1s}^i\}$. The $\{u_{1s}^i, v_{1s}^i\}$ are liquid velocities computed on the shifted interface that is approximately one cell above the actual interface and adjusting these values are equivalent to making adjustments on the interfacial stresses $\{\tau_1^i, p_1^i\}$. These five

guesses are iteratively updated with the help of five interfacial conditions, viz. two from tangential and normal stress conditions (Eq. (4) and Eq. (5)), two from interface mass balance (Eq. (8)), and one from continuity of tangential velocity (Eq. (3)).

Since the liquid flow in Fig. 8a is solvable as a "parabolic" problem for a given $\{\delta, \tau_1^i, p_1^i\}$ and the vapor flow in Fig. 8b is solvable as a "parabolic" problem for $\{\delta, u_2^i, v_2^i\}$, the question is what *overall* boundary conditions for the control volume are needed, or can be imposed, to deterministically predict these five variable $\{\delta, \tau_1^i, p_1^i, u_2^i, v_2^i\}$ at all times $t > 0$ if the flow condition at some $t = 0$ were known. To begin with, we do not *assume* the structure of the governing equations for these complex problems as the physics of the flow suggests that at least, for shear driven flows, it is possible that unsteady exit condition imposition of the type given in Eq. (15) may be feasible. To investigate this issue, the unsteady annular/stratified problems (for gravity and shear driven flows) are solved under "specified" exit conditions in formulation [B]. A more detailed algorithm for above prescribed outline is given in the Appendix A-2.

1-D Approach

The convergence, grid independence, and accuracy of the ODE solver are well known and well tested as a Matlab solver (from The MathWorks, Inc., MA) was used. Also, the agreements between the 1-D steady solutions and the 2-D steady solutions are shown in Fig. 10a and 10b. Fig. 10a is for a gravity driven flow in a vertical channel and Fig. 10b is for a shear driven flow in a horizontal/0g channel. Clearly, because of the asymmetry of the channel flow, the 1-D solution depends more significantly on the reasonableness of the choice for the vapor profile. This is why, in Fig. 10b, the 1-D simulation result is less accurate than the 2-D simulation in predicting the film thickness variation. Over the length reported in Fig. 10b, the

simulation results for a horizontal channel and 0g channel flows are same except for hydrostatic variations in the condensate pressure. However, at large downstream distances accessible by the current 1-D approach, we find (see [35]) that the transverse gravity component associated with the horizontal channel flows makes the flow quite different than the 0g channel flow.

5. COMPUTATIONAL RESULTS AND DISCUSSIONS

5.1 Key 1-D/2-D Results on Shear Driven and Gravity Driven Internal Condensing Flows

Besides the corrected version of the 2-D computations, a recent and independent 1-D analysis [35] has established that, in spite of singularity at the entrance (x = 0), these steady equations of internal condensing flows have a unique annular steady solution, and that solution does not need exit-condition prescription (i.e. parabolic boundary conditions suffice). This is a correction on our earlier reported 2-D results. The error in our earlier computational results ([30]-[34]) suggested that there were multiple steady solutions as multiple *steady* exit condition impositions were possible. The claim of existence of multiple strictly steady solutions was wrong because the computations used in that previous analysis did not satisfy one of the steady interface conditions accurately. However, new results dealing with quasi-steady solutions that are reported in section 5.2 below seem to suggest that the earlier reported multiple steady solutions correspond to quasi-steady solution under impositions of quasi-steady exit conditions.

Fig. 10a (for gravity driven flows) and Fig. 10b (for shear driven flows) compare the unique steady solutions of the strictly steady governing equations obtained by the 1-D [35] and the 2-D techniques under parabolic boundary conditions for a partially condensing flow inside a channel. The 1-D computational results shown in Figs. 11a-11b for in-tube (vertical and 0g situations) condensing flows of FC-72 vapor are also representative of in-channel flows and

indicate remarkable differences between gravity and shear driven flows with regard to the velocity profiles and film thickness. It can be seen from Fig. 11a that, for all else remaining the same, shear driven flows have much thicker condensate and, hence, much lower heat transfer rates (which is typically inversely proportional to film thickness) and interfacial mass transfer rates. The condensate velocity profile for gravity driven flow in Fig. 11a is parabolic in shape with nearly zero slope at the interface (the condensate does not need shear for its motion as in the Nusselt [6] problem) while the one for the shear driven flow is linear (which provides adequate shear for condensate motion).

For the prescribed temperature ($T_w(x)$ = constant) thermal boundary condition considered here, as shown in Fig. 11b, the pressure variations for gravity driven flows often amount to a pressure rise where as a small pressure drop is associated with shear driven 0g flows. It should be noted that the actual pressure difference that is realized needs to account for two competing effects: (i) a pressure rise needed for decelerating the vapor in order to lose mass to the condensate, and (ii) a pressure drop needed to overcome interfacial shear. For the gravity driven flow case in Fig. 10a, it is the vapor deceleration effect that dominates and for the shear driven case in Fig. 10b, it is the interfacial shear effect that *slightly* exceeds the deceleration effects. For all the steady and the unsteady simulation results reported here, interfacial mass transfer rates were very important as the interfacial mass and energy balances played a critical role. However, on the right side of the interfacial pressure condition in Eq. (4), surface tension effects (because of the straight channel geometry and low curvature waves) and the mass transfer rate effects were found to be unimportant – i.e. $p_1^i \approx p_2^i$ was a valid approximation – because the sum of these two terms contributed less than 5% to the value of the right side of Eq. (4). As a result, the solutions were nearly the same whether or not these terms were retained on the right

side. The insignificance of the Marangoni term on the right side of Eq. (5) has already been demonstrated in Liang et al. [32].

Several steady parabolic governing equations' solutions were obtained by the 1-D and the 2-D methods over the following parameter range:

$$900 \leq Re_{in} \leq 22000$$

$$0.0036 \leq Ja/Pr_1 \leq 0.0212$$

$$3.2E\text{-}4 \leq \rho_2/\rho_1 \leq 0.03 \qquad (17)$$

$$0.0113 \leq \mu_2/\mu_1 \leq 0.06$$

$$57000 \leq G_p \leq 4{,}840{,}000.$$

where $Re_{in} \equiv \rho_2 UD/\mu_2$, $G_p \equiv Fr^{-1}_x * Re_{in}^2 \equiv (\rho_2^2 g_x D_h^3) / \mu_2^2$, and $Ja/Pr_1 \equiv \Delta T.k_1/h_{fg}.\mu_1$. These results have been further synthesized and correlated in [35].

Based on the recognition of differences between gravity and shear driven flows, and computational efficiency of the 1-D tool over the 2-D tool, the 1-D tool has been used to demarcate zones (see Fig. 12) which identify gravity driven, shear driven, and the intermediary "mixed" driven region of annular/stratified flows in a 3-D parameter space (see [35]) defined by $\{x, Re_{in}, G_p\}$ while the remaining non-dimensional parameters remain fixed. Figure 12 shows, for varying values of gravitational acceleration g_x (or its non-dimensional value $G_p \equiv (\rho_2^2 g_x D_h^3) / \mu_2^2$), the resulting division of this parameter space for the in-tube cases (as shown in [35] if channel gap $h \approx D$ then the in-tube results also approximate the channel flow results). This parameter space division has been discussed in detail in [35].

5.2 Computational Results for Internal Condensing Shear Driven Flows for Different Unsteady Elliptic Boundary Condition Impositions

5.2.1 Ellipticity of the unsteady equations:

As discussed in section 2, the solutions to the unsteady equations of internal condensing shear driven flows are sought to assess the physics of the problem. For the unsteady flow, under steady parabolic boundary conditions (of steady inlet mass flow rate, steady condensing surface temperature, and steady inlet pressure) and an unsteady exit condition specification of $\dot{\bar{M}}_{L-e}(t)$ in Eq. (15) as in Fig. 2a, it is found that there is an unsteady solution whose unsteady film-thickness response is shown in Fig. 2b. This unsteady exit condition imposition (for steady parabolic boundary conditions) was computationally found to be feasible for the shear driven case and not feasible for the gravity driven (and dominated) flow cases. For gravity dominated flow cases, the film thickness profile, for $T_w(x)$ = constant cases considered in this study, is found to be same as in the Nusselt solution [6] regardless of the inlet mass-flow rate. This means that the purely elliptic behavior of the unsteady annular/stratified flows as exhibited in Figs. 2a-2b is limited to the shear driven zone in the parameter space of Fig. 12 and that the unsteady equations are strictly parabolic in the far right gravity dominated zone of Fig. 12. The steady and unsteady shear driven flows considered here are for 0g and horizontal channel flows. It has been observed that, for the relatively small condenser length involving partially condensing flows investigated, the shear driven flows for 0g (i.e. $g_x = 0$ and $g_y = 0$ in Fig. 1) are approximately the same as the shear driven horizontal channel flows with transverse gravity (i.e. $g_x = 0$ and $g_y \neq 0$ in Fig. 1). Therefore the computational results shown in this paper for 0g are also applicable for partially condensing horizontal channel flows. However, in a future

paper, we show that if the length of the condenser is long and the condensate is sufficiently thick, the 0g flows are not the same as the horizontal channel flows ($g_y \neq 0$).

Although the unsteady imposition in Fig. 2a alone is reported here, several non-periodic finite duration unsteady impositions (not shown) were implemented and they led to accurate unsteady solutions in the annular regime.

It should be further noted that unsteady solutions for the unsteady governing equations are possible without specifying the exit conditions (for example, by using parabolic exit condition formulation [A] leading to Eq. (14)) provided there are sources of unsteadiness either in the parabolic boundary conditions or in the initial conditions (see [30]-[34]).

5.2.2 Quasi-steady solutions as a result of "ellipticity" of the unsteady equations:

Figure 3 shows three different time history prescriptions for non-dimensional exit liquid mass flow rate $\dot{\hat{M}}_{L-e}(t)$ in Eq. (15). The red curve is associated with a *constant steady* value associated with the "natural" steady exit condition i.e. $\dot{\hat{M}}_{L-e}(t) = \dot{\hat{M}}_{L-e}|_{Na} \approx 0.116$ found from the unique steady solution associated with the steady shear driven parabolic problem considered in Fig. 10b. The blue curve is associated with a suitable time-periodic prescription ($\dot{\hat{M}}_{L-e}(t) = \dot{\hat{M}}_{L-e}|_{on\text{-}off}$) that is obtained by an "on-off" procedure (see Fig. 3 and definitions of time period $T_p = \tau_c + \tau_r$) in which, during the "on" time interval 'τ_c,' the exit condition in Eq. (15) is externally imposed whereas during the "off" time interval 'τ_r,' the "natural" exit condition through formulation [A] and Eq. (14) is imposed and the solution relaxes towards the "natural" solution. These values of τ_c and τ_r are so chosen that the resulting exit condition imposition in Fig. 3 as well as the associated solution in Fig. 4 are both time-periodic with mean values that are steady. The periodic on-off imposition in Fig. 3 (the blue curve) has an "off-natural" mean

($\dot{\hat{M}}_{L-e}|_{\text{on-off mean}} \approx 0.123$) above the "natural" value. This shows that the exit liquid mass flow rate can, in principle, be controlled such that during the *on* portion of the control, liquid exit mass flow rate is on the higher side of the "natural" and during the *off* portion of the prescription, the flow bounces back (with overshoot) to seek its "natural" exit condition. The green curve is an attempt to prescribe a *constant steady* exit condition ($\dot{\hat{M}}_{L-e}(t) = \dot{\hat{M}}_{L-e}|_{\text{constant}}$) at an "off-natural" mean ($\dot{\hat{M}}_{L-e}|_{\text{constant}} \approx 0.127$). The non-natural constant steady imposition in Fig. 3 (green curve) is only representative as many other non-natural constant imposition were also tested and they lead to a response similar to the one reported to this curve. Figure 13 shows another time-periodic prescription with an "off-natural" mean (dashed curve) that is slightly *below* the "natural" value. Figure 4 and Fig.14 show the respective response of the film thickness to the exit liquid mass flow rate prescriptions depicted in Fig. 3 and Fig. 13. For the *constant steady* prescription with the mean at the self-sought "natural" value of exit liquid mass flow rate, film thickness attains a steady value in time - the same (within computational error of 3%) as the film thickness obtained by solving the steady equations under parabolic boundary condition. For the time periodic quasi-steady exit condition prescription of Fig. 3, film thickness (shown by the blue curve in Fig.4) keeps on oscillating, for all times $t > 0$, in a narrow band which has a steady mean and thicknesses that are less than the one associated with the "natural" steady solutions given by the red curve. This new quasi-steady solution (steady-in-the-mean) effectively makes the condensing flow behave as if it has multiple quasi-steady solutions for multiple and suitable quasi-steady exit condition impositions. Similar but much smaller impact of the exit condition imposition in Fig. 13 leads to the film thickness response in Fig. 14 – which exhibits an oscillation in a band (the dashed curves) slightly above the strictly steady "natural" solution. Note, for the kind of imposed quasi-steady exit conditions in Fig. 3 and

Fig.13 (which has a "non-natural" mean and superposed periodic fluctuations), new quasi-steady flows are achieved with different steady-in-the-mean values of the exit liquid mass flow rate, exit vapor mass flow rate, and the rest of flow variables in the interior of the flow domain. As shown in Fig. 15, relative to the strictly steady "natural" flow, the quasi-steady flows show significant differences (about 7% for the total heat load) in the heat transfer rates $q''_w(x)$ and Nu_x values where

$$q''_w(x) \equiv h_x(\Delta T) \approx (k_l \, \Delta T) / (h \, \delta(x))$$

$$Nu_x \equiv h_x \, h / k_l \approx 1 / \delta(x) \tag{18}$$

Note that for the *constant steady* prescriptions of "natural" steady exit condition and for a time periodic quasi-steady prescription at an "off-natural" mean, the flows continue to remain in the annular/stratified flow regime for all times $t > 0$ (see Figs. 3-4). However, for a *constant steady* "off-natural" prescription given by the green curve in Fig. 3, the flow cannot remain steady as the corresponding solution for this exit condition imposition in Fig. 3 is the green curve in Fig. 4 - which shows that the solution is not possible after a certain time t^* (≈ 1170 in Fig. 4). Note that, in Fig. 4, the waves start appearing on the interface (green curve) before the annular/stratified solution becomes impossible for $t \geq t^*$. This is consistent with the result in Fig.16a where the "natural" steady solution (red curve in Fig. 4) is found to be stable to small initial disturbances and with the result in Fig. 6b where the "non-natural" strictly steady solution (the green curve in Fig. 4) is unstable to small initial disturbances and cannot be realized in practice. It is possible that the condensers exposed to "non-natural" concurrent prescription of steady inlet and exit conditions (as is the case with the red curve in Fig. 4) correspond to conditions for which appearance of self-sustained oscillations involving annular and non-annular regimes are possible. Some of this type of elliptic-sensitive issues may also be useful

and relevant for proper understanding of self-sustained oscillations in the condensing flow experiments of Wedekind and Bhatt [39]-[42].

It should be further noted that even when the film thickness in Fig. 4 significantly decreases or film thickness in Fig. 14 slightly increases under quasi-steady imposition of exit condition in Fig. 3, the mean pressure increase or decrease at the exit needed to decelerate or accelerate the vapor (see Figs. 17a-17b) is small for this partially condensing case. It is clear that the type of exit condition imposition in Fig. 13 is difficult and very small mean film thickness increases are observed in Fig. 14.

Because of the computationally intensive nature of finding the right quasi-steady imposition (as in Fig. 3 and Fig. 13) and then obtaining the associated quasi-steady solutions (as in Fig. 4 and Fig. 14), only a very limited number of other quasi-steady impositions (about 4 other cases) of this nature have been computationally investigated so far.

If a larger length condenser was considered with computational ability to simulate non-annular flows, it is possible that this type of quasi-steady response for "non-natural" quasi-steady exit condition imposition may also involve flow morphology changes because of a shift in flow regime boundaries. This important physics cannot be captured by our current simulation tool that can only handle annular/stratified morphology.

For the impositions in Fig. 3 and Fig. 13, Figs. 18a – 18b respectively show the time histories for the non-dimensional values of net mechanical energy input rate $\dot{W}_{\mathrm{Mech-in}}$ (see definition in Eq. (A.11) in the Appendix A.3) into the condenser control volume. Fig. 18a shows that the mean value of the net mechanical energy for the new quasi-steady solution (blue curve) is lower than the "natural" value whereas, in Fig. 18b, it is slightly higher than the natural value. Fig. 19 shows how the admissible range of time-averaged values of $\dot{W}_{\mathrm{Mech-in}}$ get affected by

the different mean quasi-steady exit-conditions imposition. It is possible that even though annular/stratified quasi-steady solutions exist for such *on-off* prescriptions in the vicinity of the "natural" (bounded by the two red lines); the range of available values may be limited for the realization of annular/stratified flow regimes. The reduction and increase, with respect to the "natural" parabolic value, in these overall time-averaged values are associated, for the considered case of constant condensing-surface temperature, with changes in total interface energy transfer rate $\dot{D}_{\Sigma}$ shown in Fig. 20. The interface energy transfer rate $\dot{D}_{\Sigma}$ is defined in (A.13) of the Appendix A.3 and is made up of pressure and kinetic energy transfer rates across the interface. The fact that $\dot{D}_{\Sigma}$ increases on either side of the "natural" exit condition is indicative of the energetic resistance at the interface to consume energy at non-natural rates. This energy response is limited to the assumed/ considered case of constant condensing surface temperature and explains the computationally observed "elasticity" with regard to "non-natural" quasi-steady exit condition imposition. By "elasticity," it is meant that during the "off" portion of the elliptic imposition, the quasi steady solutions in Fig. 4 and Fig. 14 tend to bounce back to the respective "natural" solutions with an overshoot.

5.2.3. Continuity of elliptic response with respect to the unsteady "elliptic/non-natural" exit condition data

The issue that needs understanding is: in what sense the natural constant exit condition $\dot{\hat{M}}_{L-e}(t) \equiv \dot{\hat{M}}_{L-e|Na}$ (red curve in Fig. 3) is "close" to the time-periodic imposition $\dot{\hat{M}}_{L-e}(t) \equiv \dot{\hat{M}}_{L-e|on-off\,periodic}$ (blue curve in Fig. 3) such that the resulting solution is close to the natural solution (as measuered by the proximity of the mean time-averaged values of the consumed mechanical energy '$\dot{W}_{Mech-in}$' shown in Fig. 19)? The analogous question is in what sense the *constant steady* off-natural prescription $\dot{\hat{M}}_{L-e}(t) \equiv \dot{\hat{M}}_{L-e} * \neq \dot{\hat{M}}_{L-e|Na}$ (green curve in Fig. 3) is

"far" from the natural constant exit condition $\dot{\hat{M}}_{L-e}(t) \equiv \dot{\hat{M}}_{L-e|Na}$ (red curve in Fig. 3) such that the average of the constantly decreasing values of the consumed mechanical energy '$\dot{W}_{Mech-in}$' as shown in Fig.18a becomes progressively farther from the "natural" value as the time duration of observation increases? Based on the above discussed response of the flow to these exit condition impositions, it appears that one suitable measure of the "distance" between an arbitary imposition $\dot{\hat{M}}_{L-e}(t)$ and the constant natural control $\dot{\hat{M}}_{L-e|Na}$ – which is the same as the magnitude or "norm" of the difference function $\dot{\hat{M}}_{L-e|Diff}(t) \equiv (\dot{\hat{M}}_{L-e}(t) - \dot{\hat{M}}_{L-e|Na})$ – can be defined as:

$$\text{dist}\,(\dot{\hat{M}}_{L-e}(t), \dot{\hat{M}}_{L-e|Na}) \equiv \left\| \dot{\hat{M}}_{L-e|Diff}(t) \right\|$$

$$\equiv \left| \int_{t*}^{t*+T} \left\{ \dot{\hat{M}}_{L-e}(t) - \dot{\hat{M}}_{L-e|Na} \right\} dt \right| + \left| \int_{t*}^{t*+T} \left(\frac{d\dot{\hat{M}}_{L-e}(t)}{d\,t} - 0 \right) dt \right|,$$

$$\equiv \left| \int_{t*}^{t*+T} \left\{ \dot{\hat{M}}_{L-e|Diff}(t) \right\} dt \right| + \left| \int_{t*}^{t*+T} \left(\frac{d\dot{\hat{M}}_{L-e|Diff}(t)}{d\,t} \right) dt \right|, \quad (19)$$

where $0 \le t^* \le t \le t^* + T$ is *time interval of interest*. For the *constant steady* off-natural or non-periodic exit condition impositions, the time period of interest is typically one in which $t^* = 0$ and T is sufficiently large. However, for time-periodic prescription with time period T_p, it is found that the resulting solution is (see Figs. 3 and 4) eventually (after some time $t > t^* > 0$) also time periodic with the same time period T_p. Therefore, it is clear that the *time duration of interest* in Eq. (19) for the quasi-steady case should be the *finite* time duration $[t^*, t^*+T_p]$ associated with the largest period T_p. With this understanding, the following can be concluded for different exit condition spedifications:

$$\text{dist}\,(\dot{\hat{M}}_{L-e|Na}, \dot{\hat{M}}_{L-e|Na}) = 0$$

$$\text{dist}\,(\dot{\hat{M}}_{L-e\,*}, \dot{\hat{M}}_{L-e|Na}) = \left| (\dot{\hat{M}}_{L-e\,*} - \dot{\hat{M}}_{L-e|Na}) \right| * T \quad (20)$$

$$\text{dist}\,(\dot{\hat{M}}_{\text{L-e|on-off periodic}}, \dot{\hat{M}}_{\text{L-e|Na}}) = \left|(\dot{\hat{M}}_{\text{L-e|on-off periodic|mean}} - \dot{\hat{M}}_{\text{L-e|Na}})\right| * T_p \,.$$

In Eq. (20) above $\dot{\hat{M}}_{\text{L-e|on-off periodic|mean}}$ refers to the time-averaged mean over the period T_P and T refers to an sufficiently long time interval. Since T is typically large and time period T_p is finite in Eq. (20), it is seen from the second equality of Eq. (20) that the "off-natural" *constant steady* specification is "far" (the distance value is large) from the natural control whereas the "periodic" specification is "close" to the "natural" prescription since the distance value is small provided the mean of the *periodic* specification (purple curve in Fig. 3) is close to the $\dot{\hat{M}}_{\text{L-e|Na}}$ (red curve in Fig. 3).

Thus, the fact that there exist "quasi-steady" solutions near the "natural" steady solution for the exit condition impositions that are "close" (in the sense of Eq. (20) above and in terms of nearby energy consumption rates in Fig. 19) to the "natural" exit condition is merely a statement that the "elliptic" problem for the unsteady shear driven flow is "well-posed" and exhibits *continuity* with respect to exit condition boundary data (i.e., the data on the right side of Eq. (14)). By *continuity* with respect to exit condition data one means that small changes in the data (in the sense of Eq. (19)), cause small changes in the solution.

5.3 Summarized Computaional Results

As discussed earlier, the flow parameters shift the flow in Fig. 12 from a shear driven regime to a gravity dominated regime (see [35]), the unsteady governing equations' character shifts gradually from one of "elliptic behavior" in the shear driven region of Fig. 12 to the purely "parabolic" behavior in the gravity dominated zone of Fig. 12. The associated steady equations always remain "parabolic" – though the strength of the "parabolic" attractor (see definition in [14]) changes. In other words, we are saying that the traditional characterization of governing

equations being parabolic, elliptic, or hyperbolic for the entire parameter space of any linear or a non-linear problem does not hold for characterizing the behavior of these complex phase-change flow problems. Instead, it is proposed that the steady and unsteady equations for internal condensing flows should not be characterized in the traditional way. Rather, it should be understood that the character of these equations change gradually –as marked in Fig. 12 - as we move in the parameter space and the flow undergoes transition between pure shear (0g) and gravity dominated (Nusselt) catagories discussed in the earlier sections. This nuance in understanding the character of the internal condensing flow equations is new for condensing flows but is not new in fluid dynamics. For example, the gas dynamics Tricomi equation (see chapter 26 of [43]) undergoes a change in character from "elliptic" to "hyperbolic" as one moves in the parameter space of Mach number (Ma) from the sub-sonic regime (Ma < 1) to the super-sonic regime (Ma > 1).

6. EXPERIMENTAL INVESTIGATION OF A SHEAR DRIVEN FLOW AND ITS QUALITATIVE COMPARISONS WITH THE COMPUTATIONAL PROBLEM/RESULTS

6.1 Physical Arrangement of the Experimental System

To study the experimental verification of the computational results regarding unsteady/quasi-steady condensing flows' "ellipticity," the 2-D flow in Fig. 1 is approximated by the 3-D situation of Fig. 5. This involves fully condensing flows of FC-72 vapor in a rectangular cross-section (2 mm gap height and 15 mm wide) duct of 1m length. Its horizontal condensing surface area (15 mm x 1 m) is the top of a 12.7 mm thick stainless plate. The channel's top and side surfaces are made of a thick transparent material (lexan), which is covered with an

insulation that can be removed to allow flow visualization. The test-section shown in Fig. 5 is used in the flow loop facility depicted in Fig. 21. For the fully condensing flow results reported here, the test-section is horizontal and the auxiliary condenser section of the flow loop in Fig. 21 is not used as the valve V is closed. Furthermore, the controllable displacement pump P_2 is also not used.

The condensing surface's "cooling approach" (which defines its thermal boundary condition) consists of:

(i) Coolant water flows under the thick condensing plate at a controlled steady flow rate and a nearly uniform temperature T_{res}.

(ii) A thermo-electric cooler underneath the heat-flux meter (HFX-1 on top of a thermo-electric cooler TEC-1 in Fig. 4) cools the condensing-surface approximately over 50 cm $\leq x \leq$ 60 cm in a fashion that keeps the mean surface temperature fixed at an average and approximate constant value. This is done with the help of feedback control of TEC-1 through a thermocouple which holds the local temperature at x = 58.5 cm fixed.

(iii) A thermo-electric cooler (TEC-2 in Fig. 13) underneath the condensing surface cools an approximate region of 80 cm $\leq x \leq$ 1 m. The thermo-electric cooler TEC2 is operated at a fixed maximum driving voltage (17.5 Volt). The thermo-electric cooler lowers the condensing surface temperature (for the reported full condensation cases) past the onset of bubbly regime – thereby ensuring that the subsequent flow morphology changes rapidly to an all liquid flow over this zone.

The above described "cooling approach" defines the following thermal boundary condition for the condensing surface:

(a) At all locations other than the ones associated with HFX-1/ TEC-1 and TEC-2 in Fig. 5, let R''_{slab} and R''_{conv} denote the respective thermal resistances – on per unit area basis – that model steady or quasi-steady heat flow through the slab and the water flow (at temp T_{res}). Furthermore, if h_{ext} is given by $1 / h_{ext} \equiv R''_{slab} + R''_{conv}$, then the thermal boundary condition at these "x" locations are of the convection type (Eq. (12)) and is given by (for $R''_{slab} << R''_{conv}$):

$$-k_1 \left.\frac{\partial T_1}{\partial y}\right|_{y=0} = h_{ext}[T_1(x, 0, t) - T_{res}], \tag{21}$$

where $0 \le x \le 50$ cm or 60 cm $\le x \le 80$ cm. For non-negligible R''_{slab}, the model above is best replaced by a conjugate analysis which correctly models the thermal inertia (effects of specific heat and the volume of the slab) issues for the transient heat flow through the slab.

(b) At the thermo-electric cooler TEC-1 and heat flux meter HFX-1 location, a nearly steady temperature boundary condition of:

$$T_1(x, 0, t) \approx 58.5\ ^\circ C \quad \text{for } 50 \text{ cm} \le x \le 60 \text{ cm} \tag{22}$$

can be assumed since the surface temperature variation in this region was measured to be small.

(c) If one respectively denotes the bottom and top temperatures of the thermo-electric cooler (TEC-2 in Fig. 5 and Fig. 7) by T_{bot} and T_{top}, and the area-averaged heat flux by $\bar{q}''$, then the constant voltage operation of TEC-2 defines a known function $\tilde{f}_{TEC}$ such that

$$\Delta T_{TEC} \equiv T_{bot} - T_{top} = \tilde{f}_{TEC}(\bar{q}''). \tag{23}$$

This non-linear function $\tilde{f}_{TEC}$ is experimentally known and follows the trends implied by the manufacturer's specification ([44]). If the per unit area thermal resistance between the top of

the TEC-2 and the condensing-surface is denoted by R''_{top}, and the thermal resistance between the bottom of TEC-2 and water flow is denoted by R''_{bot}; then the thermal boundary condition over the TEC-2, under quasi-steady conditions, is well approximated by:

$$[T_1(x,0,t) - T_{res}] = \bar{q}''\left(R''_{bot} + R''_{top}\right) - \tilde{f}_{TEC}(\bar{q}'') \qquad (24)$$

for 80 cm $\leq x \leq$ 1m, where $\bar{q}'' \equiv -k_1 \frac{\partial T_1}{\partial y}|_{y=0}$ is evaluated at a suitable x-location. For truly unsteady conditions and non-negligible conductive thermal resistance contributions to R''_{top} and R''_{bot}, the model above is best replaced by a conjugate analysis which correctly models the thermal inertia (effects of specific heat and the volume of the slab) issues for the transient conduction heat flow.

Although, both computations and experiments deal with purely shear driven horizontal channel flows, the condensing surface thermal boundary condition for the experiments – as given by Eqs. (21) – (24) above – are not the same as the one assumed for the theory (i.e. $T_1(x,0,t) = T_w(x) = \text{constant}$). The computational simulations for the above experimental thermal boundary condition and the results' comparisons with experiments are part of a forthcoming paper.

6.2 Experimental Procedure and Observations

6.2.1 Procedure and observations for the first quasi-steady realization (for $t \leq t_0$) in Figs. 6a – 6c

For the reported cases, the valve V in Fig. 21 is closed and the pump P_2 in Fig. 21 is removed and eventually attained steady operating values of $\dot{M}_{in}$, p_{in}, and $T_w(x)|_1$ are such that the point of full condensation is within the test-section and the "Collection Chamber" in Fig. 21 is filled with liquid. This procedure involves: (i) removing the compressor from the flow loop by

keeping the compressor running at a very low speed with the bypass valve (V_{BP} in Fig. 21) fully open, (ii) holding fixed the Coriolis mass flow meter F_C (in Fig. 21) reading of the mass flow rate $\dot{M}_{in}$ by a PID control of the evaporator heater, (iii) fixing the evaporator bath temperature T_{bath}, (iv) steadying condensing surface temperature T_W (x) through a control that achieves a steady coolant flow rate for the water that flows underneath the condensing surface and maintains a nearly uniform temperature, and (v) using the controllable displacement pump P_l, through a PID control, to hold the exit pressure fixed at $p_{exit} = p_{exit}^*$. This procedure allows the inlet pressure p_{in} to freely seek its natural steady value $p_{in}|_{Na}$.

As depicted in Fig. 3, it is found that the morphology of the fully condensing flow cases (depending on $\dot{M}_{in}$ and ΔT values) were found to vary from: (i) cases where the flows are annular/stratified almost up to the point of full condensation (and only a small amount of "plug/slug" flows are seen near the point of full condensation) to (ii) cases where the flows are significantly non-annular over approximately half of the test-section.

It was experimentally observed that even though fully condensing flows exhibit different flow regimes (annular, non-annular, plug-slug, bubbly, etc.) inside the test section, the observed transition locations (schematically shown in Fig. 5) by $x_{Plug/Slug}$, $x_{Bubbly,}$ etc. were experimentally found to be robust and repeatable. Along with this, the mean measured values of flow variables in Figs. 4 – 5 were also found to be repeatable for $t \leq t_0$. In Figs. 4-5, the mean values of $\dot{M}_{in}$, p_{in}, p_{exit}^*, Δp, etc. are accurate to within 5%, the temperatures are accurate to within ± 1^{o}C, but the absolute values of the mean heat-flux $q''_{W|HFX-1}$ is not representative (because the heat flux-meter was not calibrated) - though the relative magnitude of changes in $q''_{W|HFX-1}$ (i.e. $\Delta q''_{W|HFX-1}/q''_{W|HFX-1}$) are representative and correct to within 5%. Therefore the results reliably tell us that one can achieve repeatable and stable "natural" fully condensing flows if the flow

loop is designed in a way that all the "parabolic" boundary condition impositions are well controlled and repeatable and, additionally, if the flow loops design allows the flow to seek its own pressure condition at the inlet ($p_{in}|_{Na}$).

However, as discussed next, when an unsteady "elliptic" boundary condition is imposed for shear driven flows, not only do the flow regime transition boundary locations (marked $x_{Plug/Slug}$, $x_{Bubbly,}$ etc. in the schematic of Fig. 5) change in time but, also, the mean values of the flow variables changes in time.

6.2.2 Procedure for imposition of an unsteady/quasi-steady "elliptic" pressure boundary condition at the inlet

To begin with, the quasi-steady flow was "natural" for $t \leq t_0$ with the inlet mass flow rate $\dot{M}_{in}$, natural inlet pressure $p_{in|Na-1}$, fixed exit pressure p_{exit}^{*} , natural pressure difference Δp, and the heat flux $q''_{W|HFX-1}$ values were as shown in Figs 6a-b. The steady condensing - surface temperature variation $T_W(x)_{-1}$ was as in Fig. 7.

The subsequent ($t \geq t_0$) imposition of unsteady "elliptic" boundary condition procedure involves:

Use the flow controls to continue to hold fixed the earlier (for $t \leq t_0$) values of mean exit pressure p_{exit}^{*}, inlet mass flow rate $\dot{M}_{in}$, bath temperature T_{bath} (to stabilize boiler pressure variations during compressor aided imposition of inlet pressure), the coolant flow rate, and the coolant temperature for $t \geq t_0$ while increasing the inlet pressure $p_{in}(t)$ in time (over $t_0 \leq t \leq t_0 + 10$) with the help of the compressor by increasing the speed of the compressor and partly closing the bypass valve (V_{BP} in Fig. 21) to a new value $p_{in}|_2 > p_{in-1}$. Because the steady cooling approach in the experiments allows time variations in the values of condensing surface temperature $T_W(x)$, it is found that this unsteady "elliptic" imposition causes the shear driven

flow to respond unsteadily – exhibiting thermal transients (see Fig. 6c) before a final quasi-steady state is reached at $t > t_0 + 65$. This final steady state is another "quasi-steady parabolic" state associated with the new condensing surface temperature distribution $T_w(x)_{-2}$ in Fig. 7.

These results in Figs. 6-7 show that the mean inlet pressure has been successfully increased with the help of the compressor induced fluctuations while the exit pressure has remained constant. Concurrent to this imposition, at the end of the 10 minutes long hydrodynamic transient (during which the unsteady imposition occurs), the pressure-difference Δp between the inlet and the exit increases and, as in the computational results, the mean film thickness of the wavy interface decreases in the annular/stratified region and this leads to significantly enhanced heat-transfer rates (see representative $q''|_{HFX\text{-}1}$ values in Fig. 6b). It should be noted that the significant enhancement in heat-transfer rate is there because an increase in Δp by 60 Pa is quite significant compared to the original pressure difference (about 275 Pa) for the annular stratified portion of the flow (see Fig. 6b).

6.2.3 The role of fluctuations in the experimentally observed elliptic sensitivity

This imposition of non-natural quasi-steady inlet pressure $p_{in}|_2$ and associated heat-transfer enhancements (which may yield a total heat transfer rate significantly above $\dot{M}_{in|mean} \cdot h_{fg}$ due to energy contained within the inlet vapor fluctuations being absorbed by the interface) are accompanied/enabled by the time-periodic fluctuations (which have been observed and are to be measured in the forthcoming experiments) $p'_{in}(t)$ in the inlet pressure and $\dot{M}'(t)$ in the inlet mass flow rate. This makes the total inlet pressure $p_{in}(t) = p_{in\text{-}2} + p'_{in}(t)$ and total mass flow rate $\dot{M}_{in}(t) = \dot{M}_{in|mean} + \dot{M}'(t)$). For the fluctuations accompanying the mean inlet pressure, the compressor provides a significant additional flow work "$\overline{\dot{M}'p'}/\rho_2 + \dot{M}_{in|mean} \cdot (p_{in|2} - p_{in|Na})/\rho_2$"

and an additional inlet enthalpy flux "$\overline{\dot{M}'p'}(1/\rho_2 + du_g/dp|_{p0})$" - where $u_g(p)$ is the specific internal energy of the gas phase at saturation temperature $T_{sat}(p)$. Since, eventually, the mean inlet pressure is what is experimentally imposed at a non-natural quasi-steady value, the inlet fluctuations that enabled the requisite changes in the mean value of the flow variables were self-selected by the flow so as to yield the requisite non-zero values for $\overline{\dot{M}'p'}$ $(\equiv \left\{\int_0^T \dot{M}'p' \cdot dt\right\}/T$, where T is much larger than the largest time-period) that appeared in the above described energy considerations. Because the thermal transients accompany the hydrodynamic transients (see Fig. 6c), the heat-transfer enhancements gradually become permanent as the new steady temperatures $T_w(x)|_2$ are reached. Unlike the computational cases where $T_w(x)$ was constant, the new quasi-steady flow at $t > t_0 + 65$ is another parabolic flow and it does not have the feature of elastic bounce-back between the two quasi-steady states – one associated with $t \leq t_0$ and the other with $t > t_0 + 65$. These two states can only be interchanged gradually with the help of thermal transients.

7. CONCLUSIONS

1. Simulation results show that there exists a unique steady "natural" solution of the strictly steady parabolic problem for the gravity and shear driven condensing flows. This result has been verified by two independent solution techniques namely 1-D and 2-D technique. This result has also been verified in the reported experiments. It is computationally shown that shear driven internal condensing flows are stable as long as the flow is free to self-select its exit condition.

2. Both 1-D and 2-D simulation results show remarkable and understandable differences between gravity driven and shear driven steady condensing flows.

3. 2-D computational results show that there could be multiple quasi-steady/unsteady solutions of the unsteady governing equations (which exhibit "elliptic sensitivity") for shear driven cases under different quasi-steady impositions of the elliptic boundary condition. This paper presents novel categorization of internal condensing flow behavior based on its elliptic sensitivity. It is shown that steady governing equations of shear driven internal condensing flow are "parabolic" while the unsteady equations are "elliptic." However, it is also found that the unsteady behavior remains "parabolic" (even under quasi-steady/unsteady fluctuations on the parabolic boundary conditions) for: (i) gravity dominated flows, and (ii) thermal boundary conditions which hold the wall heat-flux profile fixed.

4. The results presented in this paper suggest that one of the ways to realize repeatable partially or fully condensing shear driven flows is to use "elliptic sensitivity" to control the flows in a way that ensure desired repeatability of the condenser's performance.

5. Computational and experimental results presented in this paper show that shear driven internal condensing flows are sensitive to the nature of fluctuations present at the inlet/outlet boundaries and, in addition, the condenser response also depends on the method of cooling used.

ACKNOWLEDGMENT

Parts of this work were supported by NASA grant NNX10AJ59G and NSF grant NSF-CBET-1033591.

NOMENCLATURE

C_{pl} Specific heat of the liquid condensate, J/(kg-K)

D Inner diameter of tubular test-section, m

Fr_x	Froude number U^2/g_xL_c
Fr_y	Froude number U^2/g_yL_c
H	Channel gap, m
Ja	Condensate liquid Jakob number, $C_{p1}\cdot \Delta T / h_{fg}(p_{in})$
k_1	Conductivity of condensate liquid, W/(m-K)
L	Length of the test-section, m
L_C	Characteristic length, L_C = D (diameter) for tubes and L_C = h (gap height) for channels, m
$\dot{M}_{in}$	Vapor flow rate at test-section inlet, g/s or kg/s
$\dot{\dot{M}}_{L-e}(t)$	Non-dimensional liquid mass flow rate at exit
$\dot{\dot{M}}_{V-e}(t)$	Non-dimensional vapor mass flow rate at exit
$\dot{M}_L$	Liquid flow rate at test-section exit, g/s or kg/s
p_{in}	Pressure at the test-section inlet, kPa
p_{exit}	Pressure at the test-section exit, kPa
Pr_1	Condensate liquid Prandtl number, $\mu_1 C_{p1} / k_1$
p_{xP-i}	Test-section pressures at locations $x_P = x_{P-i}$ (i = 1, 2, …), kPa
$\dot{Q}_{total}$	Net heat rate out of the test-section, W
Re_{in}	Inlet vapor Reynolds number, $\rho_2 U L_c/\mu_2$
t	Non-dimensional time
t	Physical time, s
θ	Non-dimensional temperature
$T_{sat}(p)$	Saturation temperature at pressure p, ^oC
$\overline{T}_w$	Mean condensing surface temperature, ^oC
$T_w(x_P)$	Non-uniform steady condensing surface temperature at x_P, ^oC
U	Average inlet vapor velocity in the x-direction, m/s
u_f	Non-dimensional interfacial velocity in the x-direction

u_I	Physical velocity in the x-direction, m/s
v_I	Physical velocity in the y-direction, m/s
v	Non-dimensional velocity in the y-direction
$\dot{W}_{Mech-in}$	Non-dimensional mechanical energy input rate in to the control volume of the condenser.
x, y	Physical distances along and perpendicular to the condensing surface, m
x, y	Non-dimensional distances along and perpendicular to the condensing surface
ΔT	$T_{sat}(p) - \bar{T}_w$, ^oC
Δp	$p_{in} - p_{exit}$, kPa
Δ	Physical value of condensate thickness, m
δ	Non-dimensional value of condensate thickness
ρ_2	Density of vapor, kg/m^3
ρ_1	Density of liquid, kg/m^3
μ_2	Viscosity of vapor, kg/(m-s)
μ_1	Viscosity of liquid, kg/(m-s)
π_e	Non-dimensional exit pressure
ζ	Non-dimensional pressure gradient $d\pi/dx$
Φ_L	Viscous dissipation rate for the liquid domain
Φ_V	Viscous dissipation rate for the vapor domain

Subscripts

comp	Obtained from computations
E	Test-section exit
Expt	Obtained from experiments
I	I = 1 for liquid and I = 2 for vapor

In Test-section inlet

Na Natural exit condition

8. REFERENCES

1. Carey, V. P., 1992, *Liquid-Vapor Phase-Change Phenomena*, Series in Chemical and Mechanical Engineering, Hemisphere Publishing Corporation.
2. Delhaye, J. M., 1974, "Jump Conditions and Entropy Sources in Two-phase Systems; Local Instant Formulation," *International Journal of Multiphase Flow*, Vol. 1, pp. 395-409.
3. Faghri, A., 1995, *Heat Pipe Science and Technology*, Taylor and Francis, Washington D. C.
4. Faghri, A. and Y. Zhang, 2006, *Transport Phenomena in Multiphase Systems*, Elsevier Academic Press.
5. Begg, E., D. Khrustalev, and A. Faghri, 1999, "Complete Condensation of Forced Convection Two-Phase Flow in a Miniature Tube," Vol. 121, ASME Journal of Heat Transfer, pp. 904-915. Delhaye, J. M., 1974, "Jump Conditions and Entropy Sources in Two-phase Systems; Local Instant Formulation," *International Journal of Multiphase Flow*, Vol. 1, pp. 395-409.
6. Nusselt, W., 1916, "Die Oberflächenkondesation des Wasserdampfes," *Z. Ver. Dt. Ing.*, Vol. 60, No. 27, pp. 541-546.
7. Sparrow, E. M. and, J. L. Gregg, 1959, "A Boundary Layer Treatment of Laminar Film Condensation," ASME *Journal of. Heat Transfer*, Vol. 81, pp. 13-18.
8. Koh, J. C. Y., 1962, "Film Condensation in a Forced-Convection Boundary-Layer Flow," *International Journal of Heat Mass Transfer,* Vol. 5, pp. 941-954.
9. Rohsenow, W. M., 1956, "Heat Transfer and Temperature Distribution in Laminar Film Condensation," *Transactions ASME*, Vol. 78, pp. 1645-1648.
10. Chen, M. M., 1961, "An Analytical Study of Laminar Film Condensation: Part 1 Flat Plate," *Journal of Heat Transfer,* Vol. 83, pp. 48-54.
11. Dhir, V.K. and J. H. Lienhard, 1971, "Laminar Film Condensation on Plane and Axisymmetric Bodies in Non-uniform Gravity," *Journal of Heat Transfer*, Vol. 93, pp. 97-100.

12. Fujii, T. and H. Uehara, 1972, "Laminar Filmwise Condensation on a Vertical Surface," *Inernational Journal of Heat and Mass Transfer*, Vol. 15, pp. 217-233.
13. Phan, L. and A. Narain, "Non-linear Stability of the Classical Nusselt Problem of Film Condensation and Wave-Effects," ASME *Journal of Applied Mechanics*, Vol. 74, No.2, pp. 279-290, 2007.
14. Kulkarni, S. D., A. Narain, S. Mitra, and L. Phan, 2010, "Forced Flow of Vapor Condensing over a Horizontal Plate (Problem of Cess and Koh*) - Steady and Unsteady Solutions of the Full 2D Governing Equations," ASME *Journal of Heat Transfer*, Vol. 132 (10), 101502.
15. Labuntsov, D. A., 1957, "Heat Transfer in Film Condensation of Pure Steam on Vertical Surfaces and Horizontal Tubes," *Teploenergetica,* Vol. 4, 72. Also see (in Russian) Heat Transfer During Condensation of Steam on a Vertical Surface in Conditions of Turbulent Flow of a Condensate Film, *Inghenerno-Fizicheski Zhurnal*, 3, 3-12 (1960).
16. Kutateladze, S. S., 1963, *Fundamentals of Heat Transfer,* Academic Press, New York.
17. Gregorig, R., J. Ken, and K. Turek, 1974, "Improved Correlation of Film Condensation Data Based on a More Rigorous Application of Similarity Parameters," *Wärme-und Stoffübertragung*, Vol. 7, pp. 1-30.
18. Carpenter, F. G. and A. P. Colburn, 1951, "The Effect of Vapor Velocity on Condensation Inside Tubes," *Proceedings of the General Discussion of Heat Transfer,* The Institute of Mechanical Engineers and the ASME, pp. 20-26.
19. Cavallini, A. and R. Zecchin, 1971, "High Velocity Condensation of R-11 Vapors Inside Vertical Tubes," *Heat Transfer in Refrigeration*, International Institute of Refrigeration , pp. 385-396.
20. Shah, M. M., 1979, "A General Correlation for Heat Transfer during Film Condensation inside Pipes," *International Journal of Heat and Mass Transfer,* Vol. 22, pp. 547-556.
21. Dobson, M. K. and J. C. Chato, 1998, "Condensation in Smooth Horizontal Tubes," *Journal of Heat Transfer*, Vol. 120, 193-213.
22. Shao, D. W. and E. G. Grannid, 2000, "Flow Pattern, Heat Transfer, and Pressure Drop in Flow Condensation. Part I: Pure and Azeotropic Refrigerants", HVAC & R Research, Vol. 6, No. 2, pp. 175-195.

23. Garimella, S., J. D. Killion, and J. W. Coleman, 2002, "An Experimentally Validated Model for Two-Phase Pressure Drop in the Intermittent Flow Regime for Circular Microchannels," *Journal. of Fluids Engineering*, Vol. 124, pp. 205-214.
24. Coleman, J. W., S. Garimella, 2003 "Two-phase Flow Regimes in Round, Square, and Rectangular Tubes during Condensation of Refrigerant R134a, *Int. J. Refrig.,* 26, pp. 117-128.
25. J. H. Kurita, M. Kivisalu, S. Mitra, A. Narain, 2010, "Experimental Results on Partial and Fully Condensing Flows in Vertical Tubes, Their Agreement with Theory, and Recommended Correlations," Submitted for publication in *International Journal of Heat and Mass Transfer*.
26. Hewitt, G. F., G. L. Shires, and Y. V. Polezhaev, Editors, 1997, *International Encyclopedia of Heat and Mass Transfer*, CRC Press, Boca Raton and New York.
27. Wu, H. Y., and P. Cheng, 2005, "Condensation Flow Patterns in Microchannels," *Int. J Heat Mass Transfer*,v.48, pp.2186-297, 2005.
28. Quan, X. J., P. Cheng, and H.Y. Wu, 2008, "Transition from Annular to Plug/Slug Flow in Condensation in a Microchannel," *Int. J. Heat Mass Transfer*, 51, pp. 707-716, 2008.
29. Palen, J. W., Kistler, R. S., and Frank Y. Z., 1993, "What We Still Don't Know About Condensation in Tubes," In *Condensation and Condenser Design* (Edited by J. Taborek, J. Rose and I. Tanasawa), Pub.: United Engineering Trustees, Inc. for Engineering Foundation and ASME, New York, pp. 19 – 53.
30. Narain, A., S. Kulkarni, S. Mitra, J. H. Kurita, M. Kivisalu, 2008, "Computational and Ground Based Experimental Investigations of the Effects of Specified and Unspecified (Free) Pressure Conditions at Condenser Exit for Condensing Flows in Terrestrial and Micro-Gravity Environments," Accepted for publication in *Annals of New York Academy of Sciences, Interdisciplinary Transport Phenomenon*, 2008.
31. Narain, A., J. H. Kurita, M. Kivisalu, S. D. Kulkarni, A. Siemionko, T. W. Ng, N. Kim, and L. Phan, 2007, "Internal Condensing Flows Inside a Vertical Pipe – Experimental/Computational Investigations of the Effects of Specified and Unspecified (Free) Conditions at Exit," ASME *Journal of Heat Transfer*, pp. 1352-1372, 2007.

32. Liang, Q., X. Wang, and A. Narain**,** 2004, "Effect of Gravity, Shear and Surface Tension in Internal Condensing Flows - Results from Direct Computational Simulations." ASME *Journal of Heat Transfer*, 126 (5), pp. 676-686, 2004.
33. Narain, A., Q. Liang, G. Yu, and X. Wang, 2004, "Direct Computational Simulations for Internal Condensing Flows and Results on Attainability/Stability of Steady Solutions, Their Intrinsic Waviness, and Their Noise-Sensitivity," *Journal of Applied Mechanics,* Vol. 71, pp. 69-88, 2004.
34. Phan, L., X. Wang, and A. Narain, 2006, "Exit Condition, Gravity, and Surface-Tension Effects on Stability and Noise-sensitivity Issues for Steady Condensing Flows inside Tubes and Channels," *International Journal of Heat and Mass Transfer*, Vol. 49, Issues 13-14, pp. 2058-2076, 2006.
35. Mitra, S., A. Narain, R. Naik, S.D. Kulkarni, 2010, "Quasi One-dimensional Theory for Shear and Gravity Driven Condensing Flows and their Agreement with Two-dimensional Theory and Selected Experiments," submitted for publication in the Int. J. of Heat and Mass Transfer.
36. Patankar, S. V., 1980, "*Numerical Heat Transfer and Fluid Flow*," Hemisphere, Washinton DC.'
37. Ferziger, J. H. and M. Perić, 2002, "*Computational Methods for Fluid Dynamics*," Springer, Berlin.
38. Liang, Q., 2003, ''Unsteady Computational Simulations and Code Development for a Study of Internal Film Condensation Flows' Stability, Noise-Sensitivity, and Waviness,'' Ph.D. thesis, Michigan Technological University.
39. Wedekind, G.L., B.L. Bhatt, An Experimental and Theoretical Investigation in to Thermally Governed Transient Flow Surges in Two-Phase Condensing Flow, ASME Journal of Heat Transfer 99 (4) (1977) pp.561-567.
40. Bhatt, B. L. and G. L. Wedekind, 1980 "A Self-Sustained Oscillatory Flow Phenomenon in Two-Phase Condensing Flow Systems," ASME *Journal of Heat Transfer*, Vol. 102, No. 4, pp. 695-700.
41. Bhatt, B. L., G. L. Wedekind, and K. Jung., 1989, "Effects of Two-Phase Pressure Drop on the Self-Sustained Oscillatory Instability in Condensing Flows," *Journal of Heat Transfer*, Vol. 111, pp. 538-545.

42. Bhatt, B. L., G. L. Wedekind, and K. Jung, 1989, " Effects of Two-phase pressure Drop on the Self-Sustained Oscillatory Instabilty in Condensing Flow," ASME *Journal of Heat Transfer* 111, 538-545.
43. Greenberg, M. D., 1978, *Foundations of Applied Mathematics*, Prentice Hall, New Jersey.
44. "Thermoelectric Technical Reference, 2001," Ferrotec Thermal Solutions. Ferrotec (USA) Corporation. See URL: http://www.ferrotec.com/technology/thermoelectric/thermalRef11/
45. Weatherburn, C. E., *Differential Geometry of Three Dimensions,* Cambridge University Press, New York.
46. Plesset, M. S. and Prosperetti, A., 1976, "Flow of Vapour in a Liquid Enclosure," *Journal of Fluid Mechanics*, **78** (3), pp. 433-444.
47. Whitaker, S., 1977, *Fundamental Principles of Heat Transfer*, Pergamon Press, New York.

9. APPENDIX

APPENDIX A.1

The interface conditions that apply at $\phi(x,y,t)=y-\Delta(x,t)=0$, involve values of flow variables at the interface that are denoted by a superscript 'i'. The unit normal at any point on the interface, directed from the liquid towards the vapor, is denoted by $\hat{\mathbf{n}}$ and is equal to $\nabla\phi/|\nabla\phi|$. The unit tangent at any point on the interface, directed towards increasing x, is denoted by $\hat{\mathbf{t}}$. Each phase is modeled as a viscous and incompressible Newtonian fluid with stress tensor $\mathbf{T} = -p_I\mathbf{1} + \mathbf{S}_I$ where $\mathbf{S}_I=\mu_I\{(\text{grad}\cdot\mathbf{v}_I)+(\text{grad}\cdot\mathbf{v}_I)^T\}/2$ and $\mathbf{1}$ is the identity tensor.

• The surface velocity $\mathbf{v}_s$ of a point on the interface ($\phi=0$) at time t is associated with this point's movement to a new mapped position on the interface at time t + Δt. All such mappings must be such that the normal component of this $\mathbf{v}_s$ is given by:

$$\mathbf{v}_s\cdot\hat{\mathbf{n}}=-(\partial\phi/\partial t)/|\nabla\phi| \ . \qquad \text{(A.1)}$$

• The tangential component of the vapor and liquid velocities at the interface must be continuous, i.e.

$$\mathbf{v}_1^i \bullet \hat{\mathbf{t}} = \mathbf{v}_2^i \bullet \hat{\mathbf{t}} . \tag{A.2}$$

• Allowing for variations in surface tension σ over the interface such that the vector $\nabla_s \sigma$ is in the tangent plane and ignoring the normal component of viscous stresses in comparison to interfacial pressures, the normal component of momentum balance at a point on the interface is given by:

$$\begin{aligned} p_1^i &= p_2^i + \dot{m}^2 (1/\rho_2 - 1/\rho_1) + \sigma \nabla_s \bullet \hat{\mathbf{n}} - \nabla_s \sigma \bullet \hat{\mathbf{n}} + (\mathbf{S}_1^i - \mathbf{S}_2^i)\hat{\mathbf{n}} \bullet \hat{\mathbf{n}} \\ &\cong p_2^i + \dot{m}^2 (1/\rho_2 - 1/\rho_1) - (\sigma \Delta_{xx}) / [1 + \Delta_x^2]^{2/3} . \end{aligned} \tag{A.3}$$

The symbols for the vector $\nabla_s \sigma$ and the curvature $\nabla_s \bullet \hat{\mathbf{n}}$ in the first equality of the above equation respectively denote surface-gradient operator and surface-divergence operator and their meanings are well defined in suitable differential geometry textbooks (see, e.g., Weatherburn [45]).

• The tangential component of momentum balance at any point on the interface, which allows for surface variations in the surface tension σ, reduces to:

$$\mathbf{S}_1^i \hat{\mathbf{n}} \bullet \hat{\mathbf{t}} = \mathbf{S}_2^i \hat{\mathbf{n}} \bullet \hat{\mathbf{t}} + \nabla_s \sigma \bullet \hat{\mathbf{t}} . \tag{A.4}$$

• The mass-fluxes $\dot{m}_{VK}$ and $\dot{m}_{LK}$ as determined by the kinematic restrictions imposed by interfacial values of vapor and liquid velocities are:

$$\dot{m}_{VK} \equiv -\rho_2 (\mathbf{v}_2^i - \mathbf{v}_s) \bullet \hat{\mathbf{n}} \quad \text{and} \quad \dot{m}_{LK} \equiv -\rho_1 (\mathbf{v}_1^i - \mathbf{v}_s) \bullet \hat{\mathbf{n}} . \tag{A.5}$$

• The energy balance at a point on the interface, with energy fluxes being relative to the interface, imposes a restriction on the interfacial mass flux $\dot{m}_{\text{Energy}}$, and this restriction is given by:

$$\begin{aligned}\dot{m}_{\text{Energy}} &= \frac{1}{h_{fg}}[\{k_1 \nabla T_1\big|^i \cdot \hat{\mathbf{n}} - k_2 \nabla T_2\big|^i \cdot \hat{\mathbf{n}}\} + \frac{d\sigma}{dt}\bigg|_s \quad \frac{1}{2}\dot{m}\{\left|\mathbf{v}_1^i - \mathbf{v}_s\right|^2 - \left|\mathbf{v}_2^i - \mathbf{v}_s\right|^2\} \\ &\quad + \{\mathbf{S}_1^i \hat{\mathbf{n}} \cdot (\mathbf{v}_1^i - \mathbf{v}_s) - \mathbf{S}_2^i \hat{\mathbf{n}} \cdot (\mathbf{v}_2^i - \mathbf{v}_s)\}] \\ &\cong \frac{1}{h_{fg}}[k_1 \frac{\partial T_1}{\partial n}\bigg|^i - k_2 \frac{\partial T_2}{\partial n}\bigg|^i] \,.\end{aligned} \tag{A.6}$$

In deriving the first equality in Eq. (A.6) above, the equality of surface energy per unit area to surface tension force per unit length is assumed as per usual assumption regarding equilibrium interfacial thermodynamics. The symbol $\frac{d\sigma}{dt}\bigg|_s$ denotes rate of change of surface energy per unit area per unit time and equals $\frac{\partial \sigma}{\partial t} + \mathbf{v}_s \cdot \nabla_s \sigma$. This term along with interfacial kinetic energy exchanges and exchanges associated with the workings of the normal components of the viscous stresses are considered negligible to the net interfacial heat transfer.

• Mass Balance at any point on the interface requires a single-valued interfacial mass-flux. That is:

$$\dot{m}_{\text{LK}} = \dot{m}_{\text{VK}} = \dot{m}_{\text{Energy}} \equiv \dot{m} \,. \tag{A.7}$$

• To account for the non-equilibrium thermodynamic effects of non-zero interfacial mass flux $\dot{m}$, the interfacial pressures p_1^i and p_2^i along with their difference $\Delta p^i \equiv p_1^i - p_2^i$ that appear in

Eq. (A.3) are additionally considered to be controlled by non-equilibrium thermodynamics and are thought as $p_1^i \equiv p_{1\ \text{n-eq}}^i(T_1^i)$ and $p_2^i \equiv p_{2\ \text{n-eq}}^i(T_2^i)$, where T_1^i is the liquid side interfacial temperature and T_2^i is the vapor side interfacial temperature and $p_{1\ \text{n-eq}}$ (or $p_{2\ \text{n-eq}}$) are non-equilibrium pressures to be obtained from suitable non-equilibrium thermodynamics equations. In the limit of zero mass flux $\dot{m}$, these non equilibrium thermodynamic pressures ($p_{1\ \text{n-eq}}$ and $p_{2\ \text{n-eq}}$) reach their equilibrium thermodynamic values and are denoted as $p_1^i \equiv p_{sat}(T_1^i)$ and $p_2^i \equiv p_{sat}(T_2^i)$, where p_{sat} is the inverse function of the saturation temperature $T_s(p)$. Here, the non-equilibrium and equilibrium values of the interfacial pressure differences are denoted as ($\Delta p^i)_{\text{n-eq}}$ and $(\Delta p^i)_{sat}$. To allow for a temperature discontinuity (i.e. interfacial thermal resistance) across the interface, one must also set $(\Delta p^i)_{\text{n-eq}}$ equal to $\Delta p^i \equiv p_1^i - p_2^i$ as obtained from Eq. (A.3), and, in addition, one must provide an *explicit* or *implicit model* for a function f of the type $(\Delta p^i)_{\text{n-eq}} = f\{(\Delta p^i)_{sat}, \dot{m}\}$, where f allows the two pressure differences to become the same for zero mass flux $\dot{m}$. It is common to *model* f by considerations that involve kinetic theory of gas for the vapor phase (see, e.g., section 4.5 of Carey [1], Plesset and Prosperetti [46], etc.). At all points away from x ~ 0, the assumption that use of either $(\Delta p^i)_{\text{n-eq}}$ or $(\Delta p^i)_{sat}$ as Δp^i in Eq. (A.3) do not insignificantly affect the *near zero* value of $\Delta T^i \equiv T_s(p_2^i + \Delta p^i) - T_s(p_2^i)$ is well known and well justified in the present context where interfacial thermal resistances are overshadowed by significantly larger thermal resistance of the thin condensate. Furthermore, the computations in this paper also show: (i) that the solution further downstream is not affected by the nature of the singular solution at x ~ 0 (where non-equilibrium thermodynamics is important), and, (ii) that the computed downstream values of $\Delta T^i \equiv T_s(p_2^i + \Delta p^i) - T_s(p_2^i)$, where Δp^i values are obtained

from Eq. (A.3, satisfy $\Delta T^i \cong 0$ in the sense that $\Delta T^i << \Delta T$, where ΔT is the number defined for Eq. (1). Therefore, under negligible interfacial resistance approximation, the interfacial temperature values satisfy:

$$T_1^i \cong T_2^i = T_s(p_2^i) \ . \tag{A.8}$$

• The term [t] on the right side of Eq. (5) is given by:

$$[t] = \{\frac{\mu_2}{\mu_1}\frac{\partial v_2}{\partial x}\Big|^i - \frac{\partial v_1}{\partial x}\Big|^i\} + \frac{2\delta_x}{[1-\delta_x^2]}\{\frac{\partial u_1}{\partial x}\Big|^i - \frac{\partial v_1}{\partial y}\Big|^i\} - \frac{2\delta_x}{[1-\delta_x^2]}\frac{\mu_2}{\mu_1}\{\frac{\partial u_2}{\partial x}\Big|^i - \frac{\partial v_2}{\partial y}\Big|^i\} \tag{A.9}$$

APPENDIX A.2

Summary of the algorithm used for the 2-D computational approach to solve unsteady/steady internal condensing flow problem :

1. At discrete number of spatial locations, following variables are guessed: δ, u_{1s}^i, v_{1s}^i, θ_{1s}^i, u_2^i, v_2^i, θ_2^i. These seven guess functions are adjusted with the help of the seven interface conditions and exit conditions (if imposed). The following steps implement the separate single-phase (liquid and vapor domain) calculations approach outlined in section 4 (see Figs. 8a-8b) for a "sharp interface" model.
2. After fixing $\{u_{1s}^i, v_{2s}^i, \theta_{1s}^i\}$ on a slightly shifted interface (see Fig. 8a), liquid domain is solved under the shifted interface by a *finite-volume* (SIMPLER as in [36]) method. The $\{u_{1s}^i, v_{1s}^i, \theta_{1s}^i\}$ are adjusted to satisfy tangential stress (Eq. (5)), normal stress (Eq. (4)), and saturation temperature (Eq. (9)) conditions at the interface respectively. Alternatively, a finite

volume method and other ways to directly specify the stress boundary condition (Eqs. (A.3)-(A.4)) for (τ_1^i, p_1^i) on the interface itself is also possible. If it is an unspecified exit condition case, exit condition given by formulation [A] (see Eq. (14)) is used. If it is a specified exit condition case formulation [B] (see Eq. (15)) is used. For the specified case in Eq. (15), after using an initial guess of $u_1^i = u_1^i|_{guess}$ and a desired imposition function on the right side of Eq. (15) (this function agrees with the exit mass flow rate values for the unspecified case for $t < t^*$), the tentative value of the specified imposition at $t = t^* + \Delta t$ is imposed by changing the guess for $u_1^i = u_1^i|_{guess}$ for $t = t^* + \Delta t$ as: $u_1^i|_{guess} = \beta \bullet u_1^i|_{current}$ with β found so as to equate the left and right side of Eq. (15). Based on these modified values of u_1^i, u_{1s}^i values are adjusted to satisfy tangential stress condition. Finally, in this computational approach, it is the converged value of β at $t = t^* + \Delta t$ as obtained at the end of iterative completion of all the steps (steps 1 -5) for this time ($t = t^* + \Delta t$) that determines the right side of Eq. (15) and, hence, the actual value of the imposed exit liquid mass flow rate. The value of imposed exit liquid mass flow rate is usually in the neighborhood of the original choice for the value of the function on the right side of Eq. (15). Clearly, other superior algorithms for imposing the exit condition on the right side of Eq. (15) are possible.

3. After fixing $\{u_2^i, v_2^i, \theta_2^i\}$ on interface δ (see Fig. 8b), the vapor domain *above* the interface is solved by the same *finite-volume* method (SIMPLER). The guesses for u_2^i, v_2^i, and θ_2^i are updated with the help of: continuity of tangential velocity (Eq. (3)), interfacial mass flux equality $\dot{m}_{VK} = \dot{m}_{Energy}$, and saturation temperature (Eq. (9)) conditions at the interface respectively.
4. The interface location is updated (by tracking the interface) on an adaptive Eulerian Grid which remains fixed over a time interval [t, t + Δt] of interest. This is done by numerically

solving the following equation obtained through the remaining interface condition, namely:

$\dot{m}_{LK} = \dot{m}_{Energy}$

$$\frac{\partial \delta}{\partial t} + \bar{u}(x,t)\frac{\partial \delta}{\partial x} = \bar{v}(x,t)$$
$$\delta(0,t) = 0$$
$$\delta(x,0) = \delta_{steady}(x) \quad \text{or} \quad \delta_{any}(x) \tag{A.10}$$

The numerical solution of Eq. (A.10) (see Liang [38]) yields a converged value of δ (x, t+Δt) on the fixed Eulerian grid. These values are then used to obtain the δ (x, t+Δt) values on the fixed (for all t) CFD grid being used for the liquid and vapor CFD calculations.

5. Next the newly obtained liquid and vapor domains for time t + Δt under the new interface locations define a change of the domains in Fig. 1 (i.e., $\mathcal{L}_t \rightarrow \mathcal{L}_{t+\Delta t}$ and $\mathcal{V}_t \rightarrow \mathcal{V}_{t+\Delta t}$). A simple mapping technique is used to map the computed values of the flow variables (velocity, pressure, etc.) to the newly updated extents for the vapor and liquid domains.

The above steps 1-5 are repeated in such a way that all the interface conditions, differential equations, etc. are satisfied (and, for the specified exit condition case, the specified exit flow rate is consistent with the converged values of β at all times t). It should be noted that while solving strictly steady governing equations, the same algorithm is followed but all the time dependencies are made equal to zero and, also, no exit condition is (or can be) prescribed as steady equations are essentially parabolic in nature.

APPENDIX A.3

Net mechanical energy $\dot{\mathbf{W}}_{\text{Mech-in}}$ consumed by the condenser control volume

Net rate of mechanical energy going in to the control volume $\dot{\mathbf{W}}_{\text{Mech-in}}$ is obtained from the integral form of *mechanical energy equation* (see [47]) for individual liquid and vapor domains and then adding them together. For any fixed control-volume "Cvf–total" (element volume 'dv') that represents the condenser and encloses separate liquid and vapor domains of the type shown in Figs. 8a-8b, if one denotes the bounding surface of the control volume by "Csf-total," (element area 'da') and unit normal on the bounding surface by **n**, then the expression for $\dot{\mathbf{W}}_{\text{Mech-in}}$ is defined as:

$$\dot{W}_{\text{Mech-in}} = \int_{\text{Csf-total}} -p_{rel}(\mathbf{n}\cdot\mathbf{v})\,da + \int_{\text{Csf-total}} -(1/2)\rho|\mathbf{v}|^2(\mathbf{n}\cdot\mathbf{v})\,da + \int_{\text{Cvf-total}} \{\rho\boldsymbol{g}\cdot\mathbf{v}\}\,dv \tag{A.11}$$

where $p_{\text{rel}} \equiv p - p_0$ are the relative values of the absolute pressures p_I (I = 1 or 2) with respect to the reference inlet pressure p_0 , and **v** is the velocity – these take their appropriate values in each of the two phases (I = 1 and 2).

The above expression for the net mechanical energy into the control volume is also obtained from the differential form of *mechanical energy equation* (see Eq. (5.4-13) in Whitaker [47]) integral over individual liquid ($\mathcal{L}$) and vapor ($\mathcal{V}$) volumes and then adding them together. This analysis relates $\dot{W}_{\text{Mech-in}}$ to total viscous dissipations within each of the two domains ($\Phi_L > 0$ for the liquid and $\Phi_V > 0$ for the vapor) and the net mechanical energy consumed $\dot{D}_\Sigma$ across the interface as:

$$\dot{W}_{\text{Mech-in}} = \Phi_L + \Phi_V + \dot{D}_\Sigma \tag{A.12}$$

where we have,

$$\dot{D}_{\Sigma} \equiv \int_{\Sigma}\left[\frac{\dot{m}}{\rho_2}-\frac{\dot{m}}{\rho_1}\right] p_{ref}\, da + 0.5\int_{\Sigma}\dot{m}\left[\left|\mathbf{v}_2{}^{i}\right|^2-\left|\mathbf{v}_1{}^{i}\right|^2\right] da$$

$$\Phi_L \equiv \int_{\mathcal{L}} \mu_1 \{[\nabla \mathbf{v}_1] + [\nabla \mathbf{v}_1{}^T]\} : [\nabla \mathbf{v}_1] d\upsilon \qquad (A.13)$$

$$\Phi_V \equiv \int_{\mathcal{V}} \mu_2 \{[\nabla v_2] + [\nabla v_2{}^T]\} : [\nabla v_2] d\upsilon$$

FIGURE CAPTIONS:

Fig. 1: A schematic describing a representative condensing flow problem in a horizontal channel.

Fig. 2a: For the shear driven (0g) flow of R-113 vapor with inlet vapor speed equal to 0.6 m/s and $\Delta T = 5\ ^{\circ}C$, and h = 0.004 m, the figure shows a finite duration non-dimensional exit liquid mass flow rate prescription history $\dot{\hat{M}}_{L-e}(t)$.

Fig. 2b: For the flow conditions and non-dimensional exit liquid mass flow rate prescription history given in Fig. 2a, the figure shows the film thickness profile $\delta(x, t)$ as a function of x at non-dimensional times $t = t'$, $t = t' + 5$ and $t = t' + 14$ marked in Fig. 2a.

Fig. 3: For zero gravity condensing flow in Fig. 1 has an inlet vapor speed of 0.6 m/s, and vapor-to-wall temperature difference of $5^{o}C$. This figure shows three different time histories of "specified" exit liquid flow mass rates. The vapor is R-113 and the channel gap height is 0.004 m.

Fig. 4: For the flow conditions and exit liquid mass flow-rate prescription shown in Fig. 3, this figure shows the response of film thickness values $\delta(x, t)$ versus x with t as a parameter.

Fig. 5: A schematic showing the horizontal test-section and a particular realization of a fully condensing shear driven flow inside the test section (with different flow regimes marked by their boundary locations).

Fig. 6a: This figure shows time histories of inlet mass flow rate, inlet pressure, and exit pressure for a "natural" ($t < t_0$) and an "elliptically" constrained ($t > t_0+10$) realization of a fully condensing shear driven flow in the horizontal test-section of Fig. 5.

Fig. 6b: For the flow realizations shown in Fig. 6a, this figure shows time histories of average wall heat flux q'' and pressure difference Δp ($\equiv p_{in} - p_{exit}$). The 90 Pa change in Δp is large compared to the typical pressure difference of 100 Pa – 200 Pa that exists over the annular/stratified portion of the flow (which is shown to have a total pressure difference of about 275 Pa).

Fig. 6c: For constraining shown in Figs. 6a-6b, this figure shows thermal transient response (notice the green curve for temperature takes 65 minutes to become steady after time t_0) and compares it shorter hydrodynamic response of the average heat flux q''_{HFX-1} which becomes steady in only 10 minutes after time t_0.

Fig. 7: This figure shows the steady $T_w(x)_{-1}$ values for $t < t_0$ and new steady $T_w(x)_{-2}$ for $t > t_0$ + 65 minutes in Figs. 6a-6c.

Fig. 8a: The liquid domain calculations underneath $\delta_{shift}(x,t)$ with prescribed values of u_{1s}^{i} and v_{1s}^{i} on $\delta_{shift}(x,t)$ are implemented so as to satisfy the correct shear and pressure conditions on the actual liquid domain underneath $\delta(x,t)$.

Fig. 8b: The vapor domain calculations above $\delta(x,t)$ with prescribed values of u_2^{i} and v_2^{i} on $\delta(x,t)$ satisfy the requirement of continuity of tangential velocities and equality of interfacial mass balance.

Fig 9: The above $\delta(x,t)$ predictions for $t > 0$ are for the steady solution (at $t = 0^-$) and an initial disturbance $\delta'(x,0^+)$. The $t > 0$ solutions (shown for t = 5 and 15) are obtained on two grids I and II, $\left(n_i \times n_{j|L} \times n_{j|V}\right)_I \times \Delta t = (30 \times 30 \times 20) \times 2.5$ and $\left(n_i \times n_{j|L} \times n_{j|V}\right)_{II} \times \Delta t = (50 \times 50 \times 30) \times 5$.

Fig. 10a: The figure compares steady/quasi-steady solutions for a vertical channel obtained by 2-D and 1-D techniques. The solutions are obtained for R-113 vapor with inlet speed of U = 0.41 m/s, ΔT = 5 °C, h = 0.004 m, and $g_x = 9.8\ m/s^2$.

Fig. 10b: The figure compares steady/quasi-steady solutions for a channel under 0g conditions. The results are obtained by 2-D and 1-D techniques. The solutions are obtained for R-113 vapor with inlet speed of U = 0.6 m/s, ΔT = 5 °C, and h = 0.004 m.

Fig. 11a: Figure shows film thickness versus x variation and the y-variations of the x-component of the velocity profile (at x = 20) for gravity driven vertical (1g) and shear driven (0g) flows inside a tube. The figure also shows the linearity of temperature profiles (at x = 20) for both the cases. The solutions are obtained for flow of FC-72 vapor with inlet speed of U = 0.7 m/s, ΔT = 7.5°C, and diameter = 6.6 mm.

Fig. 11b: For the cases shown in Fig. 11a, this figure shows the non-dimensional interfacial pressure variations with downstream distance.

Fig. 12: The figure suggests the boundaries in {x, Re_{in}, G_p} space that mark various transitions from gravity dominated regime to shear dominated regime for a flow of FC-72 vapor with Ja/Pr_1 = 0.004, ρ_2/ρ_1 = 0.0148 and μ_2/μ_1 = 0.0241. The nature of steady governing equations is parabolic over the entire parameter space while the nature of unsteady equations changes from "parabolic" to "parabolic with elliptic sensitivity" as one moves from gravity driven to shear driven flow conditions.

Fig. 13: For condensing flow in zero gravity with inlet vapor speed of 0.6 m/s and vapor to wall temperature difference of 5°C, this figure shows a time history of "specified" exit liquid flow mass rate for an *on-off* type time-periodic prescription such that the mean

liquid mass flow rate at the exit is slightly less than the "natural" one.

Fig. 14: For the flow conditions and the exit liquid mass flow-rate elliptic imposition in Fig. 13, this figure shows response of film thickness values with distance x and non-dimensional time t (t is a parameter). This figure shows that at all times t > 0, annular/stratified solutions exist for the *on-off* prescription as well as for the *constant steady* prescription at the "natural" exit condition.

Fig. 15: The figure shows the Nu_x values for the natural steady and two different quasi-steady impositions in Fig. 3 and Fig. 13. The Nu_x (and $q'' = (k_1 \Delta T / h\, \delta(x))$, W/m^2) values show differences in the heat transfer rates.

Fig. 16a: For condensing flow in zero gravity with inlet vapor speed of 0.6 m/s and vapor to wall temperature difference of 5ºC, this figure shows the stable response of the flow to an initial disturbance on the interface if the exit condition for the flow is free or controlled to be exactly at the "natural" value ($\dot{\hat{M}}_{L-e}(t) = \dot{\hat{M}}_{L-e}|_{Na} = 0.116$).

Fig. 16b: For flow conditions of Fig. 16a this figure shows the unstable response of flow to an initial disturbance on the interface if the exit of the flow is controlled at a *constant* "off-natural" value ($\dot{\hat{M}}_{L-e}(t) = \dot{\hat{M}}_{L-e}|_{constant} = 0.123$).

Fig. 17a: For the exit condition impositions shown in Fig. 3, this figure shows response of the non-dimensional pressure drop values between the inlet and the outlet of the condenser.

Fig. 17b: For the exit conditions impositions shown in Fig. 13, this figure shows response of

non-dimensional pressure drop values between the inlet and the outlet of the condenser.

Fig. 18a: For the flow conditions and exit liquid mass flow-rate control shown in Figs. 3, this figure shows the response of non-dimensional values of net mechanical energy in to the condenser versus non-dimensional time t. Because of the typically negative slopes associated with the constant steady "off-natural" prescription, one can also conclude that no long term quasi-steady solution exists in the annular/stratified regime.

Fig. 18b: For the flow conditions and exit liquid mass flow-rate control shown in Fig. 13, this figure shows the response of non-dimensional values of net mechanical energy in to the condenser with non-dimensional time t. It is shown that for the on-off prescriptions at "off-natural" mean, net mechanical energy in to the condenser steadies up at a mean slightly higher but near the "natural" value.

Fig. 19: For 0g shear driven flows, this figure shows eventual mean values of net mechanical energy into the condenser for quasi-steady *on-off* type periodic prescriptions with the mean prescription values on either side of the "natural" exit condition.

Fig. 20: For 0g flows, this figure shows the mean values of the total energy transfer rate ($\dot{D}_{\Sigma}$) across the interface for *on-off* type periodic prescriptions with the mean prescription values on either side of the "natural" exit condition.

Fig. 21: Schematic of the flow loop for the shear driven (fully or partially) condensing flow experiments.

FIGURES

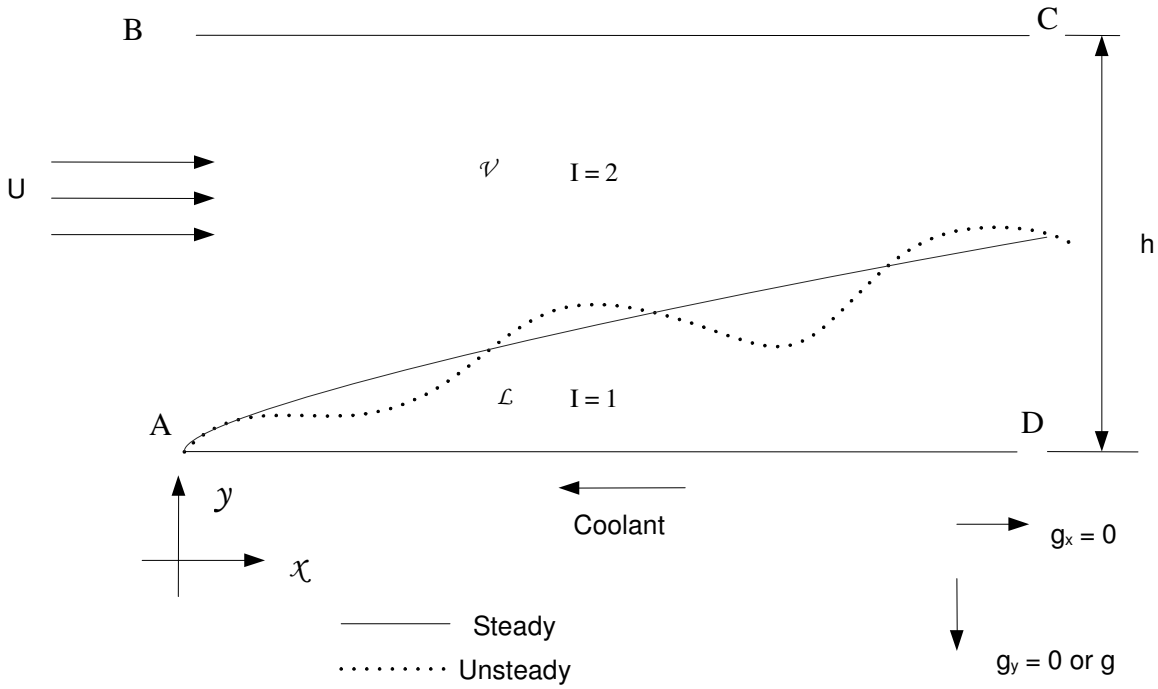

Fig. 1

.

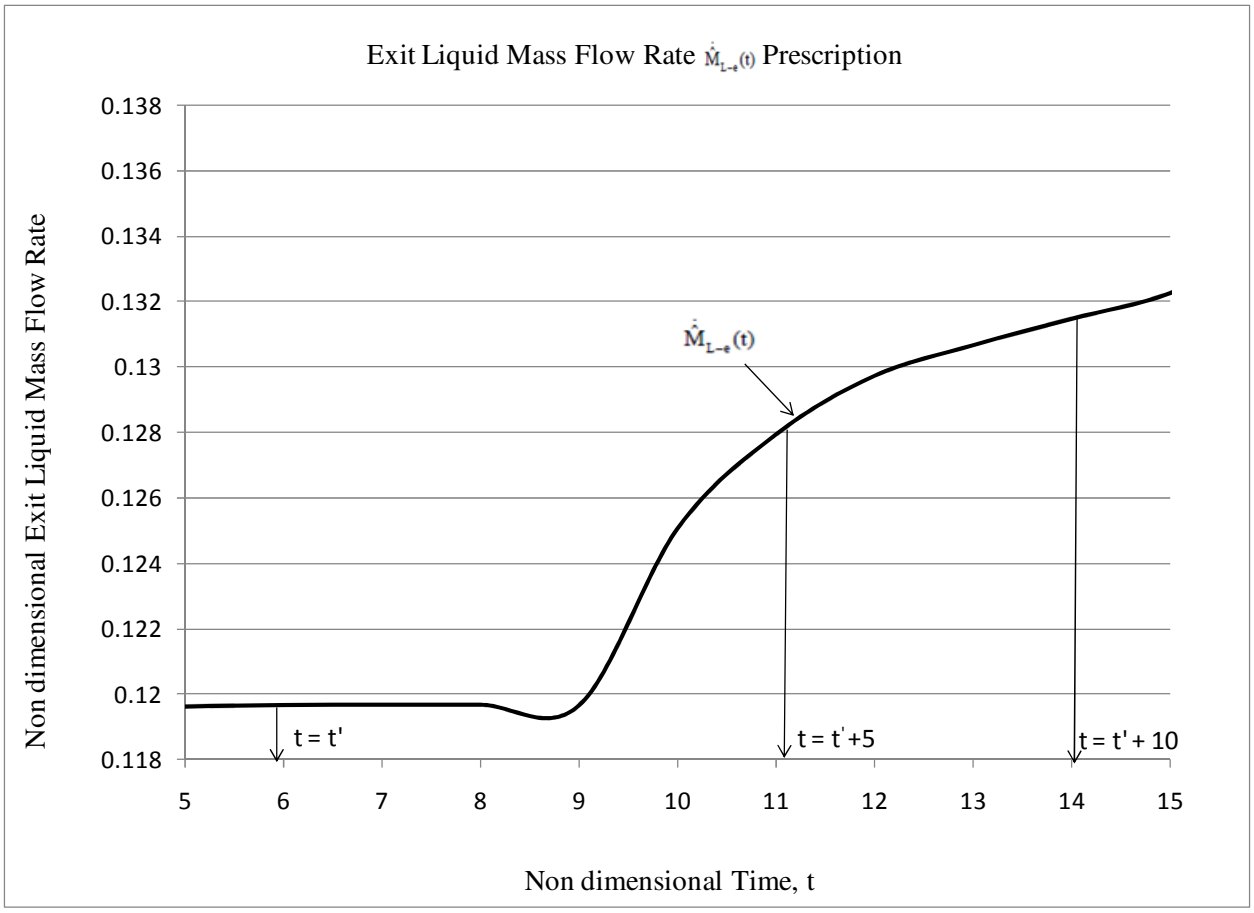
Exit Liquid Mass Flow Rate $\dot{M}_{L-e}(t)$ Prescription
Non dimensional Exit Liquid Mass Flow Rate
0.138
0.136
0.134
0.132
0.13
0.128
0.126
0.124
0.122
0.12
0.118
$\dot{M}_{L-e}(t)$
t = t'
t = t'+5
t = t' + 10
5
6
7
8
9
10
11
12
13
14
15
Non dimensional Time, t

Fig. 2a

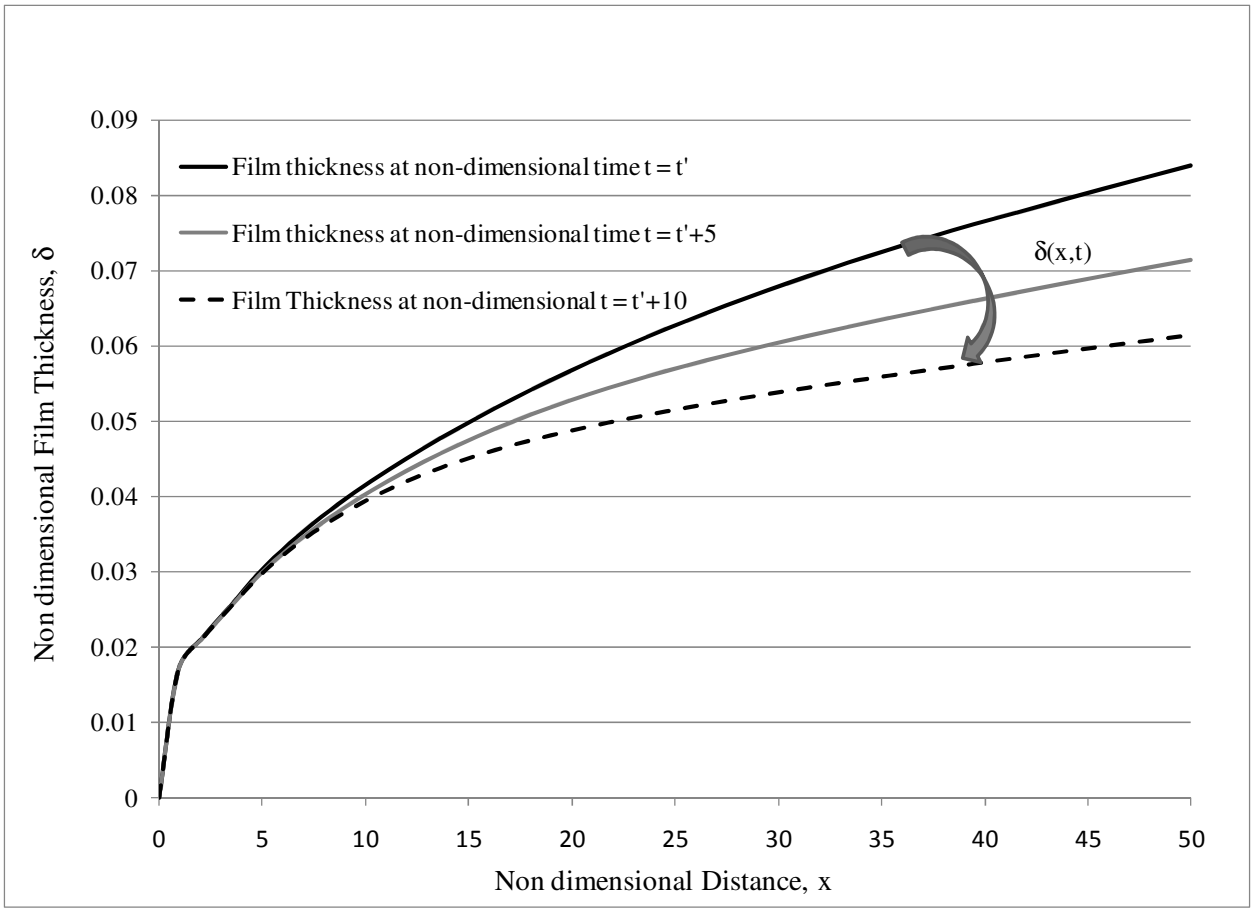
0.09
0.08
0.07
0.06
0.05
0.04
0.03
0.02
0.01
0
Non dimensional Film Thickness, δ
Film thickness at non-dimensional time t = t'
Film thickness at non-dimensional time t = t'+5
Film Thickness at non-dimensional t = t'+10
δ(x,t)
0
5
10
15
20
25
30
35
40
45
50
Non dimensional Distance, x

Fig. 2b

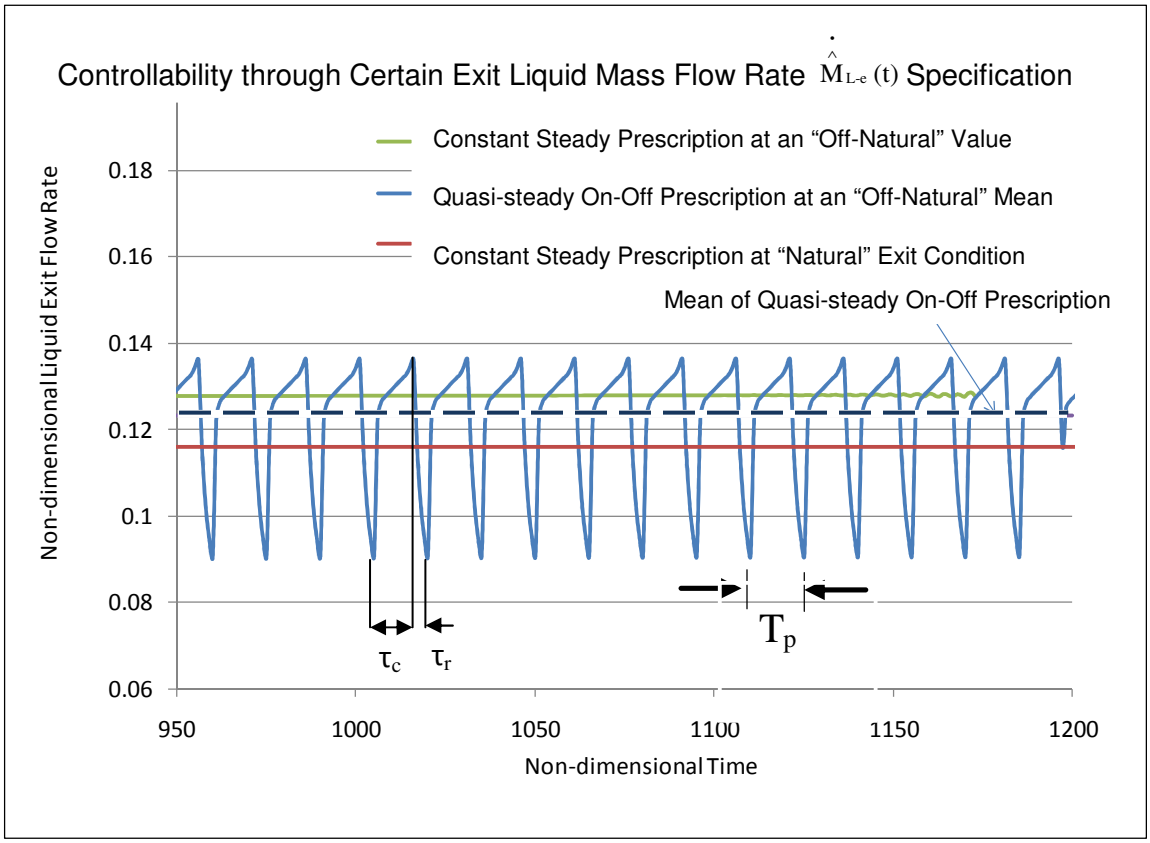
Controllability through Certain Exit Liquid Mass Flow Rate $\dot{\hat{M}}_{L\text{-}e}(t)$ Specification
Constant Steady Prescription at an "Off-Natural" Value
Quasi-steady On-Off Prescription at an "Off-Natural" Mean
Constant Steady Prescription at "Natural" Exit Condition
Mean of Quasi-steady On-Off Prescription
Non-dimensional Liquid Exit Flow Rate
0.18
0.16
0.14
0.12
0.1
0.08
0.06
950
1000
1050
1100
1150
1200
Non-dimensional Time
τ_c
τ_r
T_p

Fig. 3

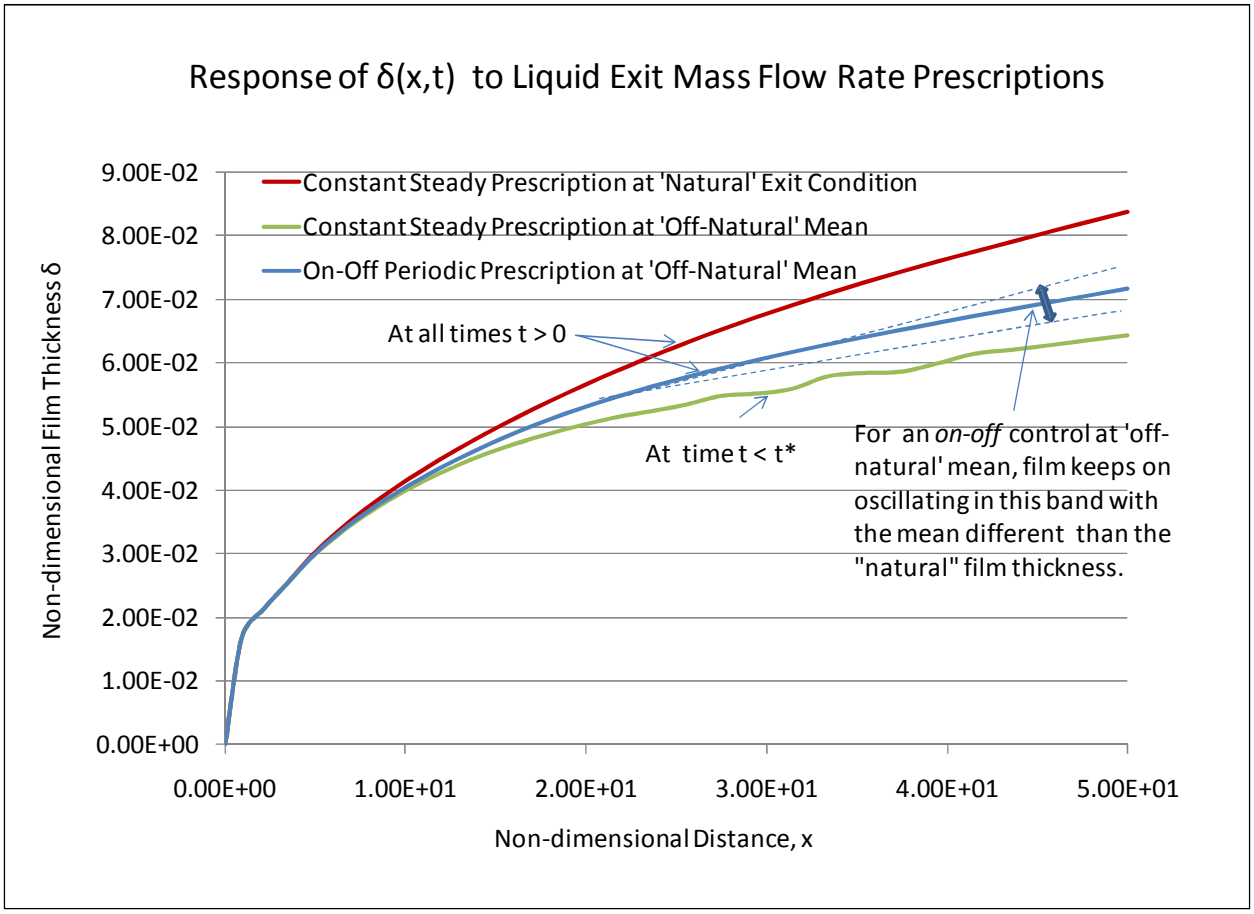
Response of δ(x,t) to Liquid Exit Mass Flow Rate Prescriptions
Constant Steady Prescription at 'Natural' Exit Condition
Constant Steady Prescription at 'Off-Natural' Mean
On-Off Periodic Prescription at 'Off-Natural' Mean
At all times t > 0
At time t < t*
For an on-off control at 'off-natural' mean, film keeps on oscillating in this band with the mean different than the "natural" film thickness.
Non-dimensional Film Thickness δ
9.00E-02
8.00E-02
7.00E-02
6.00E-02
5.00E-02
4.00E-02
3.00E-02
2.00E-02
1.00E-02
0.00E+00
0.00E+00
1.00E+01
2.00E+01
3.00E+01
4.00E+01
5.00E+01
Non-dimensional Distance, x

Fig. 4

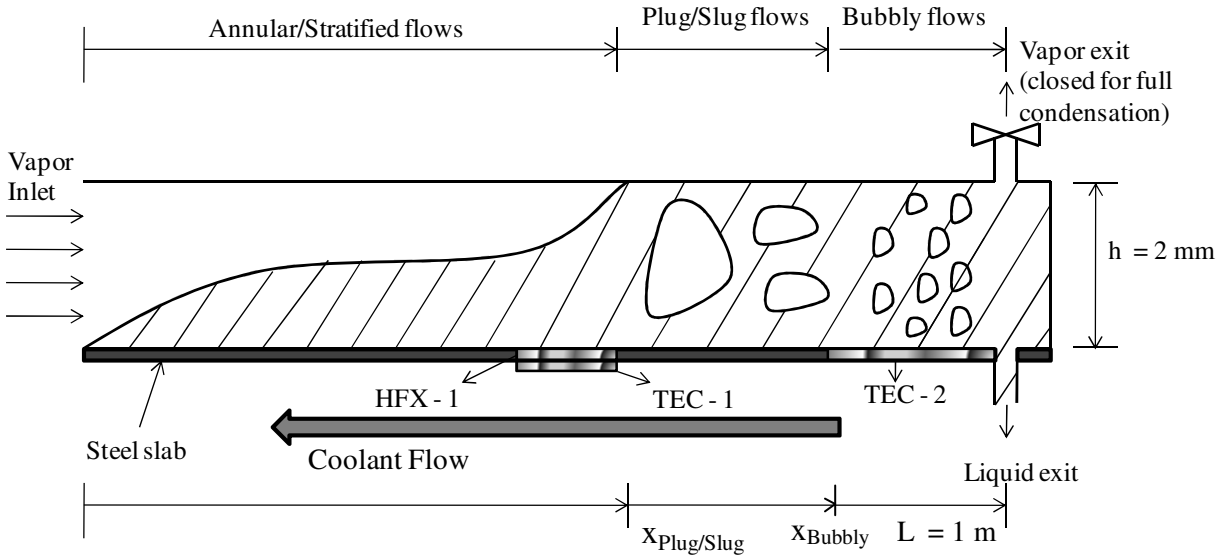
Annular/Stratified flows
Plug/Slug flows
Bubbly flows
Vapor exit
(closed for full
condensation)
Vapor
Inlet
h = 2 mm
HFX - 1
TEC - 1
TEC - 2
Steel slab
Coolant Flow
Liquid exit
$x_{Plug/Slug}$
x_{Bubbly}
L = 1 m

Fig. 5

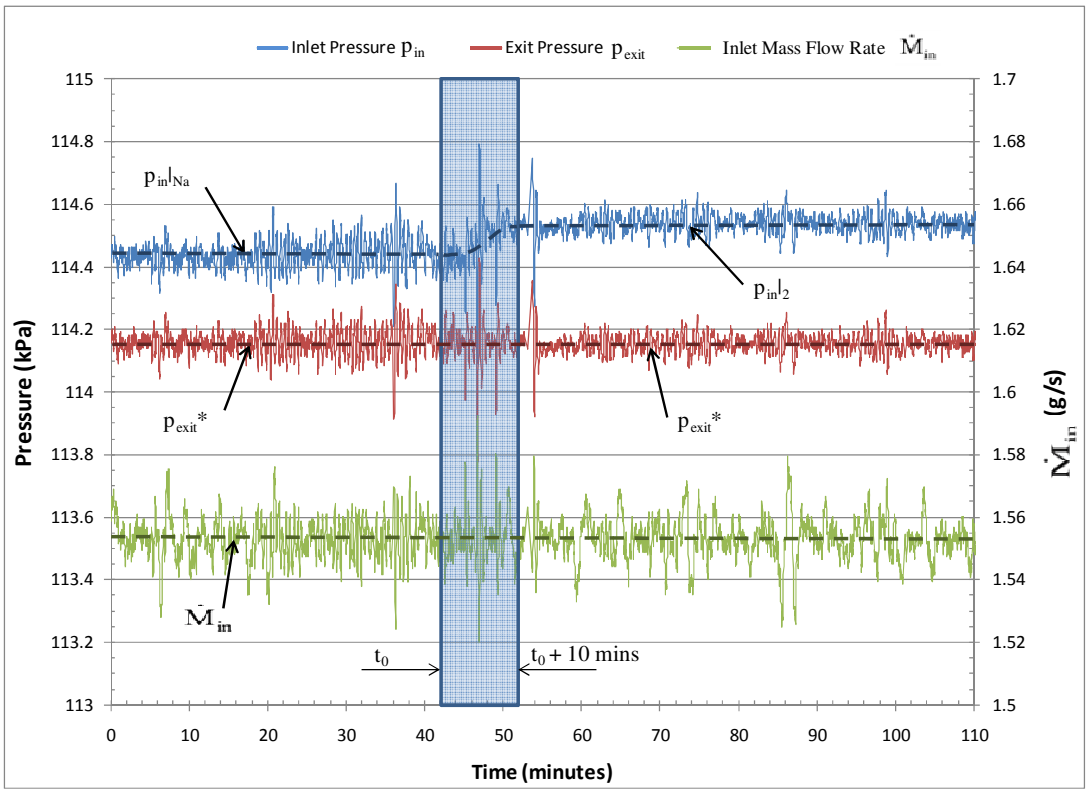
Inlet Pressure p_{in}
Exit Pressure p_{exit}
Inlet Mass Flow Rate $\dot{M}_{in}$
$p_{in}|_{Na}$
$p_{in}|_{2}$
p_{exit}*
p_{exit}*
$\dot{M}_{in}$
t_0
t_0 + 10 mins
Pressure (kPa)
$\dot{M}_{in}$ (g/s)
Time (minutes)

Fig. 6a

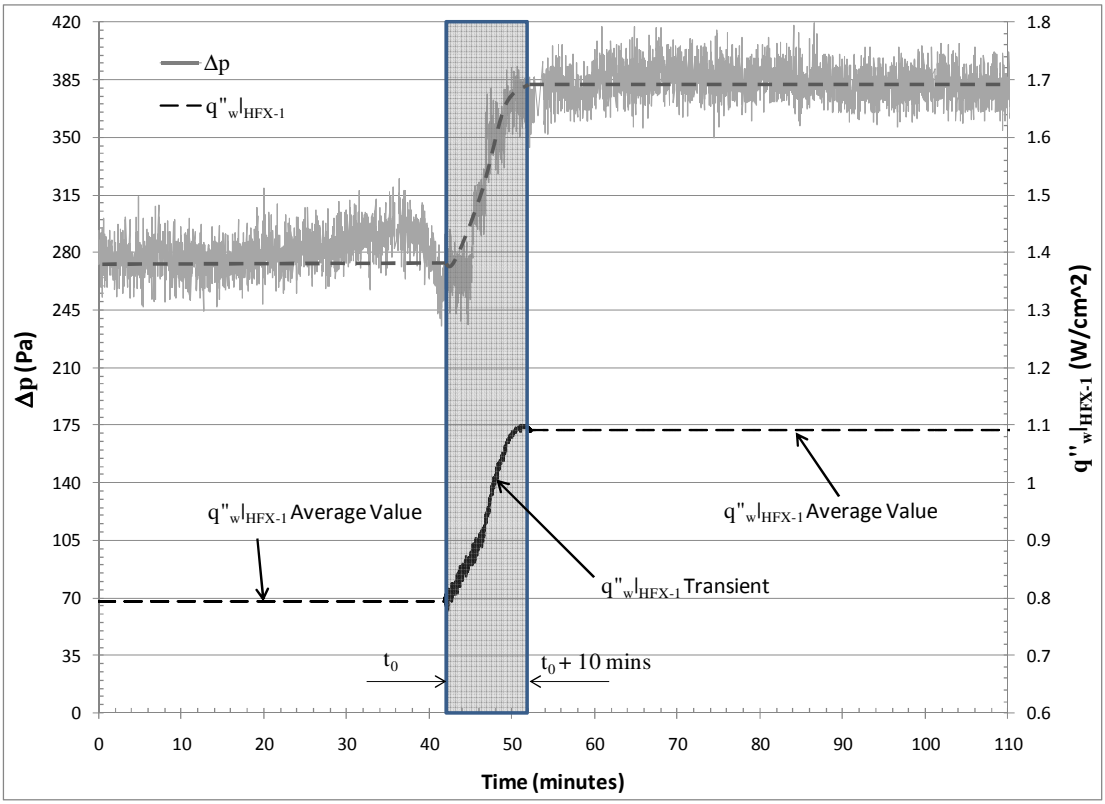
Δp
$q''_w|_{HFX-1}$
$q''_w|_{HFX-1}$ Average Value
$q''_w|_{HFX-1}$ Average Value
$q''_w|_{HFX-1}$ Transient
t_0
t_0 + 10 mins
Δp (Pa)
$q''_w|_{HFX-1}$ (W/cm^2)
Time (minutes)

Fig. 6b

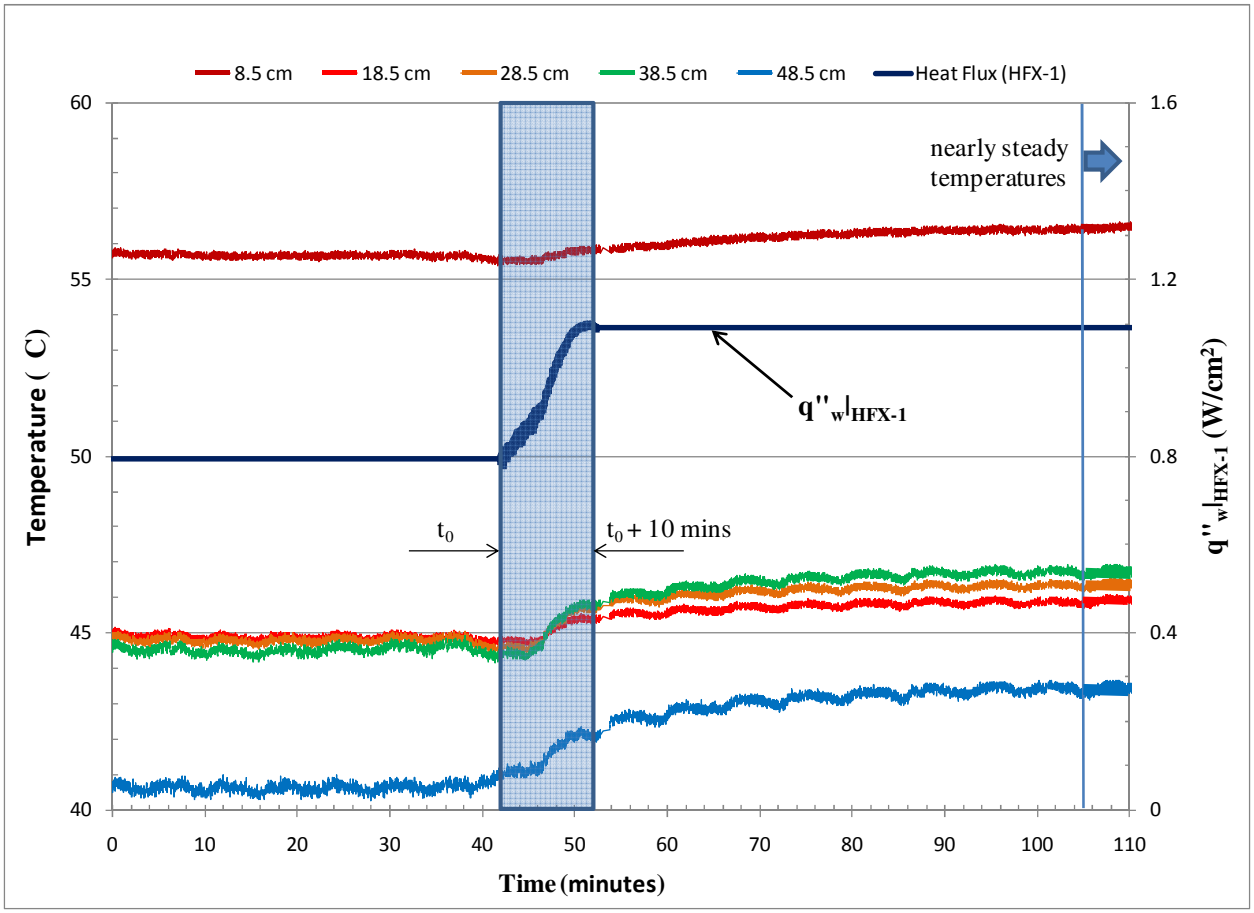
8.5 cm
18.5 cm
28.5 cm
38.5 cm
48.5 cm
Heat Flux (HFX-1)
nearly steady temperatures
$q''_w|_{HFX-1}$
t_0
t_0 + 10 mins
Temperature (C)
$q''_w|_{HFX-1}$ (W/cm^2)
Time (minutes)
60
55
50
45
40
1.6
1.2
0.8
0.4
0
0
10
20
30
40
50
60
70
80
90
100
110

Fig. 6c

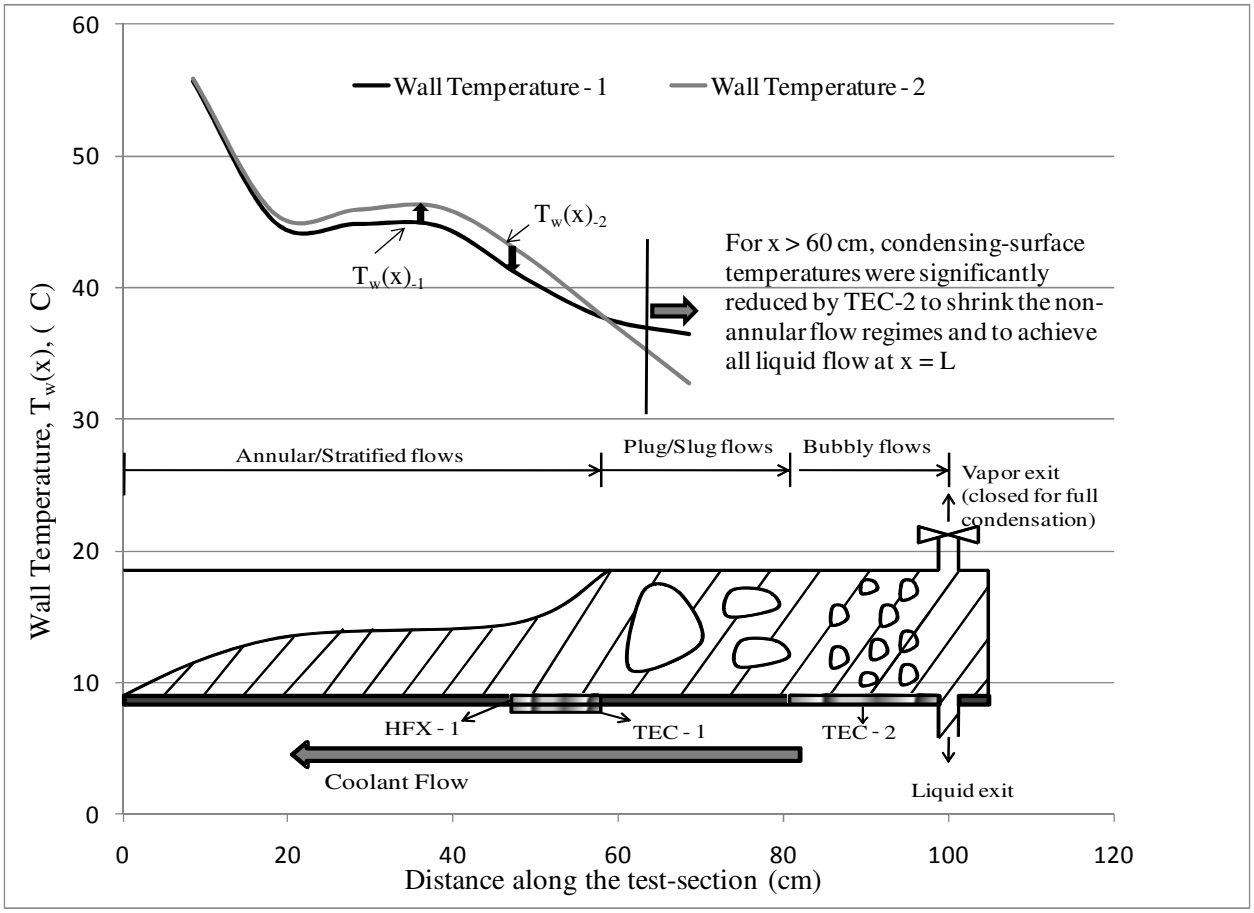
Wall Temperature - 1
Wall Temperature - 2
$T_w(x)_{-2}$
$T_w(x)_{-1}$
For x > 60 cm, condensing-surface temperatures were significantly reduced by TEC-2 to shrink the non-annular flow regimes and to achieve all liquid flow at x = L
Annular/Stratified flows
Plug/Slug flows
Bubbly flows
Vapor exit (closed for full condensation)
HFX - 1
TEC - 1
TEC - 2
Coolant Flow
Liquid exit
Wall Temperature, $T_w(x)$, (C)
Distance along the test-section (cm)
0
10
20
30
40
50
60
0
20
40
60
80
100
120

Fig. 7

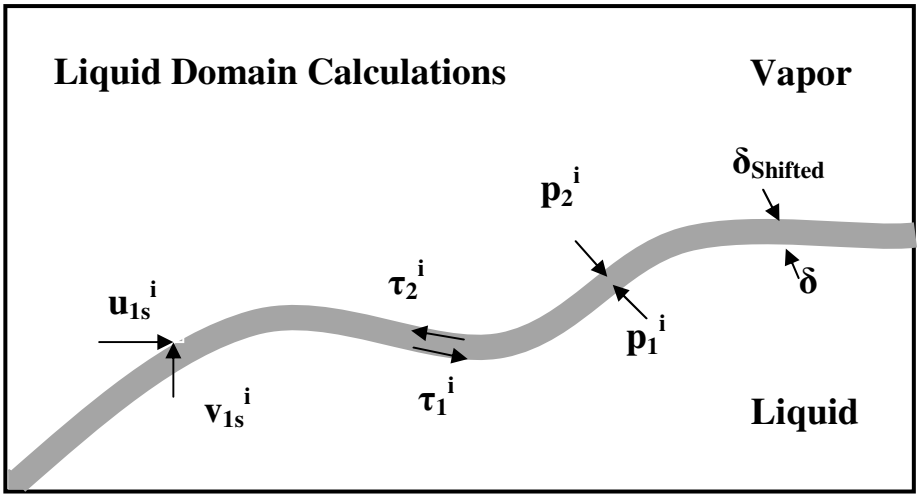
Liquid Domain Calculations
Vapor
$\delta_{Shifted}$
p_2^i
τ_2^i
u_{1s}^i
δ
p_1^i
v_{1s}^i
τ_1^i
Liquid
Ghost liquid over a single cell

Fig. 8a

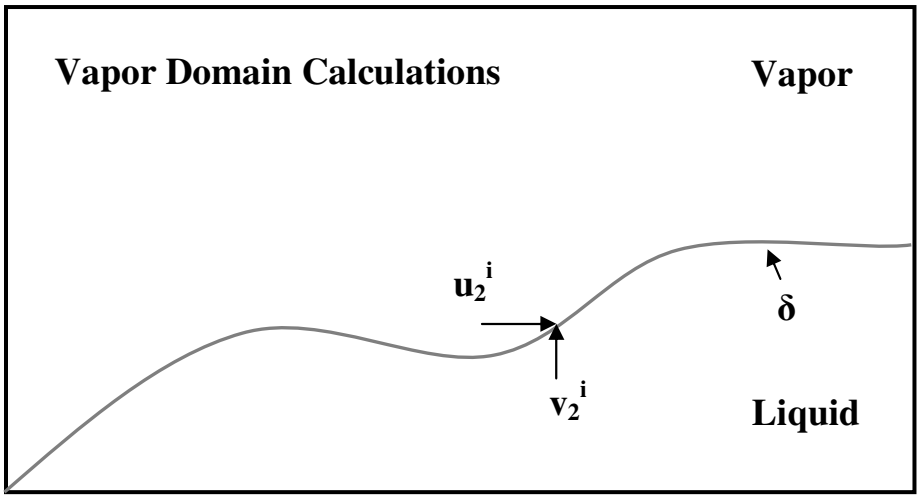
Vapor Domain Calculations
Vapor
u_2^i
δ
v_2^i
Liquid

Fig. 8b

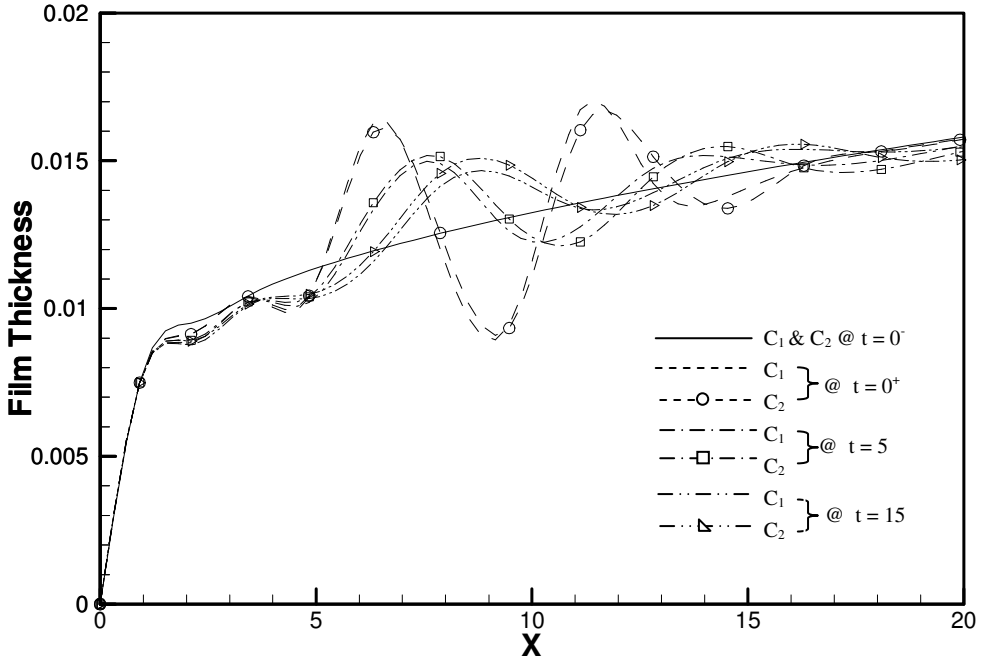
0.02
0.015
0.01
0.005
0
Film Thickness
0
5
10
15
20
X
C1 & C2 @ t = 0-
C1
C2
@ t = 0+
C1
C2
@ t = 5
C1
C2
@ t = 15

Fig. 9

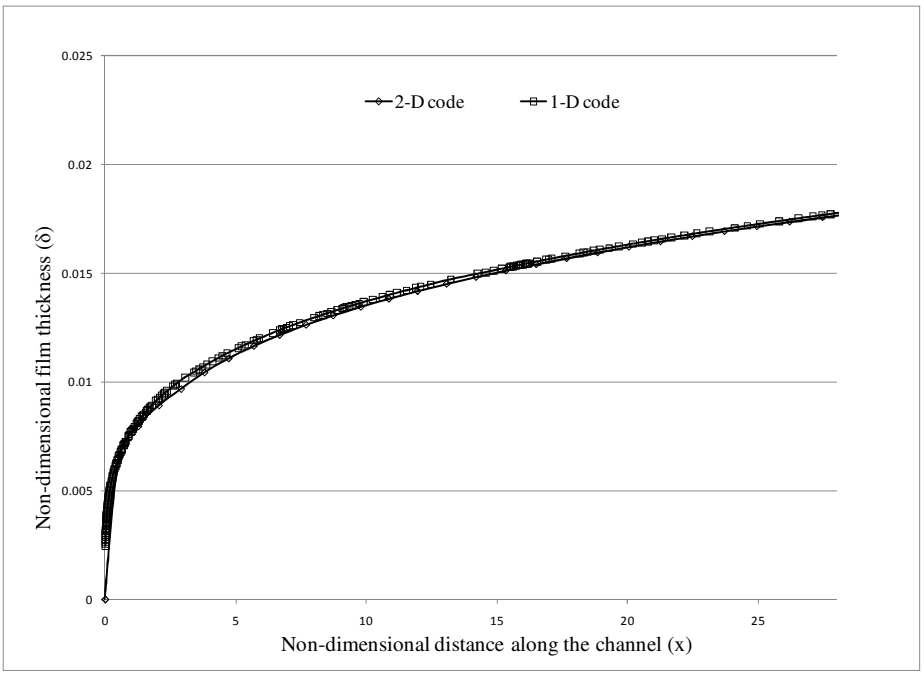

Fig. 10a

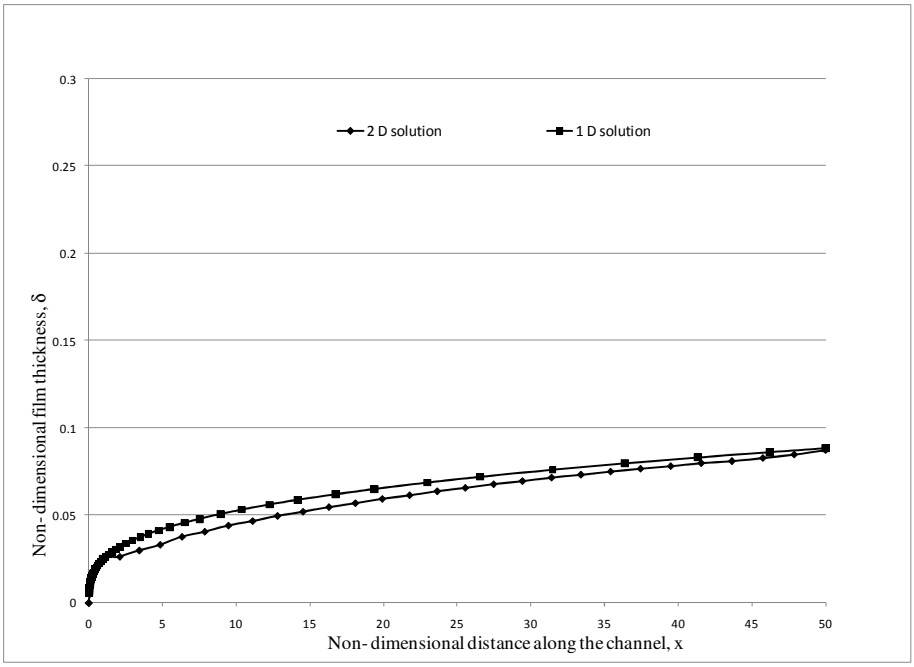

Fig. 10b

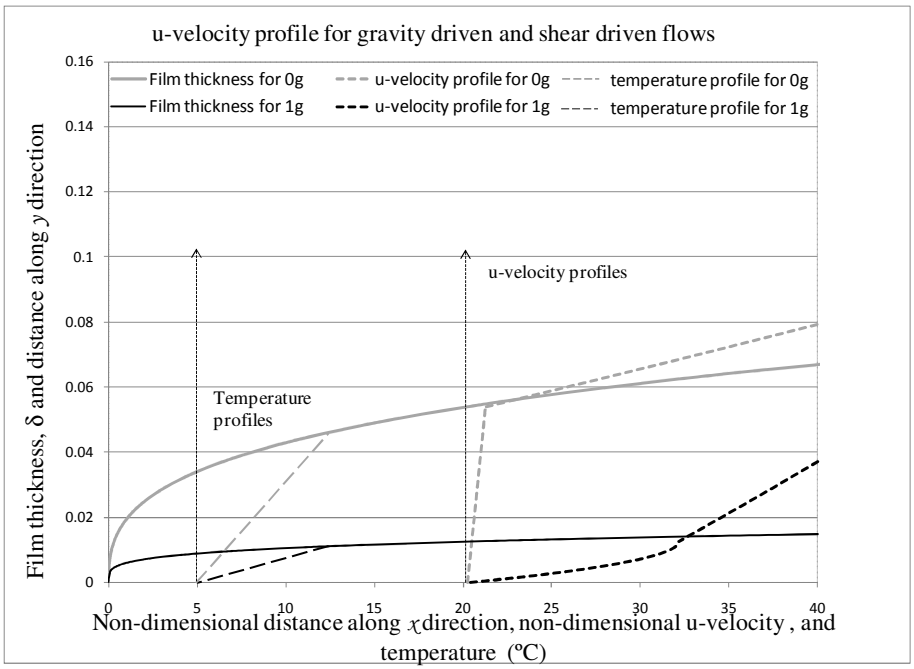

Fig. 11a

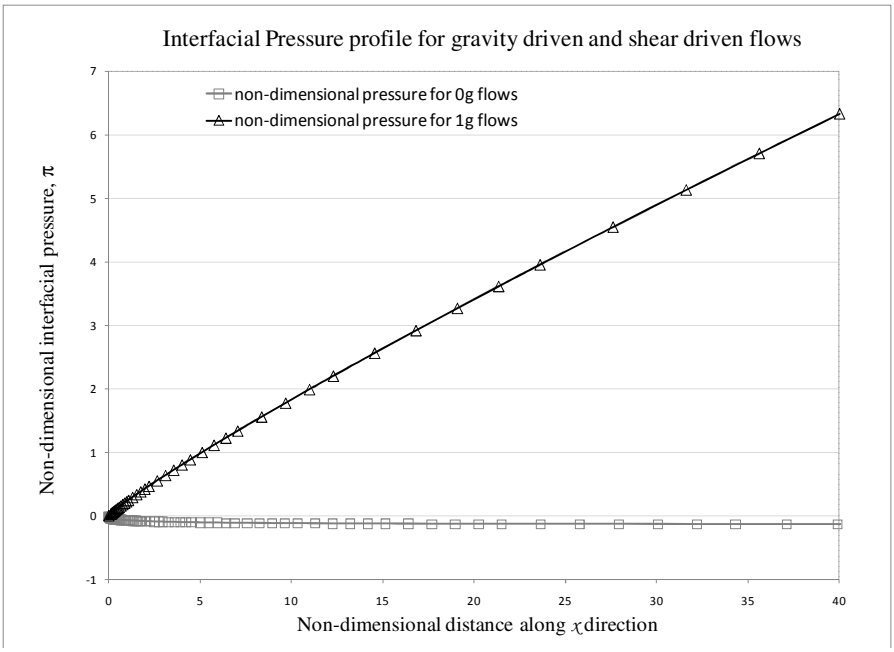

Fig. 11b

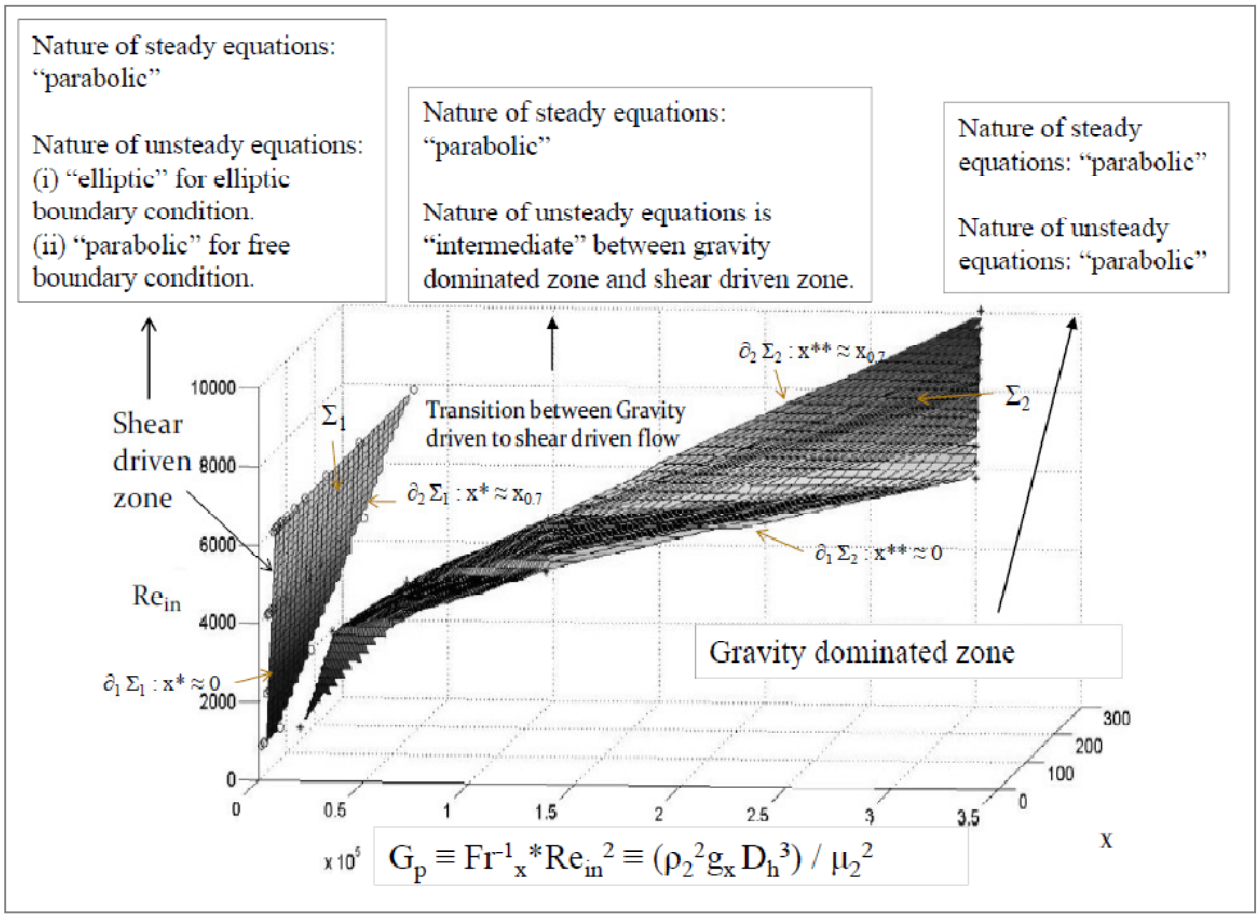
Nature of steady equations: "parabolic"
Nature of unsteady equations: (i) "elliptic" for elliptic boundary condition. (ii) "parabolic" for free boundary condition.
Nature of steady equations: "parabolic"
Nature of unsteady equations is "intermediate" between gravity dominated zone and shear driven zone.
Nature of steady equations: "parabolic"
Nature of unsteady equations: "parabolic"
Shear driven zone
Re_in
Σ1
Σ2
Transition between Gravity driven to shear driven flow
∂2 Σ2 : x** ≈ x0.7
∂2 Σ1 : x* ≈ x0.7
∂1 Σ2 : x** ≈ 0
∂1 Σ1 : x* ≈ 0
Gravity dominated zone
10000
8000
6000
4000
2000
0
0
0.5
1
1.5
2
2.5
3
3.5
x 10^5
300
200
100
0
X
G_p ≡ Fr^-1_x * Re_in^2 ≡ (ρ_2^2 g_x D_h^3) / μ_2^2

Fig. 12

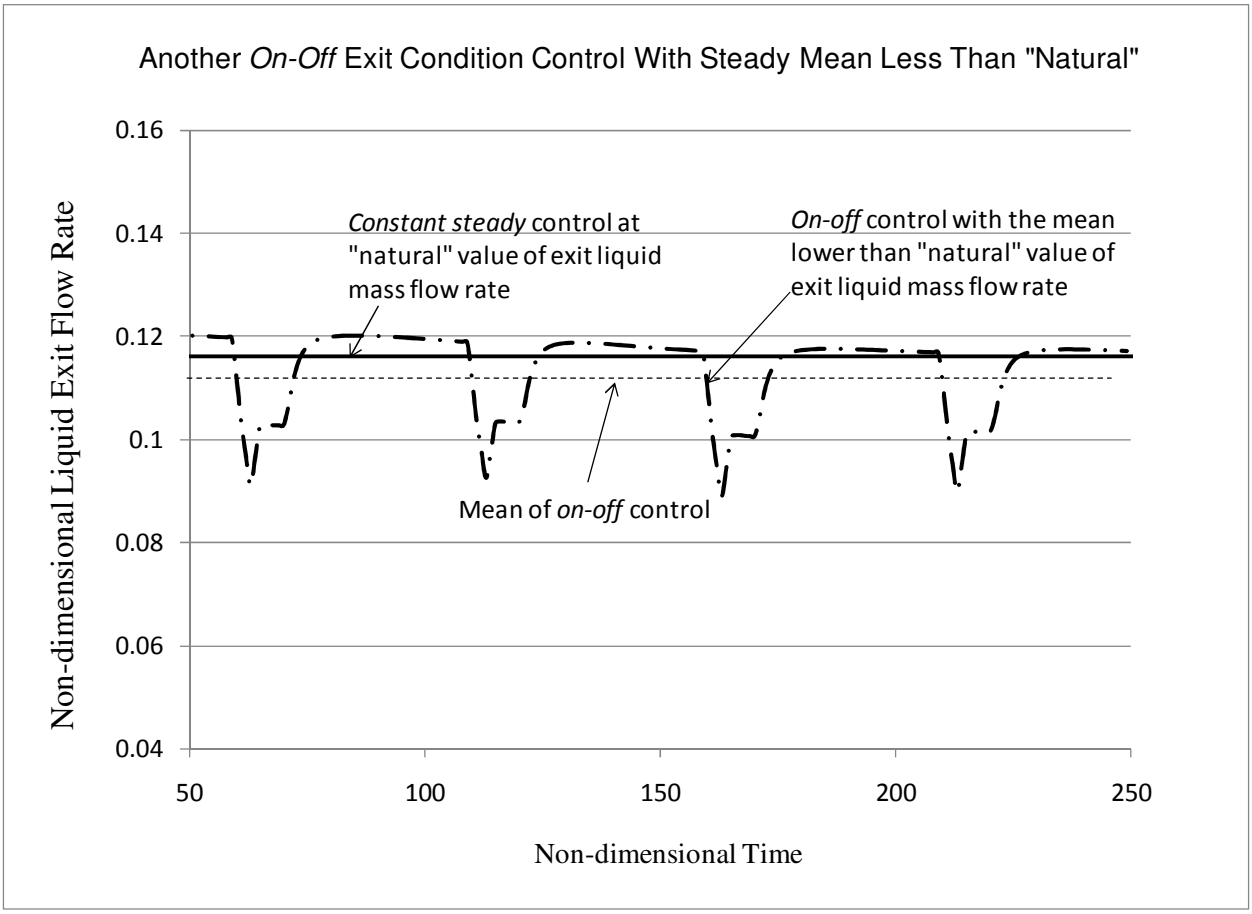
Another *On-Off* Exit Condition Control With Steady Mean Less Than "Natural"
Non-dimensional Liquid Exit Flow Rate
0.16
0.14
0.12
0.1
0.08
0.06
0.04
50
100
150
200
250
Non-dimensional Time
Constant steady control at "natural" value of exit liquid mass flow rate
On-off control with the mean lower than "natural" value of exit liquid mass flow rate
Mean of *on-off* control

Fig. 13

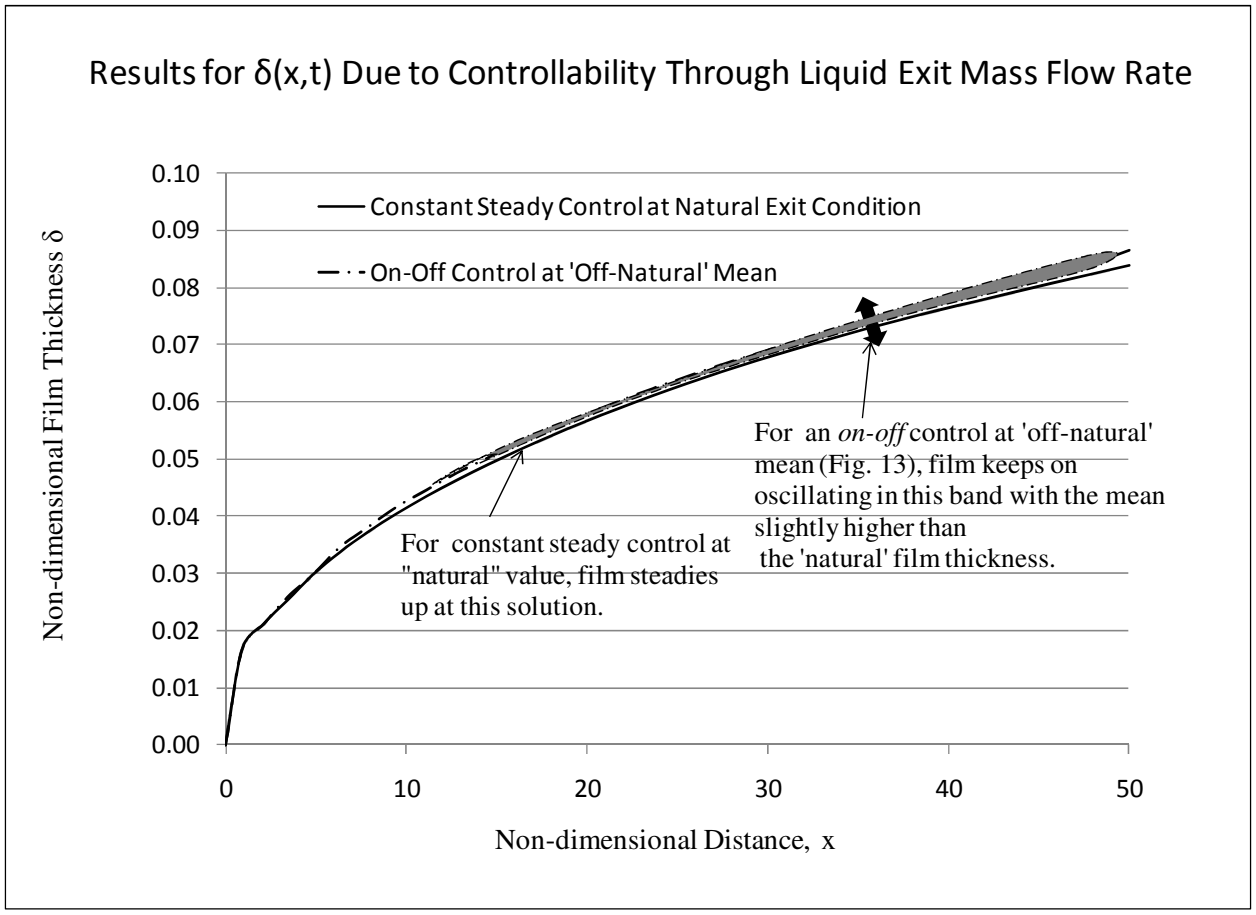
Results for δ(x,t) Due to Controllability Through Liquid Exit Mass Flow Rate
Non-dimensional Film Thickness δ
0.10
0.09
0.08
0.07
0.06
0.05
0.04
0.03
0.02
0.01
0.00
0
10
20
30
40
50
Non-dimensional Distance, x
Constant Steady Control at Natural Exit Condition
On-Off Control at 'Off-Natural' Mean
For an on-off control at 'off-natural' mean (Fig. 13), film keeps on oscillating in this band with the mean slightly higher than the 'natural' film thickness.
For constant steady control at "natural" value, film steadies up at this solution.

Fig. 14

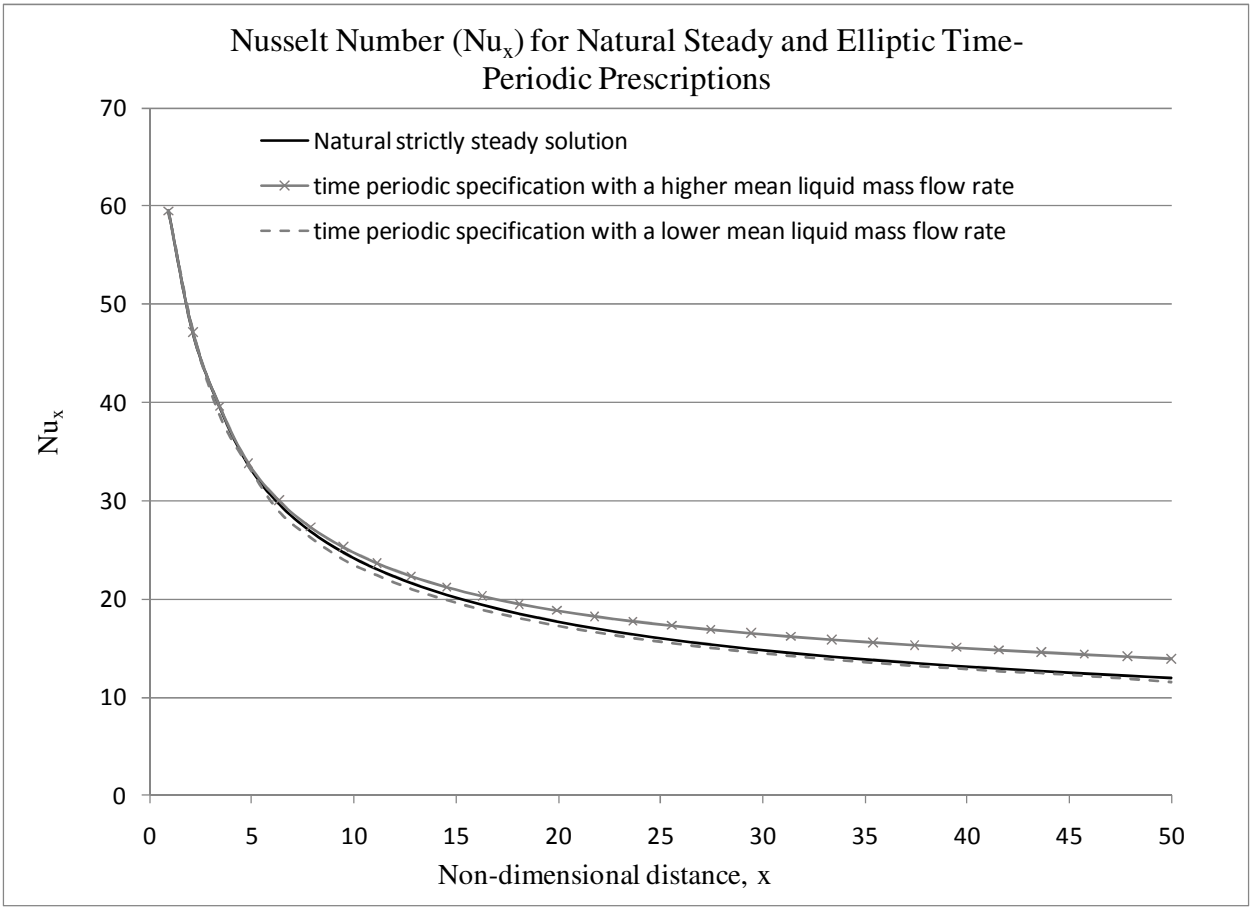
Nusselt Number (Nu_x) for Natural Steady and Elliptic Time-Periodic Prescriptions
Natural strictly steady solution
time periodic specification with a higher mean liquid mass flow rate
time periodic specification with a lower mean liquid mass flow rate
Nu_x
Non-dimensional distance, x
0
10
20
30
40
50
60
70
0
5
10
15
20
25
30
35
40
45
50

Fig. 15

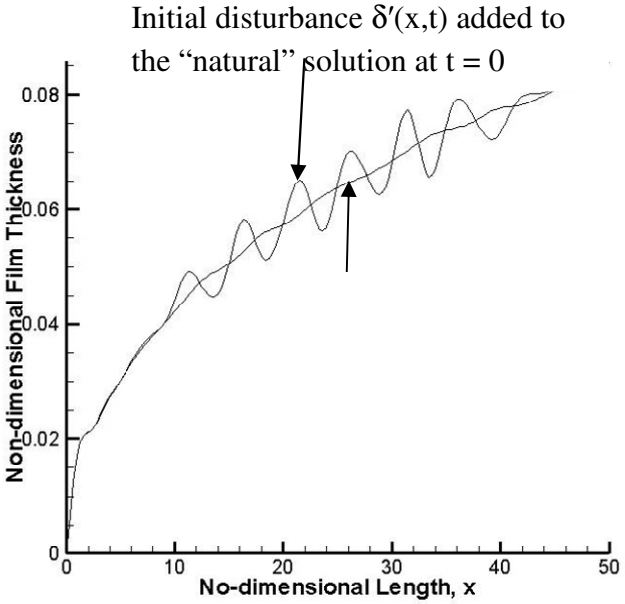

Fig. 16a

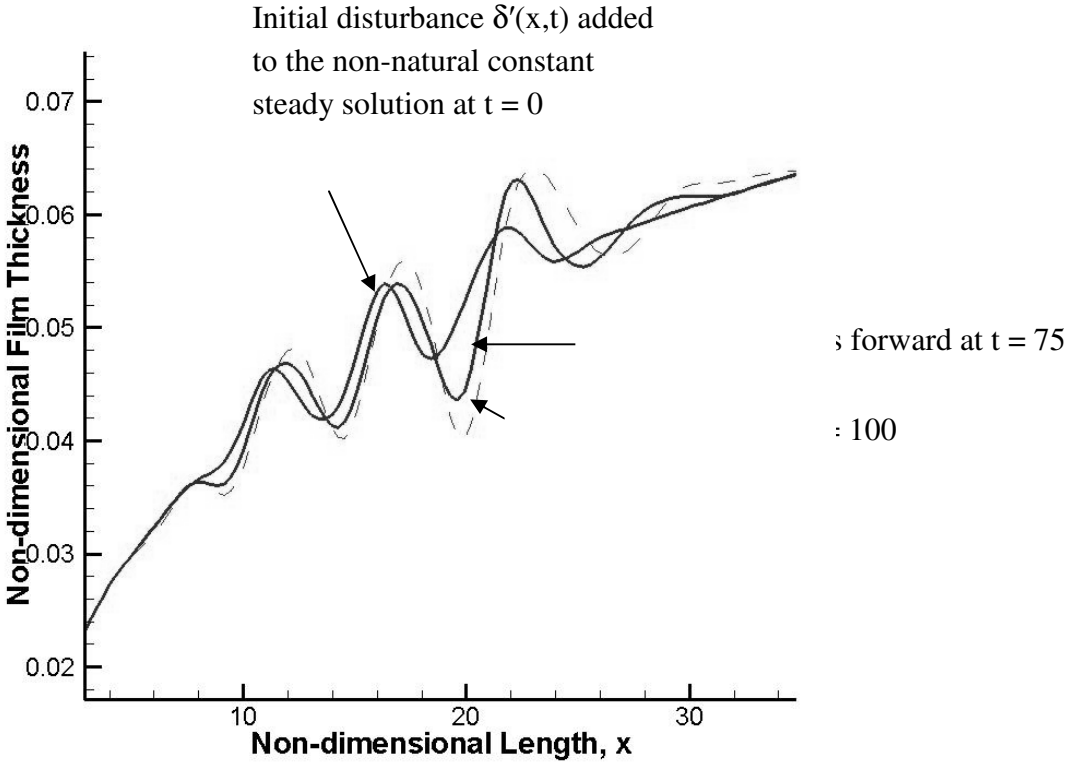

s forward at t = 75

: 100

Fig. 16b

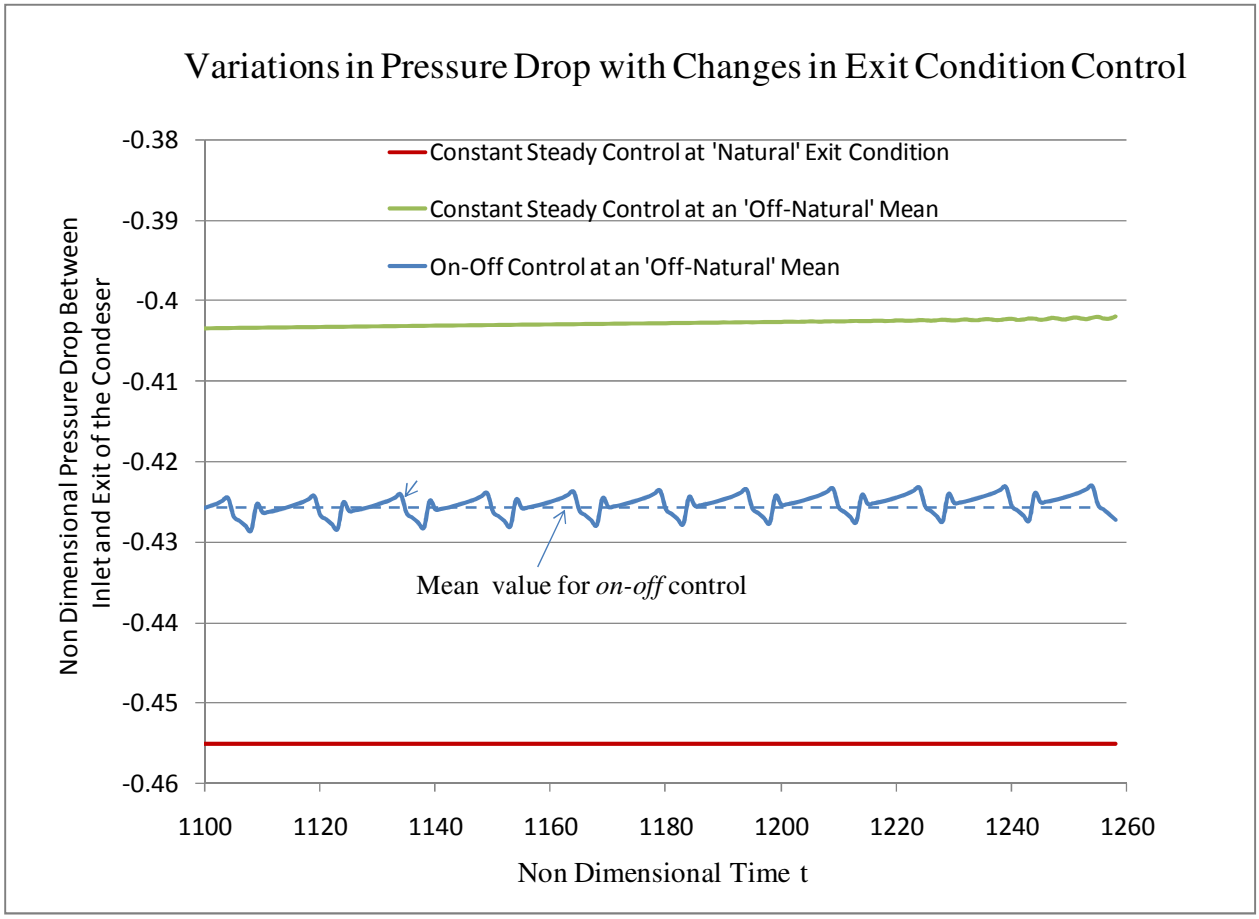
Variations in Pressure Drop with Changes in Exit Condition Control
Constant Steady Control at 'Natural' Exit Condition
Constant Steady Control at an 'Off-Natural' Mean
On-Off Control at an 'Off-Natural' Mean
Mean value for on-off control
Non Dimensional Pressure Drop Between Inlet and Exit of the Condeser
Non Dimensional Time t
-0.38
-0.39
-0.4
-0.41
-0.42
-0.43
-0.44
-0.45
-0.46
1100
1120
1140
1160
1180
1200
1220
1240
1260

Fig. 17a

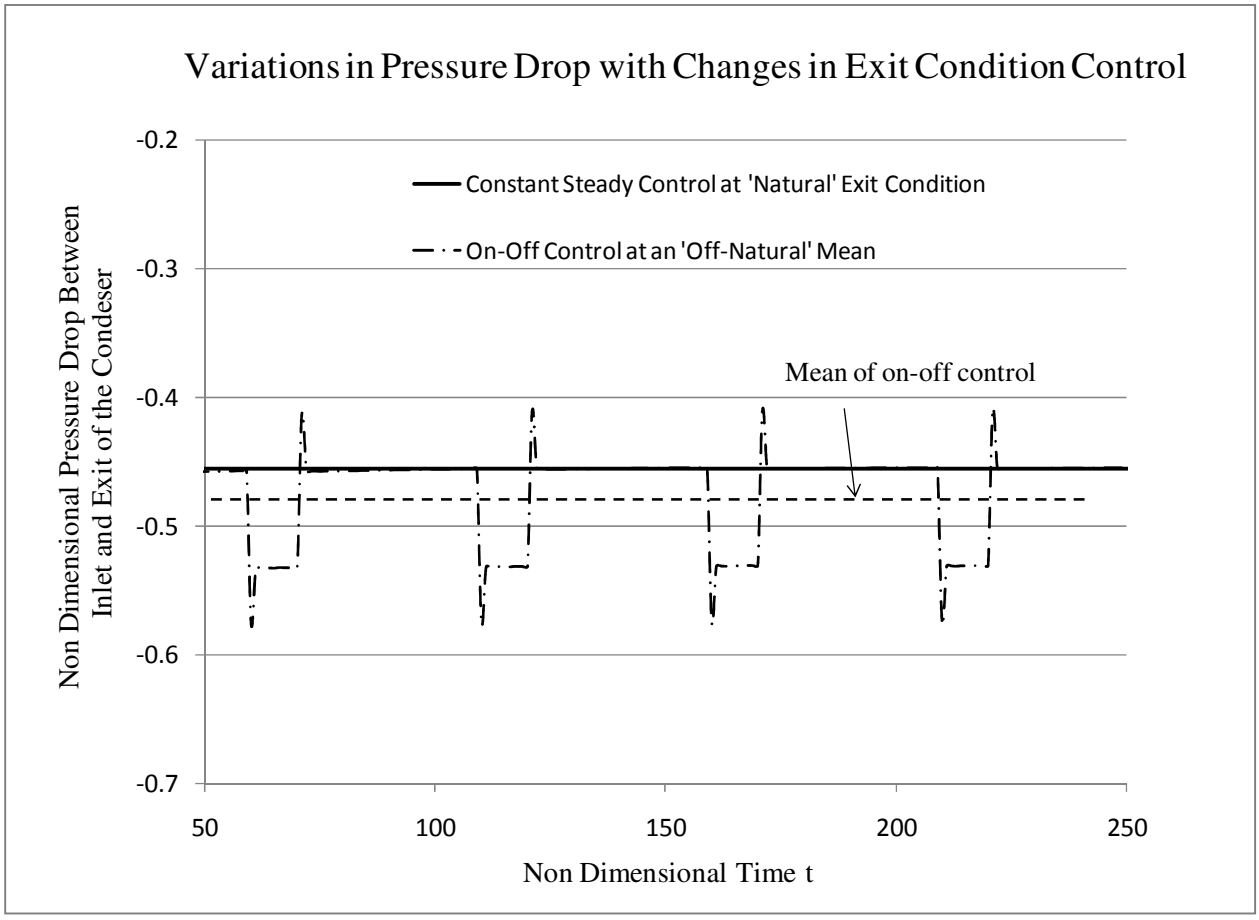
Variations in Pressure Drop with Changes in Exit Condition Control
Constant Steady Control at 'Natural' Exit Condition
On-Off Control at an 'Off-Natural' Mean
Mean of on-off control
Non Dimensional Pressure Drop Between Inlet and Exit of the Condeser
-0.2
-0.3
-0.4
-0.5
-0.6
-0.7
50
100
150
200
250
Non Dimensional Time t

Fig. 17b

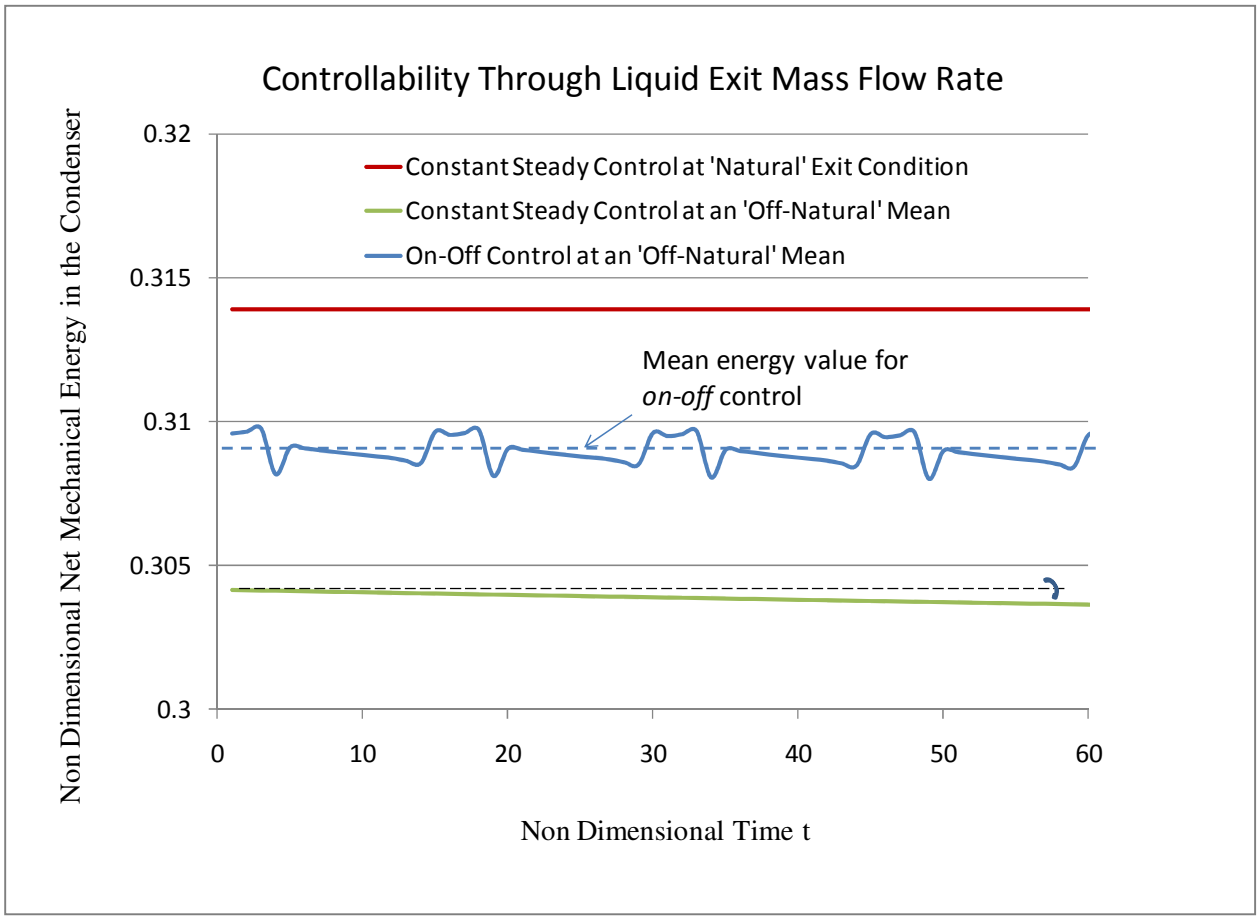
Controllability Through Liquid Exit Mass Flow Rate
Non Dimensional Net Mechanical Energy in the Condenser
0.32
0.315
0.31
0.305
0.3
Constant Steady Control at 'Natural' Exit Condition
Constant Steady Control at an 'Off-Natural' Mean
On-Off Control at an 'Off-Natural' Mean
Mean energy value for
on-off control
0
10
20
30
40
50
60
Non Dimensional Time t

Fig. 18a

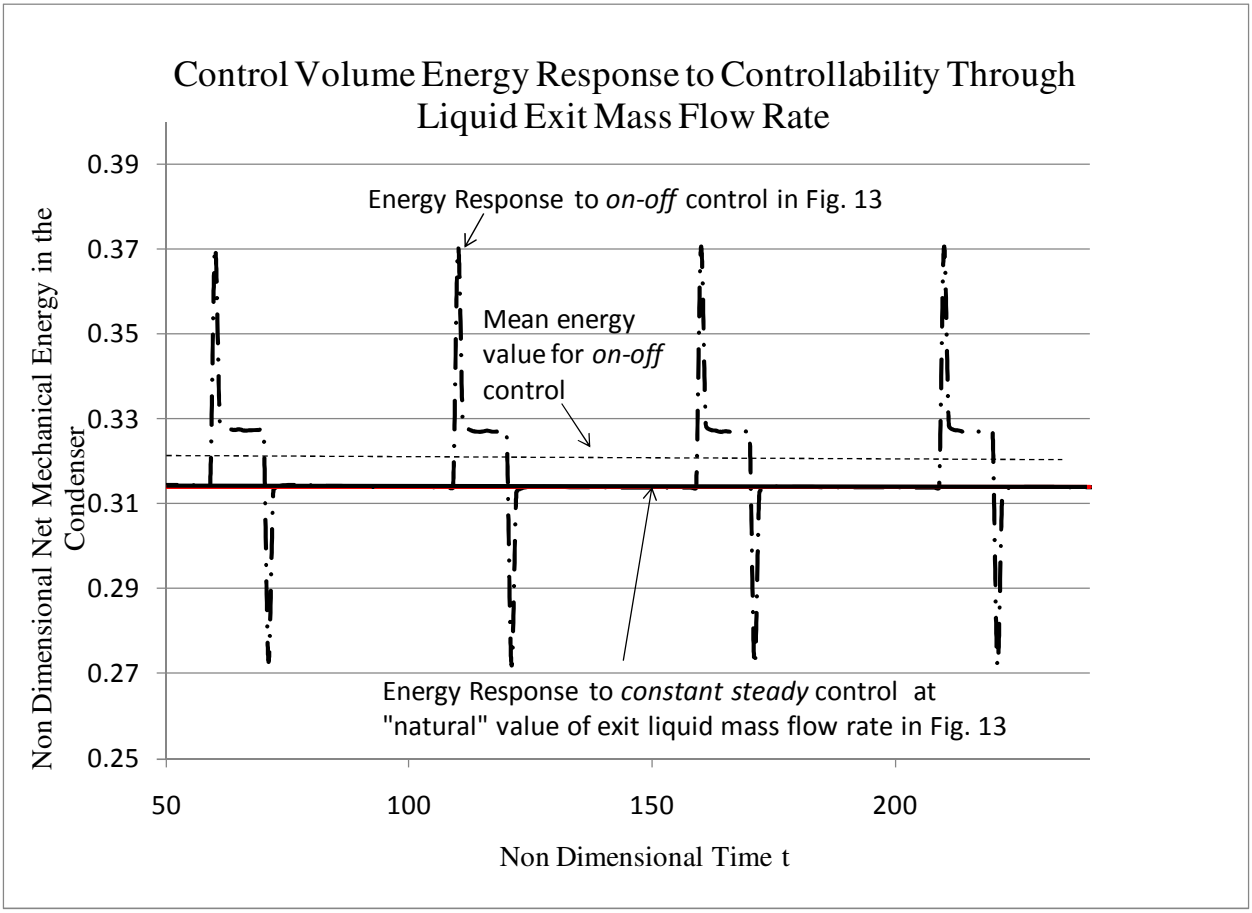
Control Volume Energy Response to Controllability Through Liquid Exit Mass Flow Rate
Non Dimensional Net Mechanical Energy in the Condenser
0.39
0.37
0.35
0.33
0.31
0.29
0.27
0.25
Energy Response to *on-off* control in Fig. 13
Mean energy value for *on-off* control
Energy Response to *constant steady* control at "natural" value of exit liquid mass flow rate in Fig. 13
50
100
150
200
Non Dimensional Time t

Fig. 18b

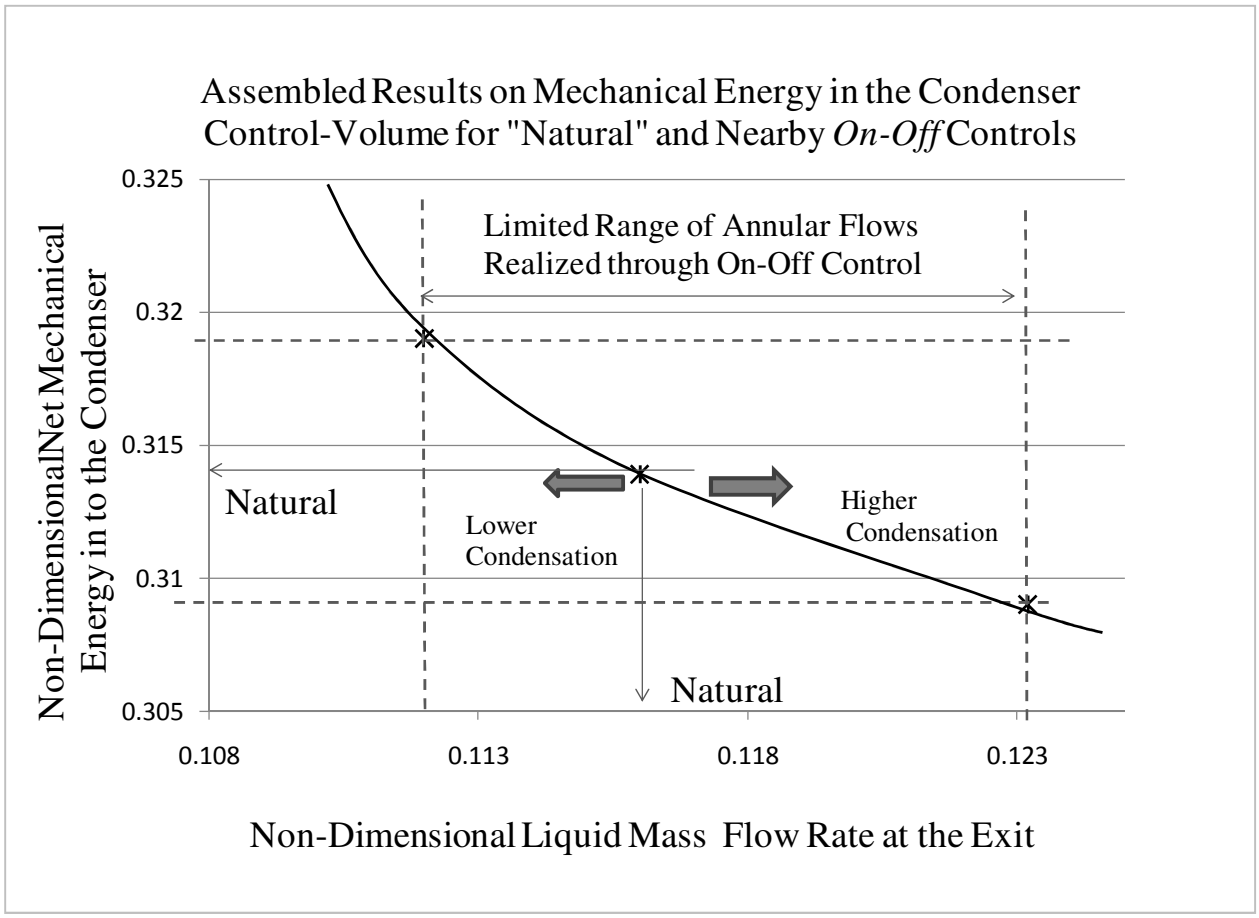
Assembled Results on Mechanical Energy in the Condenser Control-Volume for "Natural" and Nearby *On-Off* Controls
Non-DimensionalNet Mechanical Energy in to the Condenser
0.325
0.32
0.315
0.31
0.305
0.108
0.113
0.118
0.123
Limited Range of Annular Flows Realized through On-Off Control
Natural
Lower Condensation
Higher Condensation
Natural
Non-Dimensional Liquid Mass Flow Rate at the Exit

Fig. 19

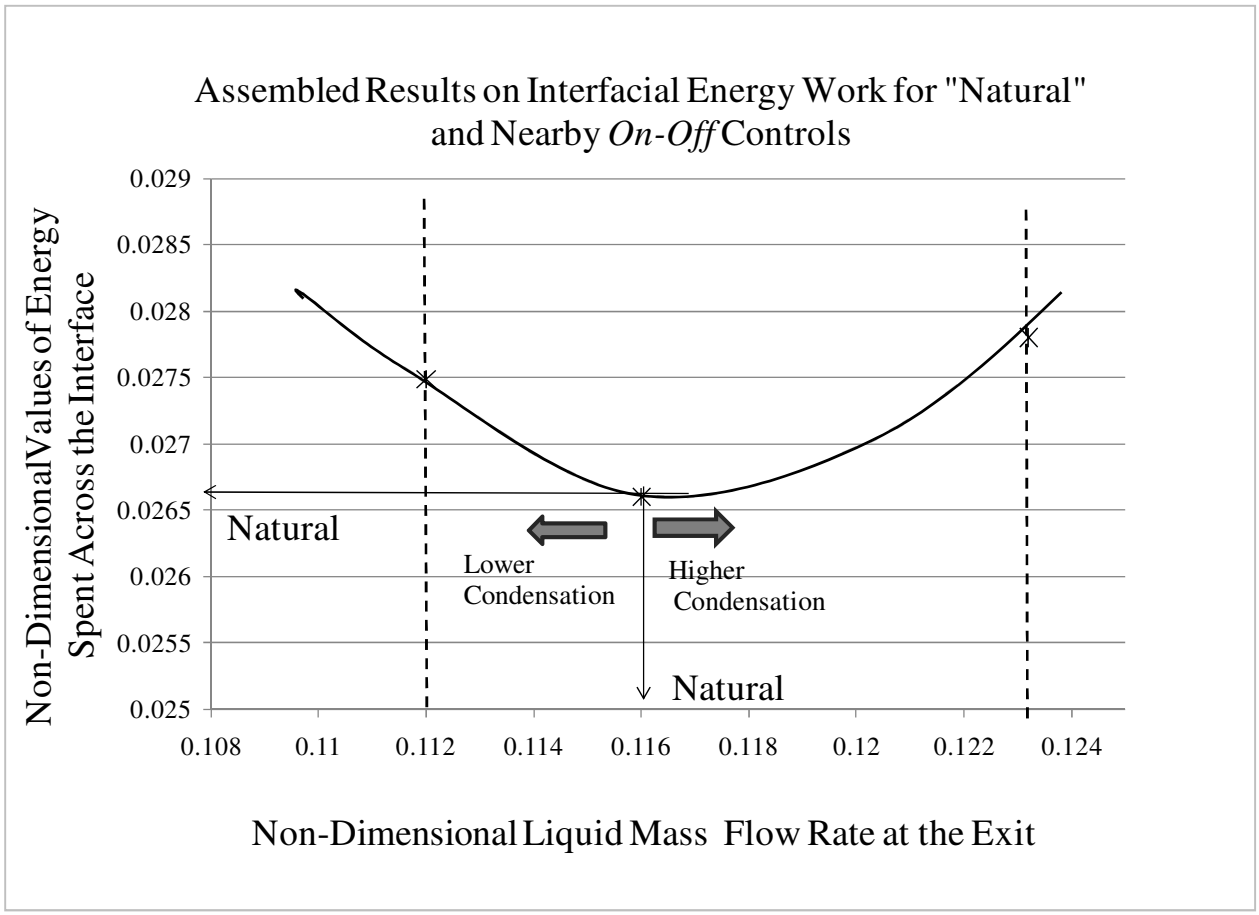
Assembled Results on Interfacial Energy Work for "Natural" and Nearby *On-Off* Controls
Non-Dimensional Values of Energy Spent Across the Interface
0.029
0.0285
0.028
0.0275
0.027
0.0265
0.026
0.0255
0.025
Natural
Lower Condensation
Higher Condensation
Natural
0.108
0.11
0.112
0.114
0.116
0.118
0.12
0.122
0.124
Non-Dimensional Liquid Mass Flow Rate at the Exit

Fig. 20

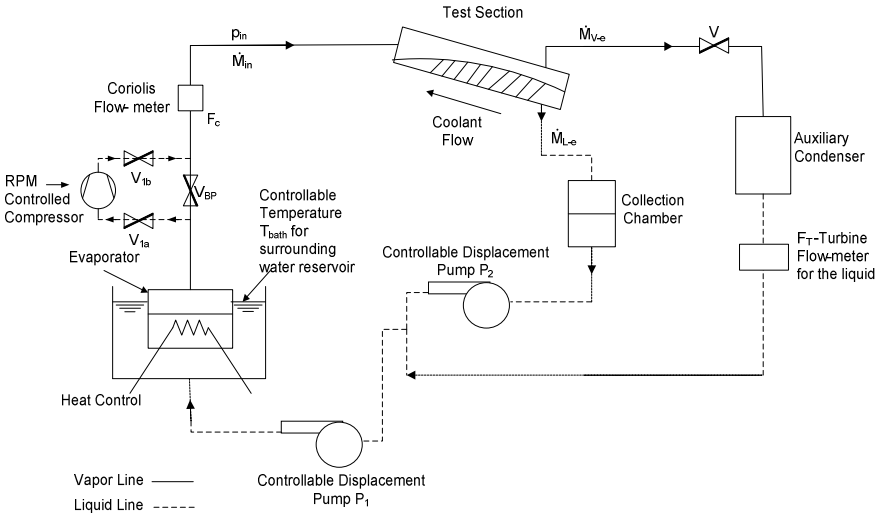
Test Section
p_{in}
$\dot{M}_{in}$
$\dot{M}_{V-e}$
V
Coriolis
Flow- meter
F_c
Coolant
Flow
$\dot{M}_{L-e}$
Auxiliary
Condenser
RPM
Controlled
Compressor
V_{1b}
V_{BP}
V_{1a}
Controllable
Temperature
T_{bath} for
surrounding
water reservoir
Collection
Chamber
F_T-Turbine
Flow-meter
for the liquid
Evaporator
Controllable Displacement
Pump P_2
Heat Control
Vapor Line
Liquid Line
Controllable Displacement
Pump P_1

Fig. 21